Manipulation of Stem Cell Functions by Micropatterned Polymer Surfaces

Wei Song

Doctoral Program in Materials Science and Engineering

Submitted to the Graduate School of
Pure and Applied Sciences
in Partial Fulfillment of the Requirements
for the Degree of Doctor of Philosophy in
Engineering

at the
University of Tsukuba

Content

List of abbreviations

AFM	Atomic force microscope
ALP	Alkaline phosphatase
ASCs	Adult stem cells
BMP	Bone morphogenetic protein
BSP	Bone sialoprotein
DMEM	Dulbecco's modified eagle medium
EGF	Epidermal growth factor
ESCs	Embryonic stem cells
FABP4	Fatty acid binding protein 4
FBS	Fetal bovine serum
FGF2	Fibroblast growth factor 2
GAG	Glycosaminoglycan
HA	Hyaluronic acid
hESCs	Human embryonic stem cells
HSCs	Hematopoietic stem cells
iPSCs	Induced pluripotent stem cells
LIF	Leukemia inhibitory factor
LPL	Lipoprotein lipase
mESCs	Mouse embryonic stem cells
MSCs	Mesenchymal stem cells
MuSCs	Muscle stem cells
NMR	Nuclear magnetic resonance
NSCs	Neural stem cells
OC	Osteocalcin
OP	Osteopontin
PAAc	Poly(acrylic acid)
PBS	Phosphate buffer saline
PDMS	Poly(dimethyl siloxane)
PPARγ2	Peroxisome proliferator-activated receptor γ2
PSt	Polystyrene
PVA	Poly(vinyl alcohol)
RT-PCR	Real-time polymerase chain reaction
RUNX2	Runt-related gene 2
SCF	Stem cell factor
TBS	Tris-buffered saline
TGF-β	Transforming growth factor-β
UV	Ultraviolet

Chapter 1

General introduction

1.1 Stem cells

In general, stem cells are described as a reservoir of non-differentiated cells that can generate highly differentiated descendant with specific function. Three main features define this cell population: self-renewal, proliferation, and multi-potentiality[1]. These features are critical to sustained generation and regeneration of cells, tissues, and organs during development and remodeling. Stem cells hold the key to a number of cellular processes from development, tissue regeneration, and aging. They also hold the promise of cures for many diseases and injuries as well as offer an opportunity to bridge the 'animal to human gap' in drug efficacy studies.

1.1.1 Origins and types

Stem cells are generally divided into three types: pluripotent embryonic stem cells (ESCs), induced pluripotent stem cells (iPSCs), and unipotent or multipotent adult stem cells (ASCs) (Figure 1.1). ESCs are derived from blastocysts and are capable of giving rise to any cell type[2-5]. IPSCs are generated by using a transcription factor cocktail to reprogram the adult somatic cells (e.g. fibroblasts) back to a pluripotent state[6,7]. ESCs and iPSCs share similar properties and have a seemingly unlimited self-renewal potential in culture. However, the reliable methods are highly required to avoid the risk of tumor formation and to direct these cells into a single tissue-specific lineage. Although iPSCs overcome the immune problem and the ethical concern faced by the use of ESCs and ASCs in patients, current methods to reprogram somatic cells and to produce iPSCs are extremely slow and inefficient[8]. In contrast, tissue-specific ASCs lack the plasticity of ESCs and iPSCs. And it is difficult to induce self-renewal of ASCs in culture and to expand the cells to reach necessary numbers in clinical therapy. Nonetheless, they are not tumorigenic and mainly used for efficiently generating highly specialized cell types[8]. Consequently, the versatile and multi-functional stem cells are the most promising cell source for the tissue engineering and regenerative medicine.

1.1.2 Mesenchymal stem cells and differentiation

Mesenchymal stem cells (MSCs), one of the well-characterized stem cells, reside in various adult

mesenchymal tissues. Thereby they are one of prospective cell sources for tissue engineering and clinical practice. The advantages of MSCs are that they can be easily harvested from the patient's donor site (e.g. bone marrow and adipose tissue), isolated and propagated *in vitro* culture, induced to differentiate into specific cell lineages, and transplanted into the patient's body where tissue regeneration is required.

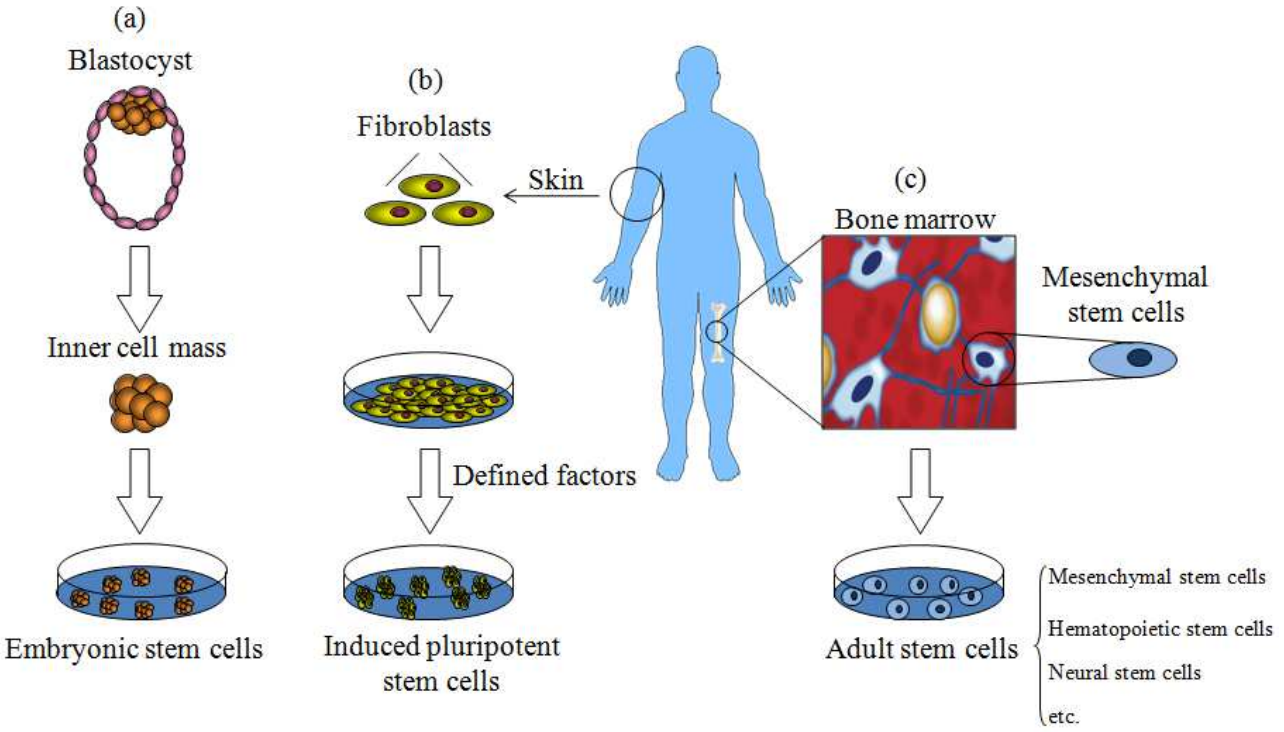

Figure 1.1 Origins and types of stem cells. (a) Embryonic stem cells, which are derived from inner cell mass of blastocysts. (b) Induced pluripotent stem cells were first generated by introducing genes encoding four proteins into somatic cells such as skin fibroblasts[6]. (c) Resident tissue-specific adult stem cells including mesenchymal stem cells, hematopoietic stem cells, neural stem cells, and so on.

The differentiation process of MSCs is simpler and more controllable than ESCs and iPSCs, and the differentiated cell populations are relatively pure[9]. MSCs are capable of differentiating into several cell types including osteocytes[10,11], chondrocytes[12,13], adipocytes[14-16], tenocytes[17], myoblasts[18-20], and stromal cells[21] (Figure 1.2). The precise manipulation of differentiation into correspondent progeny cells is extremely required to fully realize the therapeutic potential of stem cells.

1.1.2.1 Osteogenic differentiation

MSCs can differentiate into osteoblast when cultured in Dulbecco's Modified Eagle Medium (DMEM) supplemented with 10% fetal bovine serum (FBS), ascorbic acid-2-phosphate, β-glycerol phosphate, and dexamethasone[22]. The osteogenic differentiation is first noticed as the cells form aggregates or nodules at about one week. The aggregates are found to be alkaline phosphatase (ALP) positive, and they progress to form a highly mineralized bone matrix[23]. ALP can be quantitatively characterized by staining method. Alizarin Red S[24] and Von Kossa staining[25] can be used to check the mineralized bone matrix. Real-time polymerase chain reaction (RT-PCR)[26] can be used to analyze the osteogenic genes expression. At the early stage of MSCs osteogenesis, the cells express runt-related gene 2 (*RUNX2*) which is an osteogenic

transcription factor and the genes controlled by *RUNX2*, such as *ALP* and osteopontin (*OP*)[27]. Osteocalcin (*OC*) and bone sialoprotein (*BSP*) are characteristic of the late stages of osteogenesis[28,29].

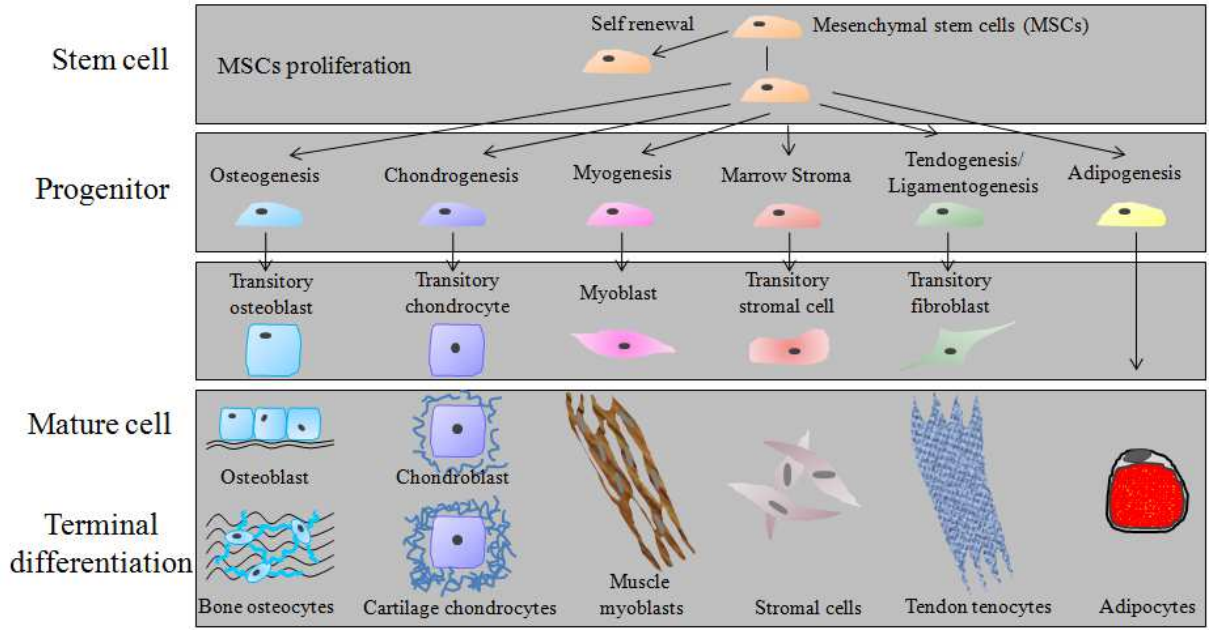

Figure 1.2 Multi-lineages potential of mesenchymal stem cells.

1.1.2.2 Adipogenic differentiation

Adipogenic differentiation of MSCs occurs in DMEM medium supplemented with 10% FBS, 0.5 mM methyl isobutylxanthine, 1 μM dexamethasone, 10 μg/mL insulin, and 100~200 μM indomethicin[9]. Small lipid vacuoles are firstly apparent in a portion of MSCs and more cells commit to the adipogenic lineage during induction culture. The adipogenic cells continue to accumulate lipid and the vacuoles enlarge and coalesce over time. The lipid vacuoles can be stained with Oil Red O[24]. The marker genes of adipogenesis include peroxisome proliferator-activated receptor γ2 (*PPARγ2*)[30,31], lipoprotein lipase (*LPL*)[32,33], and fatty acid binding protein 4 (*FABP4*)[34].

1.1.2.3 Chondrogenic differentiation

Chondrogenic differentiation of MSCs generally takes place when cultured as a micromass pellet of cells, formed by gentle centrifugation[35]. The medium composition without serum is very important. It consists of DMEM supplemented with 10 ng/mL TGF-β3, 100 nM dexamethasone, 50 μg/mL ascorbic acid-2-phosphate, and 1% ITS+1. The cell morphology changes from spindle shape to round shape. The ECM components of generated chondrocytes include type II collagen, glycosaminoglycan (GAG), and cartilage proteoglycan. Histological examinations using hematoxylin/eosin[36], safranin O/fast green[37], and toluidine blue[38] are adopted to stain nucleus, cytoplasm, and ECM. Immunohistological staining can be used to evaluate type II collagen and cartilage proteoglycan in ECM. Hoechst 33258 and Blyscan™ are used to measure the amount of DNA and GAG, respectively[39]. Chondrogenic markers of aggrecan, sox9, and type II collagen can be analyzed by RT-PCR[40,41].

1.1.3 Factors affecting stem cell functions

To fully realize the remarkable potential of stem cells in academic research and clinical application, many hurdles must be overcome, such as the directed differentiation of pluripotent stem cells and propagation of specialized adult stem cells without loss of stemness. Therefore, it is of foremost importance to be able to reliably control stem cell functions. For instance, incompletely or incorrectly differentiated cells may become tumorigenic instead of therapeutic[42] and increase the heterogeneity in derived cell population or tissue.

The intrinsic reason for the difficulty of stem cell manipulation is that the functions of stem cells are affected by various factors[1,43-45]. *In vivo*, their behaviors and functions are highly sensitive to the biochemical and physical factors from cell microenvironment such as soluble and tethered factors, ECM, and neighboring cells. *In vitro*, when seeded on cell culture dishes or biomaterials, stem cells in the first place contact the surface of materials. Consequently, the surface properties of materials play pivotal roles in cell adhesion, proliferation, migration, differentiation, and neonatal tissue formation. In short, these external factors from cell microenvironment and biomaterials alter the internal signals that ultimately regulate stem cell functions (Figure 1.3).

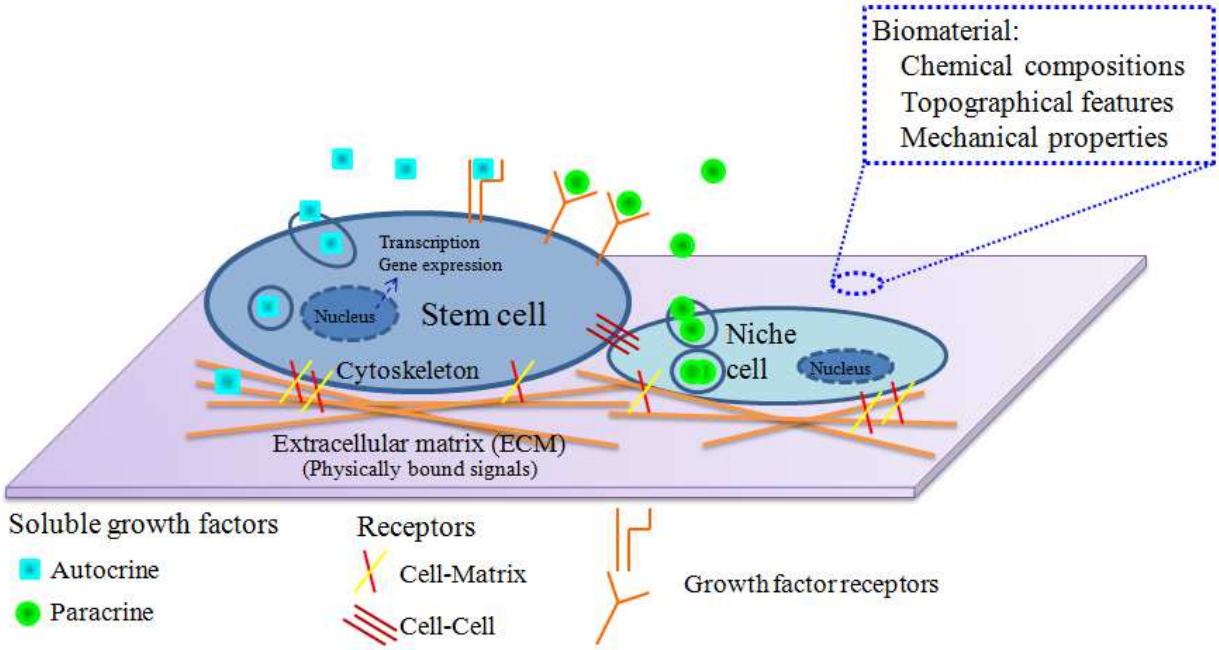

Figure 1.3 Factors affecting stem cell functions. The extracellular microenvironment including soluble and matrix-bound factors, cell-cell contact, and cell-matrix adhesion combined with biomaterial's properties including chemical compositions, topographical features, and mechanical strength direct the stem cell fate via inducing complex intracellular signaling cascades such as gene expression.

1.1.3.1 Soluble and tethered factors

Soluble factors secreted by stem cells and surrounding cells and supplemented in culture medium are potent in their effects on stem cell functions via autocrine and paracrine signaling. The most common culture method for mouse embryonic stem cells (mESCs) is co-culturing them with mouse embryonic fibroblast feeder cells in serum. The fibroblasts secrete the leukemia inhibitory factor (LIF) for self-renewal of mESCs[46]. Alternatively, feeder cells can be replaced by the addition of recombinant LIF in serum

medium[5] or the combination of LIF and bone morphogenetic protein (BMP) in serum-free medium[47]. For the maintenance of human embryonic stem cells (hESCs) pluripotency, LIF is not required but fibroblast growth factor 2 (FGF2) is indispensable[48,49]. In embryonic development, growth factors are tightly regulated in space and time[42]. However, simulating this spatiotemporal regulation of soluble factors is difficult in conventional culture systems such as culture dishes, though discrete concentrations of soluble factors can be dosed at different time point. For spatiotemporal control of soluble factors, microfluidic devices have been developed that continuously wash away factors secreted by cells while perfusing known concentrations of fresh factors[45]. For example, a microfluidic platform was developed for generating growth factors gradient across neural stem cells (NSCs). Proliferation and astrocyte differentiation of NSCs were graded and proportional to the concentrations of growth factors[50].

Soluble factors also bind to ECM and thus their diffusion is limited. This can be mimicked by synthetically tethering a growth factor to a substrate. Surface tethered epidermal growth factor (EGF) promotes both cell spreading and survival of MSCs more strongly than saturating concentrations of soluble EGF[51]. LIF immobilized to maleic anhydride copolymer thin-film coatings supported mESCs pluripotency for at least 2 weeks in the absence of added diffusible LIF[52]. Similarly, non-woven polyester fabric with immobilized LIF showed a higher percentage of undifferentiated mESCs than non-immobilized group[53]. Additionally, transforming growth factor-β (TGF β) was immobilized on hydrogel[54] and scaffold[55] via heparin, and these tethered biomaterials enhanced chondrogenic differentiation of rabbit MSCs. It should be noted that the tethering method can affect the bioactivity of growth factors. Stem cell factor (SCF) physically adsorbed to tissue culture plastic promoted the hematopoietic stem cell expansion. By contrast, cross-linking of SCF via free amines compromised its bioactivity[56].

1.1.3.2 ECM

The ECM is composed of various protein fibrils and fibers interwoven within a hydrated network of GAG chains[57]. The main compositions include collagen, fibronectin, laminin, GAGs, and growth factors. However, the exact composition is tissue-specific and alterable in the differentiation of stem cells. For instances, the composition of basement membranes is rich in laminin while stromal ECM in connective tissues consist mainly of collagen[58]. Fibronectin and versican emerge in the region of mesenchymal condensation (early stage of osteogenesis) and then disappear in mature mineralized bone[59,60]. Because of a tight connection between the cytoskeleton and the ECM through cell-surface receptors and ligands, cells sense and respond to the biochemical and biophysical signals from surrounding ECM[61,62]. Therefore, the properties of ECM impact various cell functions, such as adhesion and migration.

Gerecht *et al.* have reported that hyaluronic acid (HA) hydrogel supported self-renewal of human ESCs and maintained their full differentiation capacity, possibly because HA is a prominent ECM polymer in embryonic development[63]. In a similar way, the chondrogenic differentiation was most prominent in MSCs cultured on collagen type II hydrogel, which was one of the major components of the hyaline cartilage ECM and plays a key role in maintaining chondrocyte function[64]. Nevertheless, the substrates formed from multiple ECM proteins and components will be more beneficial for closely mimicing *in vivo* cell-ECM interactions and precisely investigating the role of ECM on the functions of stem cells.

There are mainly two methods for constructing multiple ECM molecules. One is the combinatorial library of ECM microarray established by robotic spotting. Flaim *et al.*[65] fabricated an ECM microarray platform consisting of 32 different combinations of 5 ECM molecules (collagen I, collagen III, collagen IV, laminin and fibronectin) and identified combinations of ECM that synergistically influenced both hepatocyte

function and ESCs differentiation. Such high throughout combinatorial screening using ECM microarray will provide abundant information for the formulation of complex and robust ECM mixtures for stem cell maintenance or differentiation[66]. Another is the acellular ECM matrices developed by decellularization treatments. Datta *et al.*[67,68] have prepared an ECM matrix from cultured MSCs-derived osteoblasts and found that such ECM matrix enhanced the osteogenesis of MSCs compared with titanium fibers meshes. Hoshiba *et al.*[69,70] have developed stepwise osteogenesis-mimicking and adipogenesis-mimicking ECM matrices from cultured MSCs controlled at different stages of osteogenesis and adipogenesis. These mimicking ECM matrices not only provide good *in vitro* models for analyzing the roles of ECM in stem cell differentiation, but also give fresh insights into the design of novel culture systems for the manipulation of stem cell functions.

1.1.3.3 Cell-cell interactions

In vivo, cell-cell interactions during early development play a key role in the morphogenesis of the blastocyst and mediate cell functions via membrane proteins, gap junctions, and adherens junctions. For examples, osteoblastic cells play a regulatory role in influencing function of hematopoietic stem cells (HSCs) through Notch activation[71] and cell-cell contact is required for the maintenance and expansion of embryo-derived HSCs[72]. Additionally, the cell-cell interactions between stem cells themselves are also important for their survival and self-renewal just as human ESCs have to be passaged as clumps to maintain their survival[73].

In vitro, a common method to control the extent of homotypic cell-cell interactions is to manage the cell seeding density that affect cell-to-cell paracrine signaling distance and cell-cell contact. Generally, low cell seeding density around 100-200 cells/cm^2 is good for MSCs growth[74-76]. The effect of cell density on the osteogenic differentiation is complicated. Kim, Lode, and McBeath *et al.* have reported that lower cell seeding density stimulated osteogenic differentiation of MSCs[77-79], whereas Jaiswal and Wang *et al.* have shown that higher initial seeding density is in favor of mineral deposition and osteogenic differentiation[22,80]. The contradiction is probably derived from the different origins of cells, culture systems, and divisions between low and high densities. Co-culturing stem cells with another cell type is a convenient method to study the heterotypic cell-cell interactions. One example is that co-cultured osteoclast can positively affect the late stage osteoblast differentiation markers (bone sialoprotein) of human MSCs[81]. Another is that MSCs differentiated to an nucleus pulposus-like phenotype when directly co-cultured with both non-degenerate and degenerate nucleus pulposus cells[82]. Despite the importance of cell-cell interactions in regulating stem cell functions, it is difficult for conventional culture methods to precisely control local cell densities and cell-cell contacts. Therefore, decoupling the effects of paracrine signaling from physical contact among cells is a daunting obstacle.

1.1.3.4 Chemical compositions

Biomaterial surface chemistry regulates *in vitro* and *in vivo* cell functions, including adhesion, survival, proliferation, and differentiation[83-86]. These effects on cell functions are generally attributed to chemistry-dependent differences in type, density, and bioactivity of adsorbed proteins[87,88]. Protein adsorption has profound influence on the assembly of cell membrane receptors (such as integrin binding specificity) that transfer the outside factors into the cell. The subsequent intracellular signal transductions activate gene expression and finally determine the cell fate. Therefore, surface chemical properties initiate cascade cell

responses and investigation of interactions between surface chemistry and stem cell is essential to design and develop bio-interfaces that modulate stem cell behaviors and functions.

The effects of surface chemistry on the functions of MSCs have been intensively investigated. On the two-dimensional model surfaces, the methyl group maintained the phenotype of MSCs[89], the amino, thiol, and carboxyl groups promoted the osteogenesis[89-91], and the carboxyl and hydroxyl groups facilitated the chondrogenesis[89,90,92]. On the three-dimensional hydorgel, small functional groups were immobilized into hydrogel and human MSCs were encapsulated in these hydrogels. The results showed that phosphates, carboxylic acid, and aliphatic chains led to increased expression of bone, cartilage, and fat associated markers of MSCs differentiation, respectively[93].

As a high-throughput screen method, the combinatorial library of chemistry microarrays has been developed to rapidly interrogate the interactions between biomaterials chemistry and stem cells. As proof of principle, Anderson *et al.*[94] synthesized a series of biopolymers from diverse combinations of acrylate and methacrylate monomers and then simultaneously characterize over 1,700 human ESCs-biopolymers interactions. This concept has been extended to other biomaterial microarrays to investigate various chemical effects on the functions of stem cells[95-97]. Such method would facilitate the determination of specific surface chemistry for the maintenance, proliferation, and differentiation of stem cells and accelerate the development of novel biomaterials for a range of biotechnologies and therapeutics.

1.1.3.5 Topographical features

In vivo, cells encounter many topographical features of ECM from protein folding to collagen banding. It is clear that interactions exist between cells and nanoscale/microscale features[98,99]. One example is that the topographical features within basement membranes are on sub-microscale[100]. To mimic the fibrous structure of ECM, fiber scaffolds have been fabricated by electrospinning method[101-104]. Wise *et al.*[105] reported that nanofibrous scaffold (500 nm in diameter) enhanced the chondrogenic differentiation of human MSCs. Similar to fibrous structures with controlled diameters, ridges and grooves at nanoscale/microscale have also been micropatterned to influence stem cell functions. For instance, 600 nm poly(dimethyl siloxane) (PDMS) ridges coated with fibronectin induced human ESCs alignment and elongation and altered cells morphology and proliferation[106]. Another example is that 350 nm ridge/grooves pattern effectively induced the neuronal differentiation of human ESCs[107] and MSCs[108].

Traditionally, the expansion and differentiation of stem cells mainly realized by biological medium consisting of growth factors and cytokines. However, if the functions of stem cells could be modulated by the specific surface topography rather than biological stimuli, it would be more attractive and practical in clinical applications. For instances, tissue engineered scaffold implanted into a host could elicit a specific cell response or a patient's own stem cells could be expanded on *in vitro* surface and reintroduced back to the patient in sufficient quantity to initiate *in vivo* tissue regeneration. Dalby *et al.* have prepared 120 nm pits in a square arrangement with 300 nm center-center distance. Such nanotopography with the ±50 nm offset in pit placement in x and y axes induced osteogenesis of MSCs[109]. Interestingly, by reducing the level of offset to as close to zero as possible, the prepared nanotopography switched to maintain MSCs growth and retain the multipotency of MSCs[110]. In another case, Oh *et al.* reported that small nanotubes (~30 nm in diameter) enhanced cell adhesion. In contrast, larger nanotubes (~70 to 100 nm in diameter) caused cell elongation that induced cytoskeletal stress and osteogenic differentiation of MSCs[111].

1.1.3.6 Mechanical properties

Both *in vivo* and *in vitro*, stem cells reside, experience, and respond to the mechanical properties of their microenvironment. Stem cells adhered on a substrate sense the surrounding mechanical environment and generate contractile force, resulting in tensile stress in the cytoskeleton and activation of signaling pathways that affect stem cell fate[112]. The magnitude of contractile force depends on the mechanical properties of the substrate such as stiffness. The elasticity of native tissues widely ranges from 0.1~1.0 kPa in neural tissue, ~10 kPa in muscle tissue, to on the order of GPa for completely mineralized bone tissue. Importantly, many diseases such as myocardial infarction and liver disease are accompanied by the stiffening of abnormal tissues that change cell morphology and function. Inspired by these natural phenomena, considerable attention has been paid to the manipulation of mechanical properties of biomaterials and regulation of stem cell functions. The stiffness of a biomaterial is mainly modulated by the physical structure, biochemical composition, crosslinking extent, and network organization.

Discher's group pioneered interrogation of the correlation between material's stiffness and stem cell fate[113]. They prepared a series of polyacrylamide gels with different stiffness and constant collagen I concentration by adjusting the degree of crosslinking. MSCs grown on soft (0.1~1.0 kPa), intermediate (11 kPa), and stiff (34 kPa) gels differentiated to neurogenic, myogenic, and osteogenic lineages, respectively in growth medium without differentiation induction factors. Wang *et al.*[114] also reported that the differentiation of human MSCs was highly linked to the hydrogel stiffness, that is, the cells on a softer hydrogel (600 Pa) differentiated along neurogenic lineage and cells on a harder hydrogel (12 kPa) expressed more myogenic protein markers. Similarly, neuron differentiation of NSCs is favored on soft matrices that mimic normal brain, whereas differentiation into glia is enhanced on stiffer matrices that imitate glial scars[115]. Mooney and his colleagues further investigated the effect of stiffness in three-dimensional microenvironments and they demonstrated that the commitment of MSCs relied on the rigidity of matrix, with osteogenesis occurring predominantly at 11~30 kPa[116]. Blau and co-workers modulated the substrate elasticity to regulate skeletal muscle stem cell (MuSC) self-renewal in culture[117]. The importance of their results is that MuSCs not only self-renew *in vitro* when cultured on soft hydrogel substrate that stimulates the elasticity of muscle (12 kPa) but also contribute extensively to muscle regeneration after subsequently transplanted into mice.

Although hydrogels are important in characterizing and controlling cell-material interactions, the cross-linker used to modulate stiffness influence not only bulk mechanics but also molecular-scale material properties including porosity, chemistry, backbone flexibility, and bioactivity of immobilized ligands. Hence, alternative approaches are proposed to understand the interactions between stem cells and substrate stiffness. One of the important methods is micropost system developed by Chen's group[118]. By controlling the geometry of elastomeric micropost such as height, the rigidity of micopost is managed. Stem cell morphology, focal adhesion, cytoskeletal contractility, and differentiation are impacted by the rigidity of underlying microposts[119].

1.2 Micropatterning technology

The integration of cell biology and micropatterning technology in the early 1990s has revolutionary impact on the development of cell research, biomaterials, and tissue engineering. The conventional cell culture surface is difficult to precisely control cell microenvironment, such as the location, size, and shape of individual cells, the contact between cells, the biochemical compositions, wettability, electric charges, and stiffness of local surface. In contrast, micropatterning techniques enable the precise control of most of the

important factors from cell microenvironment by modifying the physicochemical properties of cell-culture substrates at predefined locations and sub-cellular scales. Therefore, the effect of individual environmental factor on cell function and fate can be accurately assessed. For example, capillary networks[120] and connective networks[121] can be constructed by culture of endothelial cells and neural cells respectively on micropatterned surfaces. Due to the huge advantages of micropatterning technology, various patterning methods have been developed and used in biomedical research. These methods mainly include photolithography, soft lithography, photochemical immobilization, stencil-assisted patterning, laser ablation, and ink-jet printing.

1.2.1 Photolithography

Photolithography is the most successful technology in microfabrication. It has been originally developed in semiconductor industry and all integrated circuits are essentially fabricated by this technology. Generally speaking, in the photolithography process geometrical features drawn on a mask are transferred onto a substrate via ultraviolet (UV) illumination. The mask is generally made of a quartz/glass plate coated with a thin layer of non-transparent chromium. Computer-aided design software is frequently used to devise geometrical features and these geometrical features are manufactured on a mask by a projection-printing system. Such masks routinely have feature resolution down to 1~2 μm.

The general photolithography process is illustrated in Figure 1.4. Firstly, the substrate is spin-coated with a thin film of photoresist that is UV-sensitive polymer. After spin-coating, the substrate is placed on a hot plate for baking to harden the photoresist by solvent degassing. For biological applications transparent substrates such as glass and polystyrene are often used because of their compatibility with optical microscope and cell culture. Secondly, the substrate is brought in close contact with the mask in a mask-aligner device equipped with a UV source. After the substrate is aligned below UV lamp and covered by the mask, the activated UV passes through the transparent regions on the mask and irradiates the underlying photoresist. A positive-tone photoresist is that the UV exposed parts of photoresist become soluble and are removed in the subsequent development process. In contrast, a negative-tone photoresist become insoluble after irradiated by UV, thus forming opposite features to the mask after development. Upon development the substrate is covered with photoresist patterns. Thirdly, depend on one's purpose and required patterns either deposition or etching method is usually used to fabricate final patterns. A thin layer of either metals or bioactive molecules such as peptides, proteins, and polymers are deposited and then the residual photoresists are lifted off in an organic solvent. Alternatively, the exposed metal/oxide layer that was deposited prior to photoresist spin-coating is etched using patterned photoresist film as a mask and then the residual photoresists are lifted off.

Various patterns consisted of cytophilic and cytophobic regions have been created using photolithography technique[122-124]. For example, Falconnet *et al.* combined photolithographic and molecular-assembly strategies to produce functional micropatterns[125]. Firstly, a photoresist pattern was prepared by UV photolithography. Secondly, biotin or cell adhesive peptide functionalized poly(L-lysine)-graft-poly(ethylene glycol) (PLL-g-PEG) absorbed onto the photoresist pattern. Finally, the photoresist was lifted-off and the background is subsequently filled with non-functionalized PLL-g-PEG to inhibit non-specific protein adsorption. Therefore, the surface density of biotin inside adhesive islands can be quantitatively regulated and cells selectively grew on cell-adhesive peptide regions. Similarly, Jing *et al.* combined photolithography and molecular vapor deposition techniques to fabricate multielectrode arrays that supporting patterned neuronal networks[126].

There are some limitations of photolithography. Because the equipment is expensive and elaborate,

it is not easily accessible for common laboratories. It is relatively difficult for non-specialists in biology laboratory to master the operation. Additionally, the residual organic chemical regents used in procedure sometimes denature biomolecules and damage cells.

1.2.2 Soft lithography

Soft lithography was developed by Whitesides' group in Harvard University at 1990s[127,128]. The name "soft lithography" does not represent one specific method but rather a group of techniques with the common feature that an elastomeric material is used to create the chemical structure at some stage of the process[129]. These techniques mainly include microcontact printing (μCP)[130], replica molding (REM)[128], microfluidic patterning (μFLP)[131], micromolding in capillaries (MIMIC)[132], solvent-assisted micromolding (SAMIM)[133], and microtransfer molding (μTM)[134].

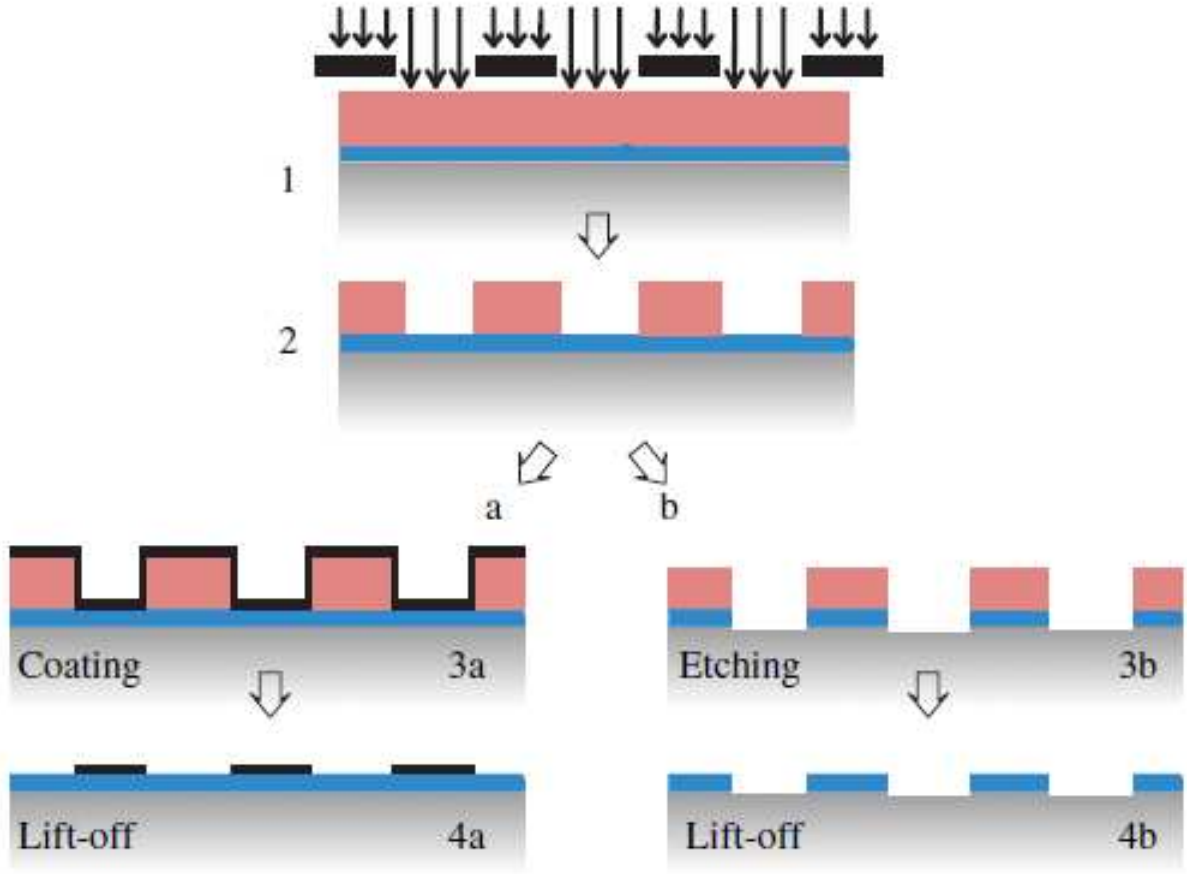

Figure 1.4 The photolithography process: 1. A spin-coated photoresist is locally exposed with UV light through a mask; 2. Photoresist development to provide local access to the underlying substrate. Depend on one's purpose and required patterns either deposition (a) or etching method (b) is usually used to fabricate final patterns. Route a: Deposition (3a) of a thin layer of either metal or bioactive molecules (peptides, proteins, polymers) and lift-off the residual photoresist in solvent (4a). Route b: Etching (3b) of the metal layer down into the underlying substrate using the patterned photoresist layer as a mask and lift-off the residual photoresist in solvent (4b). Adapted from Falconnet, D. *et al.*[129]

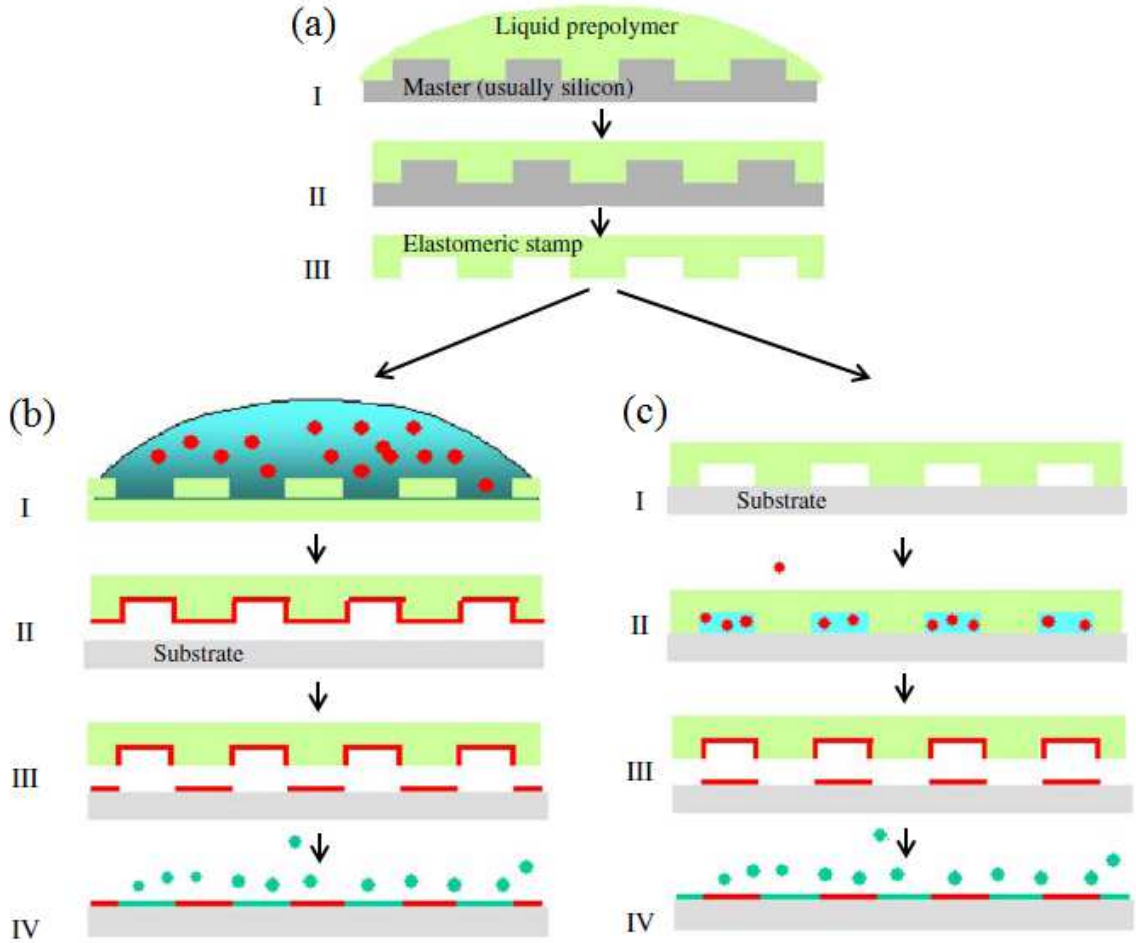

Figure 1.5 Illustration of two types of soft lithography technique: microcontact printing (μCP) and microfluidic patterning (μFLP). (a) A liquid pre-polymer is cast on the structured master surface (I) After curing (II) the elastomeric stamp is ready for use (III). (b) In μCP the stamp is inked with the solution containing the molecules to be printed (I). The molecules are transferred by printing onto the substrate (II). Following the removal of the stamp (III) the surface is backfilled with the second molecular solution for passivating (IV). (c) In μFLP the stamp is first brought into tight contact with the substrate (I). The patterning solution is afterwards introduced into the channels (II), usually using capillary forces. After adsorption of the molecules of interest the stamp is removed (III) and the remaining area backfilled with a passivating solution (IV). Adapted from Falconnet, D. *et al.*[129]

The operation process of soft lithography is simple, handy, and cost-effective. The starting step is the fabrication of master with a specifically topographical structure. The master is traditionally created by photolithography, electron beam lithography, and micromachining. Only this step requires relatively expensive facilities. The second step is the formation of stamp. The stamp is prepared by casting liquid prepolymer over master and producing the corresponding replica. The most widely used stamp material is PDMS (in ~95% of the cases Sylgard 184 from Dow Corning is used). Other alternative materials such as polyurethanes, polyimides, poly-olefin-plastomers, cross-linked Novolac reins, and agarose gels are also successfully used. The subsequent steps are versatile and most commonly adopted methods are μCP and μFLP as illustrated in Figure 1.5. In μCP the stamp is inked with the bio/chemical molecules solution. The molecules are then transferred by printing onto the substrate. Following the removal of the stamp the

substrate is backfilled with the second molecule solution to passivate the surface. In μFLP the stamp first contacts with the substrate tightly. The patterning solution is afterwards introduced into the channels, usually using capillary forces. After adsorption of the molecules of interest the stamp is removed and the remaining area is backfilled with a passivating solution.

Soft lithography is very prevalent in biomedical field due to its simplicity, cost-effectiveness, and flexibility[135]. For examples, Ameringer *et al.* prepared six armed star shaped poly(ethylene glycol) with reactive isocyanate endgroups on a glass substrate to covalently immobilize amino terminated oligonucleotides via μCP method[136]. Hyun *et al.*[137] coated an amphiphilic comb polymer presenting short oligoethylene glycol side chains onto different polymeric biomaterials including polystyrene, poly(methyl methacrylate), and poly(ethylene terephthalate). By using μCP method, the reactive COOH groups at the oligoethylene glycol chain ends were patterned with a cell adhesive peptide. Therefore, the adhesion and growth of fibroblasts were spatially confined within the micropatterned regions. Ma *et al.* created initiator patterns at micro/nano scale on a gold surface using μCP method. The initiator can trigger atom transfer radical polymerization of oligo(ethylene glycol) methyl methacrylate (OEGMA) to form poly(OEGMA) patterns. Protein adsorption result showed that proteins can only adsorbed on the regions without poly(OEGMA). Consequently, cell patterns were generated on corresponding fibronectin patterns[138].

The main disadvantage of soft lithography adopted in cell biology research is the long-term stability of micropatterns during cell culture. The self-assembled thiol molecules on gold substrate are likely to oxidize under ambient conditions[139] and micropatterned poly(ethylene glycol) for preventing non-specific protein adsorption and cell adhesion are inclined to be degraded in complex cell culture medium[140]. Furthermore, many factors have to be carefully considered during operation such as the deformation of PDMS stamp under the press[127], the time for transferring coated protein from stamp to substrate, and the compromise of protein bioactivity in operation[141].

1.2.3 Photochemical immobilization

Different methods and photo-reactive molecules have been developed to locally activate and generate chemical micropatterns for cell attachment[142-146].

Ito and colleagues introduced photo-reactive azidophenyl group into several polymers. Because the azidophenyl group was photolyzed under UV irradiation and generated highly reactive phenyl nitrene that reacted with neighboring atoms to form a covalent bond, diverse polymer micropatterns were prepared using different mask and UV photolithography. Moreover, cell adhesion and function were controlled on these micropatterns[147-152]. This modification method uses photo-generated radical reactions. Because radical reactions occur on every organic substrates including biological matrix, polymeric materials, and organic chip surfaces, this method does not require any special functional groups such as amino, carboxyl, hydroxyl, and thiol groups. Therefore, different molecules can be immobilized by the same method, distinguishing itself from other conventional immobilization methods. Moreover, there is no particular orientation of immobilized molecules when this photo-immobilization method is adopted, which is advantageous in the cases that orientation of biological molecules must be taken into account and mitigated[153].

Dillmore *et al.* reported a photochemical approach for producing micropatterns and gradients of bioactive ligands[154]. Self-assembled monolayers with nitroveratryloxycarbonyl (NVOC)-protected hydroquinone were firstly prepared. The deprotection of NVOC under photochemical irradiation revealed hydroquinone. Subsequently the hydroquinone was oxidized to benzoquinone using electric potential. The benzoquinone covalently immobilized to cell adhesive peptide via Diels-Alder reaction. Cell culture result

showed that fibroblasts only attached along the RGD peptide micropatterns. Chan *et al.* used the similar strategy to study cell polarization[155]. Instead of Diels-Alder reaction, the quinine generated by oxidation of the hydroquinone selectively bonded with aminooxy terminated ligands. Diverse geometrical and gradient micropatterns of RGD ligands were prepared and their effects on cell-cell interaction and cell polarization were conveniently investigated. More importantly, Yousaf group combined this photochemical method with μCP to develop dynamic substrate that can immobilize and release patterned ligands. And cell migration and detachment were elegantly controlled by modulating the immobilization and release of underlying ligands[156,157]. However, the synthesis procedure is so complicated for cell biologists that this platform may be difficult to be generalized for common laboratories.

1.2.4 Stencil-assisted micropatterning

A stencil is a stiff or flexible membrane with through-holes of the specific size and geometry. As a template, the stencil is brought in close contact with the substrate. Therefore, only the surfaces inside the holes can be modified by deposition or ablation of molecules and occupied by cell seeding while the surfaces outside the holes remain pristine due to the protection of the stencil. Stencil materials range from soft PDMS membranes to stiff metal grids. General procedure for cell micropattering based on the use of stencil is shown in Figure 1.6.

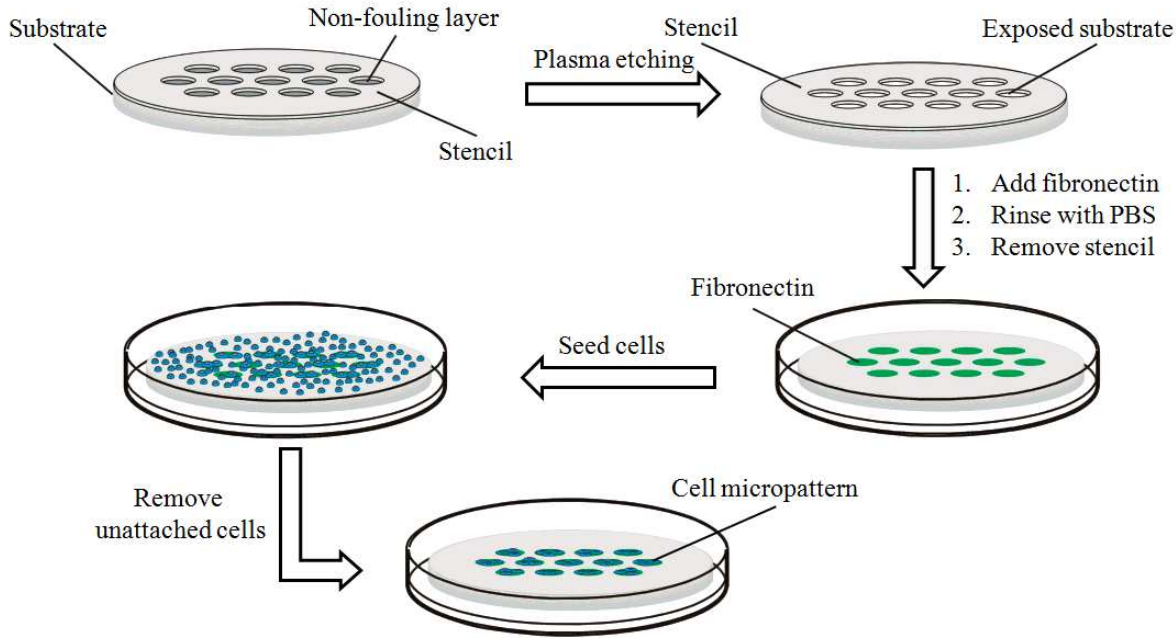

Figure 1.6 Illustration of the general procedure for cell micropattering based on the use of stencil. The stencil is placed onto a substrate with the non-fouling layer. The stencil serves as a mask for selective etching of non-fouling layer inside the hole. The etching generates islands of bare substrate surrounded by non-fouling layer. Fibronectin is adsorbed onto the etched islands of substrate and the stencil is then removed. The fibronectin patterned substrate is incubated with a cell suspension. Cell micropatterns are formed by removing unattached cells with fresh medium exchange. Adapted from Tourovskaia, A. *et al.*[158]

This method has been used to directly pattern cells without any chemical and physical modification of the substrate[159]. The stencil is sealed onto the substrate before cell seeding and manually peeled-off after cell attachment. Because there are no non-fouling materials to prevent protein adsorption and cell adhesion

between cell patterns, the locally patterned cell population will grow out of the pre-defined regions. Accordingly, such micropatterns are very useful to investigate cell migration and co-cultures of two cell types. In the co-cultures case, the first cell type adheres and spreads within the hole, while once the stencil has been removed the second cell type attaches and spreads on the surfaces where the stencil has been covered.

To keep the location, size, and geometry of cell patterns, one should use non-fouling substrate that can be prepared by various methods such as plasma polymerization[160] and physical adsorption of bovine serum albumin[161] or Pluronic co-polymers[162]. Tan *et al.* used chemical vapor deposition to deposit a thin film of parylene onto a polyethylene glycol (PEG) treated glass cover slip. And the parylene was patterned using standard photolithography. Finally, the patterned substrate was incubated with fibronection solution and the parylene template was mechanically peeled off with sterile tweezers. This micropattern was used to culture cell and probe the role of cell-cell interactions in tumor angiogenesis[141]. Similarly, an interpenetrating network (IPN) layer of poly(acrylamide-*co*-ethyleneglycol) (PAAm-*co*-EG) was grafted onto a glass substrate. The stencil was then placed on the substrate as a template and exposed to O_2 plasma. Hence the local etching removed non-fouling layer of PAAm-*co*-EG within the holes of stencil. After incubating with fibronectin solution and peeling off stencil, cell micropatterns formed because the surrounding highly swelling IPN effectively resisted protein adsorption and cell adhesion[158].

1.2.5 Other methods

Laser ablation. Yamato *et al.* reported the fabrication of cell micropatterns using electron beam irradiated polymer grafting and laser ablation[163]. Poly(*N*-isopropylacrylamide) (PIPAAm) was covalently grafted onto commercial tissue culture polystyrene (TCPS) dishes using electron beam irradiation. Subsequently selected surface regions were irradiated with a UV excimer laser and the basal TCPS substrate re-exposed on ablated regions. Hepatocytes specifically adhered onto and confined within the ablated regions adsorbed with fibronectin. In another case, poly(vinyl alcohol) (PVA) molecules were conjugated to a glass coverslip through 3-(amino)propyl-trimethyloxysilane and glutaraldehyde. And then PVA-coated surfaces were ablated using an LSM 510 NLO META system. The generated micropatterns were used to study cell migration[164]. The main limitation of laser ablation is that the laser system is not easy to be accessible for common laboratories.

Ink-jet patterning. Tissue engineers have adapted and modified existing ink-jet technology for biological research and applications. Alkanethiols[165] and proteins[166] have been directly jetted onto substrates and formed various micropatterns to manipulate cell functions such as neuronal adhesion[167,168]. The advantages of ink-jet patterning are inexpensive, flexible substrate choice, and time-saving. Moreover, multifunctional micropatterns can be prepared using a multiple nozzle device and different compounds can be printed on the same spot. The disadvantage of this technology is the limitation of spot size and resolution. The spot size is usually larger than 100 μm. To modulate the size and resolution, the nozzle diameter, liquid-solid interfacial tension, and pressure should be finely adjusted.

1.3 Micropatterning of stem cells

Recently, stem cell research has been significantly boosted by integrating the stem cell biology with

micropatterning technology. Through careful control of local physicochemical properties, micropatterned substrates provide an insight into how surfaces with contrastive chemistries and culture conditions affect cell interactions and stem cell developmental processes. Definitively, micropatterning is a powerful tool to decipher stem cell morphogenesis and functions.

1.3.1 Micropatterning of embryonic stem cells

Embryonic stem cells (ESCs) are promising cell sources for tissue engineering and regenerative medicine because of their pluripotency and unlimited self-renewal capacity. To realize the therapeutic potential of ESCs, it is necessary to regulate their self-renewal and differentiation in a reproducible manner. The differentiation of ESCs can be induced to three germ layers (endoderm, ectoderm, and mesoderm) by forming either attached colonies or embryoid bodies (EBs). Therefore, the size of colonies and EBs is one of the most important factors for ESCs functions. Micropatterning technology is very useful to precisely control the size of colonies and EBs by generating a series of circular micropatterns with different diameters. Zandstra and co-workers pioneered the research on the sized effects. One important result is that larger colonies with high local cell density microenvironments promote the maintenance of self-renewal ability of human ESCs by suppressing Smad1 activation via increased activity of BMP antagonists such as GDF3[169]. Another one is that the differentiation trajectories are also affected by colony and EB size. The ratio of *Gata6* (endoderm-associated marker) to *Pax6* (neural-associated marker) expression increases with decreasing colony size. Additionally, larger EB size is in favor of mesoderm and cardiac induction when micropatterned EBs were generated from endoderm-biased (high *Gata6*/*Pax6*) input human ESCs. Conversely, higher cardiac induction exhibits in smaller EBs generated from neural-biased (low *Gata6*/*Pax6*) input human ESCs[170]. Similarly, Sasaki *et al.* prepared size controlled mouse ESC aggregates on circular micropatterns (100~400 μm in diameters) using a maskless photolithography technique. They found that the optimal diameter for the cardiac differentiation in the ESC aggregates was 200 μm[171].

1.3.2 Micropatterning of mesenchymal stem cells

Classically, the fate of stem cells is regulated by genetic and molecular mediators (e.g. transcription factors and growth factors). However, more and more evidences have recently highlighted the crucial roles of physical factors from cell microenvironment on the overall control of stem cell functions. Micropatterning methods are particularly suitable for investigation of these physical effects. Chen *et al.* generated force gradient in micropatterned cell sheets and demonstrated that such force gradient can direct patterned differentiation of mesenchymal stem cells (MSCs)[172]. A group of micropatterns including circle, rectangle, ellipse, half-ellipse, offset annulus, elliptical annulus, and sinusoidal bands were prepared by microcontact printing. In the presence of soluble factors for both osteogenic and adipogenic differentiation, human MSCs at the regions of high stress differentiated along osteogenic lineage whereas regions of low stress resulted in adipogenesis. Similarly, Luo *et al.* manipulated the geometries of human MSC aggregates using octagon, triangle, trapezoid, square, pentagon, and circle micropatterns. And their result indicated that the rate of adipogenic differentiation was influenced by the geometries of cell aggregates[173]. The sole effect of cell shape without supplemental soluble factors on the differentiation of MSCs was also investigated using micropatterning method[174]. The strips of fibronectin (20 μm in wide) were printed on poly(lactic-co-glycolic acid) film and the attached bone marrow derived human MSCs were highly oriented and elongated along fibronectin strip. Compared with spread MSCs on unpatterned substrate, highly elongated MSCs

up-regulated the gene markers associated with neurogenesis and myogenesis as well as protein expression of cardiac myosin heavy chain.

1.3.3 Micropatterning of neural stem cells

Neural stem cells (NSCs) offer great potential in tissue engineering and regenerative medicine because of their ability to generate the main phenotypes in the nervous system[175]. The direction, connection, and structural polarization of axonal growth should be precisely controlled for therapeutic applications such as repairing damaged nerves. To elucidate the fundamental factors important for never regeneration, micropattening technology has been integrated with neurology research. Ruiz *et al.* produced cell adhesive poly-L-lysine (PLL) on non-adhesive poly(ethylene oxide)-like surface by microcontact printing[176]. The prepared micropatterns were consisted of isolated and interconnected squares. NSCs derive from human cord blood showed good attachment and long-term confinement on the PLL patterns. Moreover, random and guided axonal outgrowth as well as migration was monitored by micropatterning the NSCs in specific configurations. Recently, micropatterning method has been integrated with carbon nanotube (CNT) technology to manipulate the functions of stem cells[177]. Park *et al.* reported a method for selective growth and polarization-controlled differentiation of human NSCs into neurons using CNT network patterns[178]. The good performance of human NSCs is due to the synergistic cues of selective laminin adsorption and optimal nanotopography provided by the CNT network patterns.

1.4 Motivation and objectives

The inherent plasticity and multi-lineage potential of stem cells make them promising cell sources for tissue engineering and regenerative medicine. However, controlling over behaviors and functions of stem cells, such as proliferation and differentiation, is extremely required to fully realize the therapeutic potential of stem cells.

Either *in vivo* or *in vitro* stem cell functions are regulated by intricate reciprocal interactions between cells and their microenvironment. Stem cell behaviors are highly sensitive to the biochemical and physical factors from surrounding microenvironment such as the extracellular matrix (ECM), neighboring cells, and surface properties. Due to the limitation of current technology to track *in vivo* cells, it is still very difficult to directly investigate cell behaviors in vivo. Accordingly, in vitro cell culture is the indispensable approach for stem cell research. Nonetheless, the conventional cell culture surface is difficult to precisely control cell microenvironment, such as the location, size, and shape of individual cells, contact between cells, and to directly compare the effects of various microenvironmental factors, such as biochemical compositions, topographical features, wettability, electric charges, and stiffness of local surface.

In contrast, micropatterning techniques enable the precise control of most of the important factors from cell microenvironment by modifying the physicochemical properties of cell-culture substrates at predefined locations and sub-cellular scales. Therefore, the effect of individual environmental factor on cell function and fate can be accurately assessed.

In this thesis, we integrated a simple and robust micropatterning method with the stem cell research on the purpose of manipulation of stem cell functions. Various micropatterns with particular features were designed by using different photomasks to investigate the pivotal components of cell microenvironment in a highly controllable manner. Photo-reactive poly(vinyl alcohol) (PVA) were synthesized by coupling PVA

with UV-sensitive azidophenyl group and locally grafted to the commonly used cell-culture polystyrene (PSt) surface by UV irradiation through photomasks. PVA was chosen as non-fouling polymer due to its superior ability to resist protein adsorption and cell adhesion. Long-term cell culture at either multiple- or single-cell level was realized on the PVA-micropatterned polymer surfaces because the micro-patterned PVA hydrogel was very stable and highly hydrated in the aqueous culture medium. Cell density, spreading, and shape of human bone marrow-derived mesenchymal stem cells (MSCs) were regulated by the ratio of PSt area to PVA area, size, and geometry of the micropatterns, respectively. The effect of cell density, spreading area, and cell shape on the functions of MSCs such as proliferation and differentiation were directly compared on the PVA-micropatterned PSt surface. Moreover, PVA-poly(acrylic acid) (PAAc)-micropatterned PSt surface was prepared to study the electrostatic effect on the functions of individual MSCs with highly controlled and uniform cell shape.

1.5 References

1. Watt, F. M., Out of Eden: stem cells and their niches. *Science* **287**, 1427-1430 (2000).
2. Evans, M. J., Kaufman, M. H., Establishment in culture of pluripotential cells from mouse embryos. *Nature* **292**, 154-156 (1981).
3. Martin, G. R., Isolation of a pluripotent cell line from early mouse embryos cultured in medium conditioned by teratocarcinoma stem cells. *Proc Natl Acad Sci USA* **78**, 7634-7638 (1981).
4. Thomson, J. A., Embryonic stem cell lines derived from human blastocysts. *Science* **282**, 1145-1147 (1998).
5. Smith, A. G., Embryo-derived stem cells: of mice and men. *Annu Rev Cell Dev Biol* **17**, 435-462 (2001).
6. Takahashi, K., Tanabe, K., Ohnuki. M., Narita. M., Ichisaka. T., Tomoda. K., Yamanaka. S., Induction of pluripotent stem cells from adult human fibroblasts by defined factors. *Cell* **131**, 861-872 (2007).
7. Takahashi, K., Yamanaka, S., Induction of pluripotent stem cells from mouse embryonic and adult fibroblast cultures by defined factors. *Cell* **126**, 663-676 (2006).
8. Lutolf, M. P., Gilbert, P. M., Blau, H. M., Designing materials to direct stem-cell fate. *Nature* **462**, 433-441 (2009).
9. Pittenger, M. F., Mackay, A. M., Beck, S. C., Jaiswal, R. K., Douglas, R., Mosca, J. D., Moorman, M. A., Simonetti, D. W., Craig, S., Marshak, D. R., Multilineage potential of adult human mesenchymal stem cells. *Science* **284**, 143-147 (1999).
10. Mauney, J. R., Kirker-Head, C., Abrahamson, L., Gronowicz, G., Volloch, V., Kaplan, D. L., Matrix-mediated retention of in vitro osteogenic differentiation potential and in vivo bone-forming capacity by human adult bone marrow-derived mesenchymal stem cells during ex vivo expansion. *J Biomed Mater Res A* **79**, 464-475 (2006).
11. Ohgushi, H., Kotobuki, N., Funaoka, H., Machida, H., Hirose, M., Tanaka, Y., Takakura, Y., Tissue engineered ceramic artificial joint--ex vivo osteogenic differentiation of patient mesenchymal cells on total ankle joints for treatment of osteoarthritis. *Biomaterials* **26**, 4654-4661 (2005).
12. Hofmann, S., Knecht, S., Langer, R., Kaplan, D. L., Vunjak-Novakovic, G., Merkle, H. P., Meinel, L., Cartilage-like tissue engineering using silk scaffolds and mesenchymal stem cells. *Tissue Eng* **12**, 2729-2738 (2006).

13. Cui, J. H., Park, K., Park, S. R., Min, B. H., Effects of low-intensity ultrasound on chondrogenic differentiation of mesenchymal stem cells embedded in polyglycolic acid: an in vivo study. *Tissue Eng* **12**, 75-82 (2006).
14. Neubauer, M., Hacker, M., Bauer-Kreisel, P., Weiser, B., Fischbach, C., Schulz, M. B., Goepferich, A., Blunk, T., Adipose tissue engineering based on mesenchymal stem cells and basic fibroblast growth factor in vitro. *Tissue Eng* **11**, 1840-1851 (2005).
15. Choi, Y. S., Park, S. N., Suh, H., Adipose tissue engineering using mesenchymal stem cells attached to injectable PLGA spheres. *Biomaterials* **26**, 5855-5863 (2005).
16. Alhadlaq, A., Tang, M., Mao, J. J., Engineered adipose tissue from human mesenchymal stem cells maintains predefined shape and dimension: implications in soft tissue augmentation and reconstruction. *Tissue Eng* **11**, 556-566 (2005).
17. Nöth, U., Schupp, K., Heymer, A., Kall, S., Jakob, F., Schütze, N., Baumann, B., Barthel, T., Eulert, J., Hendrich, C., Anterior cruciate ligament constructs fabricated from human mesenchymal stem cells in a collagen type I hydrogel. *Cytotherapy* **7**, 447-455 (2005).
18. Tian, H., Bharadwaj, S., Liu, Y., Ma, H., Ma, P. X., Atala, A., Zhang, Y., Myogenic differentiation of human bone marrow mesenchymal stem cells on a 3D nano fibrous scaffold for bladder tissue engineering. *Biomaterials* **31**, 870-877 (2010).
19. Gang, E. J., Jeong, J. A., Hong, S. H., Hwang, S. H., Kim, S. W., Yang, I. H., Ahn, C., Han, H., Kim, H., Skeletal myogenic differentiation of mesenchymal stem cells isolated from human umbilical cord blood. *Stem Cells* **22**, 617-624 (2004).
20. Gang, E. J., Bosnakovski, D., Simsek, T., To, K., Perlingeiro, R. C. R., Pax3 activation promotes the differentiation of mesenchymal stem cells toward the myogenic lineage. *Exp Cell Res* **314**, 1721-1733 (2008).
21. Galmiche, M. C., Koteliansky, V. E., Brière, J., Hervé, P., Charbord, P., Stromal cells from human long-term marrow cultures are mesenchymal cells that differentiate following a vascular smooth muscle differentiation pathway. *Blood* **82**, 66-76 (1993).
22. Jaiswal, N., Haynesworth, S. E., Caplan, A. I., Bruder, S. P., Osteogenic differentiation of purified, culture-expanded human mesenchymal stem cells in vitro. *J Cell Biochem* **64**, 295-312 (1997).
23. Kotobuki, N., Ioku, K., Kawagoe, D., Fujimori, H., Goto, S., Ohgushi, H., Observation of osteogenic differentiation cascade of living mesenchymal stem cells on transparent hydroxyapatite ceramics. *Biomaterials* **26**, 779-785 (2005).
24. Penney, D. P., Powers, J. M., Frank, M., Willis, C., Churukian, C., Analysis and testing of biological stains--the Biological Stain Commission Procedures. *Biotechnic* **77**, 237-275 (2002).
25. Drury, R., Theory and practice of histotechnology. *J Clin Pathol* **34**, 1406 (1981).
26. VanGuilder, H. D., Vrana, K. E., Freeman, W. M., Twenty-five years of quantitative PCR for gene expression analysis. *Biotechniques* **44**, 619-626 (2008).
27. Malaval, L., Modrowski, D., Gupta, A. K., Aubin, J. E., Cellular expression of bone-related proteins during in vitro osteogenesis in rat bone marrow stromal cell cultures. *J Cell Physiol* **158**, 555-572 (1994).
28. Igarashi, M., Kamiya, N., Hasegawa, M., Kasuya, T., Takahashi, T., Takagi, M., Inductive effects of dexamethasone on the gene expression of Cbfa1, Osterix and bone matrix proteins during differentiation of cultured primary rat osteoblasts. *J Mol Histol* **35**, 3-10 (2004).
29. Zur Nieden, N. I., Kempka, G., Ahr, H. J., In vitro differentiation of embryonic stem cells into mineralized osteoblasts. *Differentiation* **71**, 18-27 (2003).

30. Wahli, W., Braissant, O., Desvergne, B., Peroxisome proliferator activated receptors: transcriptional regulators of adipogenesis, lipid metabolism and more.... *Chem Biol* **2**, 261-266 (1995).
31. Schoonjans, K., Staels, B., Auwerx, J., The peroxisome proliferator activated receptors (PPARS) and their effects on lipid metabolism and adipocyte differentiation. *Biochim Biophys Acta* **1302**, 93-109 (1996).
32. Hietanen, E., Greenwood, M. R., A comparison of lipoprotein lipase activity and adipocyte differentiation in growing male rats. *J Lipid Res* **18**, 480-490 (1977).
33. Park, J. S., Chu, J. S., Tsou, A. D., Diop, R., Tang, Z., Wang, A., Li, S., The effect of matrix stiffness on the differentiation of mesenchymal stem cells in response to TGF-β. *Biomaterials* **32**, 3921-3930 (2011).
34. Mauney, J. R., Volloch, V., Kaplan, D. L., Matrix-mediated retention of adipogenic differentiation potential by human adult bone marrow-derived mesenchymal stem cells during ex vivo expansion. *Biomaterials* **26**, 6167-6175 (2005).
35. Mackay, A. M., Beck, S. C., Murphy, J. M., Barry, F. P., Chichester, C. O., Pittenger, M. F., Chondrogenic differentiation of cultured human mesenchymal stem cells from marrow. *Tissue Eng* **4**, 415-428 (1998).
36. Arufe, M. C., De la Fuente, A., Fuentes-Boquete, I., De Toro, F. J., Blanco, F. J., Differentiation of synovial CD-105(+) human mesenchymal stem cells into chondrocyte-like cells through spheroid formation. *J Cell Biochem* **108**, 145-155 (2009).
37. Cui, J. H., Park, S. R., Park, K., Choi, B. H., Min, B. H., Preconditioning of mesenchymal stem cells with low-intensity ultrasound for cartilage formation in vivo. *Tissue Eng* **13**, 351-360 (2007).
38. Yoneno, K., Ohno, S., Tanimoto, K., Honda, K., Tanaka, N., Doi, T., Kawata, T., Tanaka, E., Kapila, S., Tanne, K., Multidifferentiation potential of mesenchymal stem cells in three-dimensional collagen gel cultures. *J Biomed Mater Res A* **75**, 733-741 (2005).
39. Lee, C. R., Grad, S., Gorna, K., Gogolewski, S., Goessl, A., Alini, M., Fibrin-polyurethane composites for articular cartilage tissue engineering: A preliminary analysis. *Tissue Eng* **11**, 1562-1573 (2005).
40. Shanmugasundaram, S., Chaudhry, H., Arinzeh, T. L., Microscale versus nanoscale scaffold architecture for mesenchymal stem cell chondrogenesis. *Tissue Eng A* **17**, 831-840 (2011).
41. Richardson, S. M., Curran, J. M., Chen, R., Vaughan-Thomas, A., Hunt, J. A., Freemont, A. J., Hoyland, J. A., The differentiation of bone marrow mesenchymal stem cells into chondrocyte-like cells on poly-L-lactic acid (PLLA) scaffolds. *Biomaterials* **27**, 4069-4078 (2006).
42. Murry, C. E., Keller, G., Differentiation of embryonic stem cells to clinically relevant populations: lessons from embryonic development. *Cell* **132**, 661-680 (2008).
43. Fuchs, E., Tumbar, T., Guasch, G., Socializing with the neighbors: stem cells and their niche. *Cell* **116**, 769-778 (2004).
44. Reilly, G. C., Engler, A. J., Intrinsic extracellular matrix properties regulate stem cell differentiation. *J Biomech* **43**, 55-62 (2010).
45. Discher, D. E., Mooney, D. J., Zandstra, P. W., Growth factors, matrices, and forces combine and control stem cells. *Science* **324**, 1673-1677 (2009).
46. Sasaki, N., Shinomi, M., Hirano, K., Ui-Tei, K., Nishihara, S., Lacdinac (Galnacβ1-4glcnac) Contributes to Self-Renewal of Mouse Embryonic Stem Cells by Regulating LIF/STAT3 Signaling. *Stem Cells* **29**, 641-650 (2011).

47. Ying, Q. L., Nichols, J., Chambers, I., Smith, A., BMP induction of Id proteins suppresses differentiation and sustains embryonic stem cell self-renewal in collaboration with STAT3. *Cell* **115**, 281-292 (2003).
48. Yao, S., Chen, S., Clark, J., Hao, E., Beattie, G. M., Hayek, A., Ding, S., Long-term self-renewal and directed differentiation of human embryonic stem cells in chemically defined conditions. *Proc Natl Acad Sci USA* **103**, 6907-6912 (2006).
49. Rao, B. M., Zandstra, P. W., Culture development for human embryonic stem cell propagation: molecular aspects and challenges. *Curr Opin Biotechnol* **16**, 568-576 (2005).
50. Chung, B. G., Flanagan, L. A., Rhee, S. W., Schwartz, P. H., Lee, A. P., Monuki, E. S., Jeon, N. L., Human neural stem cell growth and differentiation in a gradient-generating microfluidic device. *Lab Chip* **5**, 401-406 (2005).
51. Fan, V. H., Tamama, K., Au, A., Littrell, R., Richardson, L. B., Wright, J. W., Wells, A., Griffith, L. G., Tethered epidermal growth factor provides a survival advantage to mesenchymal stem cells. *Stem Cells* **25**, 1241-1251 (2007).
52. Alberti, K., Davey, R. E., Onishi, K., George, S., Salchert, K., Seib, F. P., Bornhäuser, M., Pompe, T., Nagy, A., Werner, C., Zandstra, P. W., Functional immobilization of signaling proteins enables control of stem cell fate. *Nat Methods* **5**, 645-650 (2008).
53. Cetinkaya, G., Türkoğlu, H., Arat, S., Odaman, H., Onur, M. A., Gümüşderelioğlu, M., Tümer, A., LIF-immobilized nonwoven polyester fabrics for cultivation of murine embryonic stem cells. *J Biomed Mater Res A* **81**, 911-919 (2007).
54. Park, J. S., Woo, D. G., Yang, H. N., Lim, H. J., Chung, H. M., Park, K. H., Heparin-bound transforming growth factor-beta3 enhances neocartilage formation by rabbit mesenchymal stem cells. *Transplantation* **85**, 589-596 (2008).
55. Park, K., Cho, K. J., Kim, J. J., Kim, I. H., Han, D. K., Functional PLGA scaffolds for chondrogenesis of bone-marrow-derived mesenchymal stem cells. *Macromol Biosci* **9**, 221-229 (2009).
56. Doran, M. R., Markway, B. D., Aird, I. A., Rowlands, A. S., George, P. A., Nielsen, L. K., Cooper-White, J. J., Surface-bound stem cell factor and the promotion of hematopoietic cell expansion. *Biomaterials* **30**, 4047-4052 (2009).
57. Lutolf, M. P., Hubbell, J. A., Synthetic biomaterials as instructive extracellular microenvironments for morphogenesis in tissue engineering. *Nat Biotechnol* **23**, 47-55 (2005).
58. Rosso, F., Giordano, A., Barbarisi, M., Barbarisi, A., From Cell-ECM interactions to tissue engineering. *J Cell Physiol* **199**, 174-180 (2004).
59. Nakamura, M., Sone, S., Takahashi, I., Mizoguchi, I., Echigo, S., Sasano, Y., Expression of versican and ADAMTS1, 4, and 5 during bone development in the rat mandible and hind limb. *J Histochem Cytochem* **53**, 1553-1562 (2005).
60. Sasano, Y., Li, H. C., Zhu, J. X., Imanaka-Yoshida, K., Mizoguchi, I., Kagayama, M., Immunohistochemical localization of type I collagen, fibronectin and tenascin C during embryonic osteogenesis in the dentary of mandibles and tibias in rats. *Histochem J* **32**, 591-598 (2000).
61. Galbraith, C. G., Sheetz, M. P., Forces on adhesive contacts affect cell function. *Curr Opin Cell Biol* **10**, 566-571 (1998).
62. Geiger, B., Bershadsky, A., Pankov, R., Yamada, K. M., Correspondence, B. G., Transmembrane extracellular matrix–cytoskeleton crosstalk. *Nat Rev Mol Cell Biol* **2**, 793-805 (2001).

63. Gerecht, S., Burdick, J. A., Ferreira, L. S., Townsend, S. A., Langer, R., Vunjak-Novakovic, G., Hyaluronic acid hydrogel for controlled self-renewal and differentiation of human embryonic stem cells. *Proc Natl Acad Sci USA* **104**, 11298-11303 (2007).
64. Bosnakovski, D., Mizuno, M., Kim, G., Takagi, S., Okumura, M., Fujinaga, T., Chondrogenic differentiation of bovine bone marrow mesenchymal stem cells (MSCs) in different hydrogels: influence of collagen type II extracellular matrix on MSC chondrogenesis. *Biotechnol Bioeng* **93**, 1152-1163 (2006).
65. Flaim, C. J., Chien, S., Bhatia, S. N., An extracellular matrix microarray for probing cellular differentiation. *Nat Methods* **2**, 119-125 (2005).
66. Toh, Y. C., Blagović, K., Voldman, J., Advancing stem cell research with microtechnologies: opportunities and challenges. *Integr Biol* **2**, 305-325 (2010).
67. Datta, N., Pham, Q. P., Sharma, U., Sikavitsas, V. I., Jansen, J. A., Mikos, A. G., In vitro generated extracellular matrix and fluid shear stress synergistically enhance 3D osteoblastic differentiation. *Proc Natl Acad Sci USA* **103**, 2488-2493 (2006).
68. Datta, N., Holtorf, H. L., Sikavitsas, V. I., Jansen, J. A., Mikos, A. G., Effect of bone extracellular matrix synthesized in vitro on the osteoblastic differentiation of marrow stromal cells. *Biomaterials* **26**, 971-977 (2005).
69. Hoshiba, T., Kawazoe, N., Tateishi, T., Chen, G., Development of extracellular matrices mimicking stepwise adipogenesis of mesenchymal stem cells. *Adv Mater* **22**, 3042-3047 (2010).
70. Hoshiba, T., Kawazoe, N., Tateishi, T., Chen, G., Development of stepwise osteogenesis-mimicking matrices for the regulation of mesenchymal stem cell functions. *J Biol Chem* **284**, 31164-31173 (2009).
71. Calvi, L. M., Adams, G. B., Weibrecht, K. W., Weber, J. M., Olson, D. P., Knight, M. C., Martin, R. P., Schipani, E., Divieti, P., Bringhurst, F. R., Milner, L. A., Kronenberg, H. M., Scadden, D. T., Osteoblastic cells regulate the haematopoietic stem cell niche. *Nature* **425**, 841-846 (2003).
72. Harvey, K., Dzierzak, E., Cell-cell contact and anatomical compatibility in stromal cell-mediated HSC support during development. *Stem Cells* **22**, 253-258 (2004).
73. Ludwig, T. E., Bergendahl, V., Levenstein, M. E., Yu, J., Probasco, M. D., Thomson, J. A., Feeder-independent culture of human embryonic stem cells. *Nat Methods* **3**, 637-646 (2006).
74. Neuhuber, B., Swanger, S. A., Howard, L., Mackay, A., Fischer, I., Effects of plating density and culture time on bone marrow stromal cell characteristics. *Exp Hematol* **36**, 1176-1185 (2008).
75. Both, S. K., van der Muijsenberg, A. J. C., van Blitterswijk, C. A., de Boer, J., de Bruijn, J. D., A rapid and efficient method for expansion of human mesenchymal stem cells. *Tissue Eng* **13**, 3-9 (2007).
76. Lund, P., Pilgaard, L., Duroux, M., Fink, T., Zachar, V., Effect of growth media and serum replacements on the proliferation and differentiation of adipose-derived stem cells. *Cytotherapy* **11**, 189-197 (2009).
77. McBeath, R., Pirone, D. M., Nelson, C. M., Bhadriraju, K., Chen, C. S., Cell shape, cytoskeletal tension, and RhoA regulate stem cell lineage commitment. *Dev Cell* **6**, 483-495 (2004).
78. Lode, A., Bernhardt, A., Gelinsky, M., Cultivation of human bone marrow stromal cells on three-dimensional scaffolds of mineralized collagen : influence of seeding density on colonization , proliferation and osteogenic differentiation. *Tissue Eng* 400-407 (2008).

79. Kim, K., Dean, D., Mikos, A. G., Fisher, J. P., Effect of initial cell seeding density on early osteogenic signal expression of rat bone marrow stromal cells cultured on cross-linked poly(propylene fumarate) disks. *Biomacromolecules* **10**, 1810-1817 (2009).
80. Wang, L., Dormer, N. H., Bonewald, L. F., Detamore, M. S., Osteogenic differentiation of human umbilical cord mesenchymal stromal cells in polyglycolic acid scaffolds. *Tissue Eng A* **16**, 1937-1948 (2010).
81. Sinclair, S. S. K., Burg, K. J. L., Effect of osteoclast co-culture on the differentiation of human mesenchymal stem cells grown on bone graft granules. *J Biomater Sci Polym Ed* **22**, 789-808 (2011).
82. Strassburg, S., Richardson, S. M., Freemont, A. J., Hoyland, J. A., Co-culture induces mesenchymal stem cell differentiation and modulation of the degenerate human nucleus pulposus cell phenotype. *Regen Med* **5**, 701-711 (2010).
83. Brodbeck, W. G., Shive, M. S., Colton, E., Nakayama, Y., Matsuda, T., Anderson, J. M., Influence of biomaterial surface chemistry on the apoptosis of adherent cells. *J Biomed Mater Res* **55**, 661-668 (2001).
84. Shen, M., Horbett, T. A., The effects of surface chemistry and adsorbed proteins on monocyte/macrophage adhesion to chemically modified polystyrene surfaces. *J Biomed Mater Res* **57**, 336-345 (2001).
85. McClary, K. B., Ugarova, T., Grainger, D. W., Modulating fibroblast adhesion, spreading, and proliferation using self-assembled monolayer films of alkylthiolates on gold. *J Biomed Mater Res* **50**, 428-439 (2000).
86. García, A. J., Vega, M. D., Boettiger, D., Modulation of cell proliferation and differentiation through substrate-dependent changes in fibronectin conformation. *Mol Biol Cell* **10**, 785-798 (1999).
87. Keselowsky, B. G., Collard, D. M., García, A. J., Surface chemistry modulates focal adhesion composition and signaling through changes in integrin binding. *Biomaterials* **25**, 5947-5954 (2004).
88. Keselowsky, B. G., Collard, D. M., García, A. J., Integrin binding specificity regulates biomaterial surface chemistry effects on cell differentiation. Proc Natl Acad Sci USA **102**, 5953-5957 (2005).
89. Curran, J. M., Chen, R., Hunt, J. A., The guidance of human mesenchymal stem cell differentiation in vitro by controlled modifications to the cell substrate. *Biomaterials* **27**, 4783-93 (2006).
90. Curran, J. M., Chen, R., Hunt, J. A., Controlling the phenotype and function of mesenchymal stem cells in vitro by adhesion to silane-modified clean glass surfaces. *Biomaterials* **26**, 7057-7067 (2005).
91. Guo, L., Kawazoe, N., Hoshiba, T., Tateishi, T., Chen, G., Zhang, X., Osteogenic differentiation of human mesenchymal stem cells on chargeable polymer-modified surfaces. *J Biomed Mater Res A* **87**, 903-912 (2008).
92. Guo, L., Kawazoe, N., Fan, Y., Ito, Y., Tanaka, J., Tateishi, T., Zhang, X., Chen, G., Chondrogenic differentiation of human mesenchymal stem cells on photoreactive polymer-modified surfaces. *Biomaterials* **29**, 23-32 (2008).
93. Benoit, D. S. W., Schwartz, M. P., Durney, A. R., Anseth, K. S., Small functional groups for controlled differentiation of hydrogel-encapsulated human mesenchymal stem cells. *Nat Mater* **7**, 816-823 (2008).
94. Anderson, D. G., Levenberg, S., Langer, R., Nanoliter-scale synthesis of arrayed biomaterials and application to human embryonic stem cells. *Nat Biotechnol* **22**, 863-866 (2004).
95. Anderson, D. G., Putnam, D., Lavik, E. B., Mahmood, T. A., Langer, R., Biomaterial microarrays: rapid, microscale screening of polymer-cell interaction. *Biomaterials* **26**, 4892-4897 (2005).

96. Mei, Y., Gerecht, S., Taylor, M., Urquhart, A. J., Bogatyrev, S. R., Cho, S. W., Davies, M. C., Alexander, M. R., Langer, R. S., Anderson, D. G., Mapping the Interactions among Biomaterials, Adsorbed Proteins, and Human Embryonic Stem Cells. *Adv Mater* **21**, 2781-2786 (2009).
97. Luo, W., Chan, E. W. L., Yousaf, M. N., Tailored electroactive and quantitative ligand density microarrays applied to stem cell differentiation. *J Am Chem Soci* **132**, 2614-2621 (2010).
98. Stevens, M. M., George, J. H., Exploring and engineering the cell surface interface. *Science* **310**, 1135-1138 (2005).
99. Curtis, A., Wilkinson, C., Nanotechniques and approaches in biotechnology. *Mater Today* **19**, 97-101 (2001).
100. Abrams, G. A., Schaus, S. S., Goodman, S. L., Nealey, P. F., Murphy, C. J., Nanoscale topography of the corneal epithelial basement membrane and Descemet's membrane of the human. *Cornea* **19**, 57-64 (2000).
101. Shih, Y. R. V., Chen, C. N., Tsai, S. W., Wang, Y. J., Lee, O. K., Growth of mesenchymal stem cells on electrospun type I collagen nanofibers. *Stem Cells* **24**, 2391-2397 (2006).
102. Christopherson, G. T., Song, H., Mao, H. Q., The influence of fiber diameter of electrospun substrates on neural stem cell differentiation and proliferation. *Biomaterials* **30**, 556-564 (2009).
103. Xie, J., Willerth, S. M., Li, X., Macewan, M. R., Rader, A., Sakiyama-Elbert, S. E., Xia, Y., The differentiation of embryonic stem cells seeded on electrospun nanofibers into neural lineages. *Biomaterials* **30**, 354-362 (2009).
104. Xin, X., Hussain, M., Mao, J. J., Continuing differentiation of human mesenchymal stem cells and induced chondrogenic and osteogenic lineages in electrospun PLGA nanofiber scaffold. *Biomaterials* **28**, 316-325 (2007).
105. Wise, J. K., Yarin, A. L., Megaridis, C. M., Cho, M., Chondrogenic differentiation of human mesenchymal stem cells on oriented nanofibrous scaffolds: engineering the superficial zone of articular cartilage. *Tissue Eng A* **15**, 913-921 (2009).
106. Gerecht, S., Bettinger, C. J., Zhang, Z., Borenstein, J. T., Vunjak-Novakovic, G., Langer, R., The effect of actin disrupting agents on contact guidance of human embryonic stem cells. *Biomaterials* **28**, 4068-4077 (2007).
107. Lee, M. R., Kwon, K. W., Jung, H., Kim, H. N., Suh, K. Y., Kim, K., Kim, K. S., Direct differentiation of human embryonic stem cells into selective neurons on nanoscale ridge/groove pattern arrays. *Biomaterials* **31**, 4360-4366 (2010).
108. Yim, E. K. F., Pang, S. W., Leong, K. W., Synthetic nanostructures inducing differentiation of human mesenchymal stem cells into neuronal lineage. *Exp Cell Res* **313**, 1820-1829 (2007).
109. Dalby, M. J., Gadegaard, N., Tare, R., Andar, A., Riehle, M. O., Herzyk, P., Wilkinson, C. D., Oreffo, R. O., The control of human mesenchymal cell differentiation using nanoscale symmetry and disorder. *Nat Mater* **6**, 997-1003 (2007).
110. McMurray, R. J., Gadegaard, N., Tsimbouri, P. M., Burgess, K. V., McNamara, L. E., Tare, R., Murawski, K., Kingham, E., Oreffo, R. O., Dalby, M. J., Nanoscale surfaces for the long-term maintenance of mesenchymal stem cell phenotype and multipotency. *Nat Mater* **10**, 637-644 (2011).
111. Oh, S., Brammer, K. S., Li, Y. S., Teng, D., Engler, A. J., Chien, S., Jin, S., Stem cell fate dictated solely by altered nanotube dimension. *Proc Natl Acad Sci USA* **106**, 2130-2135 (2009).
112. Guilak, F., Cohen, D. M., Estes, B. T., Gimble, J. M., Liedtke, W., Chen, C. S., Control of stem cell fate by physical interactions with the extracellular matrix. *Cell Stem Cell* **5**, 17-26 (2009).

113. Engler, A. J., Sen, S., Sweeney, H. L., Discher, D. E., Matrix elasticity directs stem cell lineage specification. *Cell* **126**, 677-689 (2006).
114. Wang, L. S., Boulaire, J., Chan, P. P. Y., Chung, J. E., Kurisawa, M., The role of stiffness of gelatin-hydroxyphenylpropionic acid hydrogels formed by enzyme-mediated crosslinking on the differentiation of human mesenchymal stem cell. *Biomaterials* **31**, 8608-8616 (2010).
115. Saha, K., Keung, A. J., Irwin, E. F., Li, Y., Little, L., Schaffer, D. V., Healy, K. E., Substrate Modulus Directs Neural Stem Cell Behavior. *Biophys J* **95**, 4426-4438 (2008).
116. Huebsch, N., Arany, P. R., Mao, A. S., Shvartsman, D., Ali, O. A., Bencherif, S. A., Rivera-Feliciano, J., Mooney, D. J., Harnessing traction-mediated manipulation of the cell/matrix interface to control stem-cell fate. *Nat Mater* **9**, 518-526 (2010).
117. Gilbert, P. M., Havenstrite, K. L., Magnusson, K. E., Sacco, A., Leonardi, N. A., Kraft, P., Nguyen, N. K., Thrun, S., Lutolf, M. P., Blau, H. M., Substrate elasticity regulates skeletal muscle stem cell self-renewal in culture. *Science* **329**, 1078-1081 (2010).
118. Tan, J. L., Tien, J., Pirone, D. M., Gray, D. S., Bhadriraju, K., Chen, C. S., Cells lying on a bed of microneedles: an approach to isolate mechanical force. *Proc Natl Acad Sci USA* **100**, 1484-1489 (2003).
119. Fu, J., Wang, Y. K., Yang, M. T., Desai, R. A., Yu, X., Liu, Z., Chen, C. S., Mechanical regulation of cell function with geometrically modulated elastomeric substrates. *Nat Methods* **7**, 733-736 (2010).
120. Tsuda, Y., Yamato, M., Kikuchi, A., Watanabe, M., Chen, G., Takahashi, Y., Okano, T., Thermoresponsive Microtextured Culture Surfaces Facilitate Fabrication of Capillary Networks. *Adv Mater* **19**, 3633-3636 (2007).
121. Song, H. K., Toste, B., Ahmann, K., Hoffman-Kim, D., Palmore, G. T. R., Micropatterns of positive guidance cues anchored to polypyrrole doped with polyglutamic acid: a new platform for characterizing neurite extension in complex environments. *Biomaterials* **27**, 473-484 (2006).
122. Chiang, E. N., Dong, R., Ober, C. K., Baird, B. A., Cellular responses to patterned poly(acrylic acid) brushes. *Langmuir* **27**, 7016-7023 (2011).
123. Sweetman, M. J., Shearer, C. J., Shapter, J. G., Voelcker, N. H., Dual silane surface functionalization for the selective attachment of human neuronal cells to porous silicon. *Langmuir* **27**, 9497-9503 (2011).
124. Flavel, B. S., Sweetman, M. J., Shearer, C. J., Shapter, J. G., Voelcker, N. H., Micropatterned arrays of porous silicon: toward sensory biointerfaces. *ACS Appl Mater Interfaces* **3**, 2463-2471 (2011).
125. Falconnet, D., Koenig, A., Assi, F., Textor, M., A combined photolithographic and molecular-assembly approach to produce functional micropatterns for applications in the biosciences. *Adv Funct Mater* **14**, 749-756 (2004).
126. Jing, G., Wang, Y., Zhou, T., Perry, S. F., Grimes, M. T., Tatic-Lucic, S., Cell patterning using molecular vapor deposition of self-assembled monolayers and lift-off technique. *Acta Biomater* **7**, 1094-1103 (2011).
127. Xia, Y., Whitesides, G. M., Soft lithography. *Angew Chem Int Edit* **37**, 550-575 (1998).
128. Xia, Y., Whitesides, G. M., Soft Lithography. *Annu Rev Mater Sci* **28**, 153-184 (1998).
129. Falconnet, D., Csucs, G., Grandin, H. M., Textor, M., Surface engineering approaches to micropattern surfaces for cell-based assays. *Biomaterials* **27**, 3044-3063 (2006).
130. Kumar, A., Whitesides, G. M., Features of gold having micrometer to centimeter dimensions can be formed through a combination of stamping with an elastomeric stamp and an alkanethiol "'ink'" followed by chemical etching. *Appl Phys Lett* **63**, 2002 (1993).

131. Delamarche, E., Bernard, A., Schmid, H., Bietsch, A., Michel, B., Biebuyck, H., Microfluidic networks for chemical patterning of substrates: design and spplication to bioassays. *J Am Chem Soc* **120**, 500-508 (1998).
132. Trau, M., Yao, N., Kim, E., Xia, Y., Whitesides, G. M., Aksay, I. A., Microscopic patterning of orientated mesoscopic silica through guided growth. *Nature* **390**, 674-676 (1997).
133. Rogers, J. A., Bao, Z., Dhar, L., Fabrication of patterned electroluminescent polymers that emit in geometries with feature sizes into the submicron range. *Appl Phys Lett* **73**, 294 (1998).
134. Zhao, X. M., Smith, S. P., Waldman, S. J., Whitesides, G. M., Prentiss, M., Demonstration of waveguide couplers fabricated using microtransfer molding. *Appl Phys Lett* **71**, 1017 (1997).
135. Singhvi, R., Kumar, A., Lopez, G. P., Stephanopoulos, G. N., Wang, D. I., Whitesides, G. M., Ingber, D. E., Engineering cell shape and function. *Science* **264**, 696-698 (1994).
136. Ameringer, T., Hinz, M., Mourran, C., Seliger, H., Groll, J., Moeller, M., Ultrathin functional star PEG coatings for DNA microarrays. *Biomacromolecules* **6**, 1819-1823 (2005).
137. Hyun, J. Ma, H., Banerjee, P., Cole, J., Gonsalves, K., Chilkoti, A., Micropatterns of a cell-adhesive peptide on an amphiphilic comb polymer film. *Langmuir* **18**, 2975-2979 (2002).
138. Ma, H., Hyun, J., Stiller, P., Chilkoti, A., "Non-fouling" oligo(ethylene glycol)-functionalized polymer brushes synthesized by surface-initiated atom transfer radical polymerization. *Adv Mater* **16**, 338-341 (2004).
139. Bearinger, J. P., Terrettaz, S., Michel, R., Tirelli, N., Vogel, H., Textor, M., Hubbell, J. A., Chemisorbed poly(propylene sulphide)-based copolymers resist biomolecular interactions. *Nat Mater* **2**, 259-264 (2003).
140. Peng, R., Yao, X., Ding, J., Effect of cell anisotropy on differentiation of stem cells on micropatterned surfaces through the controlled single cell adhesion. *Biomaterials* **32**, 8048-8057 (2011).
141. Tan, C. P., Seo, B. R., Brooks, D. J., Chandler, E. M., Craighead, H. G., Fischbach, C., Parylene peel-off arrays to probe the role of cell-cell interactions in tumour angiogenesis. *Integr Biol* **1**, 587-594 (2009).
142. Kikuchi, Y., Nakanishi, J., Nakayama, H., Shimizu, T., Yoshino, Y., Yamaguchi, K., Yoshida, Y., Horiike, Y., Grafting poly(ethylene glycol) to a glass surface via a photocleavable linker for light-induced cell micropatterning and cell proliferation control. *Chem Lett* **37**, 1062-1063 (2008).
143. Fu, C. Y., Lin, C. Y., Chu, W. C., Chang, H. Y., A simple cell patterning method using magnetic particle-containing photosensitive poly (ethylene glycol) hydrogel blocks: a technical note. *Tissue Eng C* **17**, 871-877 (2011).
144. Tseng, Q., Wang, I., Duchemin-Pelletier, E., Azioune, A., Carpi, N., Gao, J., Filhol, O., Piel, M., Théry, M., Balland, M., A new micropatterning method of soft substrates reveals that different tumorigenic signals can promote or reduce cell contraction levels. *Lab Chip* **11**, 2231-2240 (2011).
145. Nakanishi, J., Kikuchi, Y., Inoue, S., Yamaguchi, K., Takarada, T., Maeda, M., Spatiotemporal control of migration of single cells on a photoactivatable cell microarray. *J Am Chem Soc* **129**, 6694-6695 (2007).
146. Lee, H. J., Kim, D. N., Park, S., Lee, Y., Koh, W. G., Micropatterning of a nanoporous alumina membrane with poly(ethylene glycol) hydrogel to create cellular micropatterns on nanotopographic substrates. *Acta Biomater* **7**, 1281-1289 (2011).
147. Kang, I. K., Kim, G. J., Kwon, O. H., Ito, Y., Co-culture of hepatocytes and fibroblasts by micropatterned immobilization of beta-galactose derivatives. *Biomaterials* **25**, 4225-4232 (2004).

148. Liu, H., Ito, Y., Cell attachment and detachment on micropattern-immobilized poly(N-isopropylacrylamide) with gelatin. *Lab Chip* **2**, 175-178 (2002).
149. Ito, Y., Hasuda, H., Terai, H., Kitajima, T., Culture of human umbilical vein endothelial cells on immobilized vascular endothelial growth factor. *J Biomed Mater Res A* **74**, 659-665 (2005).
150. Konno, T., Hasuda, H., Ishihara, K., Ito, Y., Photo-immobilization of a phospholipid polymer for surface modification. *Biomaterials* **26**, 1381-1388 (2005).
151. Ito, Y., Nogawa, M., Preparation of a protein micro-array using a photo-reactive polymer for a cell-adhesion assay. *Biomaterials* **24**, 3021-3026 (2003).
152. Hasuda, H., Kwon, O. H., Kang, I. K., Ito, Y., Synthesis of photoreactive pullulan for surface modification. *Biomaterials* **26**, 2401-2406 (2005).
153. Ito, Y., Photoimmobilization for microarrays. *Biotechnol Progr* **22**, 924-932 (2006).
154. Dillmore, W. S., Yousaf, M. N., Mrksich, M., A photochemical method for patterning the immobilization of ligands and cells to self-assembled monolayers. *Langmuir* **20**, 7223-7231 (2004).
155. Chan, E. W. L., Yousaf, M. N., A photo-electroactive surface strategy for immobilizing ligands in patterns and gradients for studies of cell polarization. *Mol Biosyst* **4**, 746-753 (2008).
156. Luo, W., Yousaf, M. N., Tissue morphing control on dynamic gradient surfaces. *J Am Chem Soc* **133**, 10780-10783 (2011).
157. Chan, E. W. L., Park, S., Yousaf, M. N., An electroactive catalytic dynamic substrate that immobilizes and releases patterned ligands, proteins, and cells. *Angew Chem Int Edit* **47**, 6267-6271 (2008).
158. Tourovskaia, A., Barber, T., Wickes, B. T., Hirdes, D., Grin, B., Castner, D. G., Healy, K. E., Folch, A., Micropatterns of chemisorbed cell adhesion-repellent films using oxygen plasma etching and elastomeric masks. *Langmuir* **19**, 4754-4764 (2003).
159. Folch, A., Jo, B. H., Hurtado, O., Beebe, D. J., Toner, M., Microfabricated elastomeric stencils for micropatterning cell cultures. *J Biomed Mater Res* **52**, 346-353 (2000).
160. Cheng, Q., Li, S., Komvopoulos, K., Plasma-assisted surface chemical patterning for single-cell culture. *Biomaterials* **30**, 4203-4210 (2009).
161. Ostuni, E., Kane, R., Chen, C. S., Ingber, D. E., Whitesides, G. M., Patterning Mammalian Cells Using Elastomeric Membranes. *Langmuir* **16**, 7811-7819 (2000).
162. Cheng, Q., Komvopoulos, K., Li, S., Surface chemical patterning for long-term single-cell culture. *J Biomed Mater Res A* **96**, 507-512 (2011).
163. Yamato, M., Konno, C., Koike, S., Isoi, Y., Shimizu, T., Kikuchi, A., Makino, K., Okano, T., Nanofabrication for micropatterned cell arrays by combining electron beam-irradiated polymer grafting and localized laser ablation. *J Biomed Mater Res A* **67**, 1065-1071 (2003).
164. Doyle, A. D., Wang, F. W., Matsumoto, K., Yamada, K. M., One-dimensional topography underlies three-dimensional fibrillar cell migration. *J Cell Biol* **184**, 481-490 (2009).
165. Pardo, L., Wilson, W. C., Boland, T., Characterization of patterned self-assembled monolayers and protein arrays generated by the Ink-jet method. *Langmuir* **19**, 1462-1466 (2003).
166. Roth, E. A., Xu, T., Das, M., Gregory, C., Hickman, J. J., Boland, T., Inkjet printing for high-throughput cell patterning. *Biomaterials* **25**, 3707-3715 (2004).
167. Sanjana, N. E., Fuller, S. B., A fast flexible ink-jet printing method for patterning dissociated neurons in culture. *J Neurosci Methods* **136**, 151-163 (2004).
168. Turcu, F., Tratsk-Nitz, K., Thanos, S., Schuhmann, W., Heiduschka, P., Ink-jet printing for micropattern generation of laminin for neuronal adhesion. *J Neurosci Methods* **131**, 141-148 (2003).

169. Peerani, R., Rao, B. M., Bauwens, C., Yin, T., Wood, G. A., Nagy, A., Kumacheva, E., Zandstra, P. W., Niche-mediated control of human embryonic stem cell self-renewal and differentiation. *EMBO J* **26**, 4744-4755 (2007).
170. Bauwens, C. L., Peerani, R., Niebruegge, S., Woodhouse, K. A., Kumacheva, E., Husain, M., Zandstra, P. W., Control of human embryonic stem cell colony and aggregate size heterogeneity influences differentiation trajectories. *Stem Cells* **26**, 2300-2310 (2008).
171. Sasaki, D., Shimizu, T., Masuda, S., Kobayashi, J., Itoga, K., Tsuda, Y., Yamashita, J. K., Yamato, M., Okano, T., Mass preparation of size-controlled mouse embryonic stem cell aggregates and induction of cardiac differentiation by cell patterning method. *Biomaterials* **30**, 4384-4389 (2009).
172. Ruiz, S. A., Chen, C. S., Emergence of patterned stem cell differentiation within multicellular structures. *Stem Cells* **26**, 2921-2927 (2008).
173. Luo, W., Jones, S. R., Yousaf, M. N., Geometric control of stem cell differentiation rate on surfaces. *Langmuir* **24**, 12129-12133 (2008).
174. Tay, C. Y., Yu, H., Pal, M., Leong, W. S., Tan, N. S., Ng, K. W., Leong, D. T., Tan, L. P., Micropatterned matrix directs differentiation of human mesenchymal stem cells towards myocardial lineage. *Exp Cell Res* **316**, 1159-1168 (2010).
175. Gage, F. H., Mammalian neural stem cells. *Science* **287**, 1433-1438 (2000).
176. Ruiz, A., Buzanska, L., Gilliland, D., Rauscher, H., Sirghi, L., Sobanski, T., Zychowicz, M., Ceriotti, L., Bretagnol, F., Coecke, S., Colpo, P., Rossi, F., Micro-stamped surfaces for the patterned growth of neural stem cells. *Biomaterials* **29**, 4766-4774 (2008).
177. Park, S. Y., Park, S. Y., Namgung, S., Kim, B., Im, J., Kim, J. Y., Sun, K., Lee, K. B., Nam, J. M., Park, Y., Hong, S., Carbon nanotube monolayer patterns for directed growth of mesenchymal stem cells. *Adv Mater* **19**, 2530-2534 (2007).
178. Park, S. Y., Choi, D. S., Jin, H. J., Park, J., Byun, K. E., Lee, K. B., Hong, S., Polarization-controlled differentiation of human neural stem cells using synergistic cues from the patterns of carbon nanotube monolayer coating. *ACS Nano* **5**, 4704-4711 (2011).

Chapter 2

Manipulation of cell density and its effect on osteogenic and chondrogenic differentiation of MSCs

2.1 Summary

In this chapter, azidophenyl-derivatized poly(vinyl alcohol) (PVA) was synthesized by coupling the hydroxyl groups of PVA with 4-azidobenzoic acid. A photomask with designed micropattern was fabricated using laser lithography system. PVA-micropatterned polystyrene (PSt) surface was created using prepared photomask and UV photolithography. The micropatterned surface consisted of different area ratios of cell-adhesive PSt to non-adhesive PVA regions. A gradient pattern of human mesenchymal stem cells (MSCs) with different cell densities was generated by culturing the cells on prepared micropatterned surface. The effects of cell density gradient on stem cell functions such as proliferation and differentiation were investigated. MSCs seeded at a low density proliferated faster than those seeded at a high density. Although MSCs seeded at both low and high densities showed osteogenic differentiation, the higher cell seeding density could initiate osteogenic differentiation at a faster rate than the low cell seeding density. Additionally, high cell density was required to induce chondrogenic differentiation of MSCs.

2.2 Introduction

Mesenchymal stem cells (MSCs) are a promising cell source for tissue engineering and regenerative medicine because they are relatively easy to obtain from a small aspirate of bone marrow, and are capable of differentiating into lineages of mesenchymal tissues, including bone, cartilage, and fat[1,2,3]. However, manipulation of stem cell functions remains a great challenge in tissue engineering because many factors affect the fate of stem cells[4-11]. Those factors including soluble growth factors[1], matrix elasticity[12], surface topography[13], chemistry[14] and charge[15], mechanical stimuli[16], and culture conditions[17] can externally affect the differentiation of the MSCs. On the other hand, cell-related internal factors are equally important in determining cell behavior and function.

Cell density, which can affect cell morphology and intercellular signaling, is just one of the internal factors for optimal differentiation of MSCs. McBeath *et al.*[18] reported that human mesenchymal stem cells

(hMSCs) seeded at low density (e.g., 1,000 and 3,000 cells/cm^2) on tissue culture polystyrene (TCPS) tended to differentiate along the osteoblast lineage whereas hMSCs seeded at high density (e.g., 21,000 and 25,000 cells/cm^2) tended to differentiate along the adipocyte lineage. In another report, Kim *et al.*[19] found that rat bone marrow stromal cells (rBMSCs) seeded at a low density (e.g., 30,000 cells/cm^2) on TCPS stimulated early osteogenic differentiation. The low cell density (30,000 cells/cm^2) in this study was actually higher than the 'high' cell density (25,000 cells/cm^2) as referred to in the McBeath's study. In addition, Jaiswal *et al.*[20] reported that higher initial seeding density of hMSCs could significantly enhance mineral deposition, which indicated that the cells had differentiated to osteoblasts and had matured. Therefore, current researches on the cell density and its effect on the differentiation of MSCs are still controversial.

Moreover, the effect of cell density on the differentiation of MSCs was investigated by conventional seeding procedure. In this method, different cell densities are separately seeded one by one onto a series of culture dishes/plates. This is a lengthy process with expensive reagents and the interference by other factors is negative aspects of this method. Therefore, control over different cell densities on the same plate/surface would be a valuable method to more direct, explicit, and systematic comparison of the effect of cell seeding density on cell function.

Micropatterning techniques are of great importance in studying cell biology[21], biomaterials, and tissue engineering[22]. Spatial control of cells has been achieved by various micropatterning methods[23-26]. In this chapter, a square micropattern was used to control the location of MSCs to generate a wide range of cell density (2.6 - 112.5 × 10^3 cells/cm^2). Photo-reactive poly(vinyl alcohol) (PVA) was synthesized and micropatterned on commonly used cell-culture polystyrene (PSt) surface to obtain different cell densities. The effects of various cell densities on the osteogenic and chondrogenic differentiation of MSCs were investigated on such a single micropatterned surface.

2.3 Materials and methods

2.3.1 Synthesis of azidophenyl-derivatized PVA

Azidophenyl-derivatized poly(vinyl alcohol) (AzPhPVA) was synthesized by coupling the hydroxyl groups of PVA with 4-azidobenzoic acid. Dimethyl sulfoxide (DMSO, 1 mL) containing dicyclohexylcarbodiimide (234 mg, 1.13 mmol, Watanabe Chemical Industries, Ltd) was added dropwise to 2.5 mL of DMSO containing 4-azidobenzoic acid (185 mg, 1.13 mmol, Tokyo Chemical Industry Co., Ltd) under stirring at room temperature in the dark. Then, 1 mL of DMSO with 16.8 mg of 4-(1-pyrrolidinyl) pyridine (0.113 mmol, Wako Pure Chemical Industries, Ltd) was added dropwise to the reaction mixture under stirring. After 10 min, 8 mL of DMSO solution containing 100 mg of PVA (MW 44,000, 1.13 mmol in monomer units, Wako Pure Chemical Industries, Ltd) was added dropwise to the above reaction mixture under stirring in the dark. After 24 h, dicyclohexylurea formed during the reaction was removed by filtration, and the filtrate was collected and purified by precipitation in methanol twice. The precipitated photo-reactive PVA was collected by centrifuging at 2,000 rpm for 10 min at 25 ºC and then dissolved in Milli-Q water. The chemical equation for the synthesis process was shown in Figure 2.1.

The azidophenyl groups introduced to photo-reactive PVA were characterized by UV-Visible Spectrophotometer (JASCO V-660) and ^{1}H-NMR (JEOL 300/BZ). The percentage of azidophenyl groups in photo-reactive PVA was calculated by ^{1}H-NMR from the peak integration of the azidophenyl protons around 7.2 and 8.0 ppm, and that of the methylene protons of PVA main chain around 1.4 ppm, respectively.

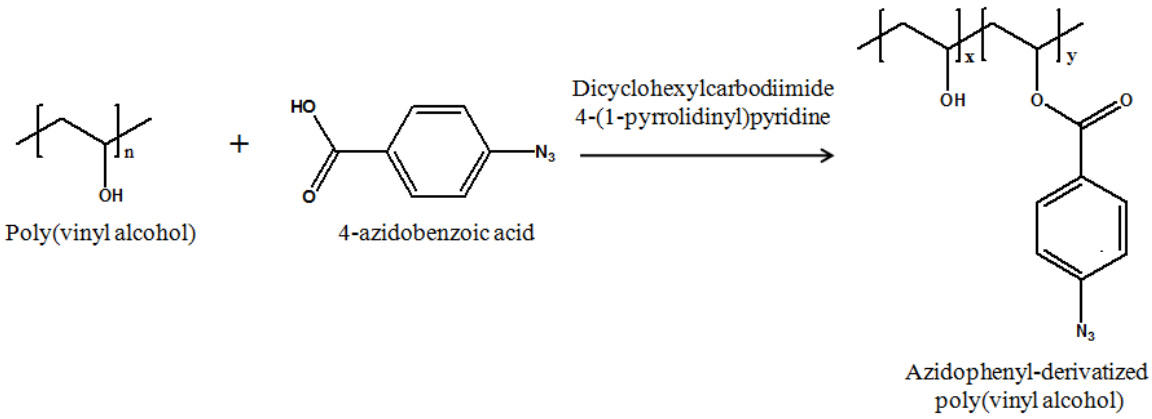

Figure 2.1 The chemical equation for the synthesis of azidophenyl-derivatized poly(vinyl alcohol).

2.3.2 Fabrication of photomask

Quartz wafer coated with chromium layer was thoroughly cleaned with nitrogen gas. After cleaning, the wafer was baked for 2 min at 120 ºC to evaporate adsorbed water molecules. And then positive-tone photoresist OFPR-800 (Tokyo Ohka Kogyo Co., Ltd) was spin-coated at 500 rpm for 3 sec, 1500 rpm for 3 sec, and 4500 rpm for 30 sec on a K-359SD-1 spinner system (Kyowa Riken). After coating, the wafer was baked for 2 min at 120 ºC. A DWL66 laser lithography system (Heidelberg Instruments) was used to irradiate the photoresist according to the pattern designed with VectorWorks (A & A Co., Ltd). After irradiation, the photoresist was developed by immersing in NMD-3 (Tokyo Ohka Kogyo Co., Ltd) developer for 30 sec, rinsed with water, dried with compressed air, and immediately transferred to the chromium etchant ($(NH_4)_2[Ce(NO_3)_6]/HClO_4$) solution to remove the exposed chromium. The residual photoresist was then removed with acetone. The prepared photomask was checked with an optical microscope. The preparation process was shown in Figure 2.2.

2.3.3 Micropatterning of PVA with a photomask

PSt plates (3.0 × 2.5 cm^2) were cut from a cell-culture PSt flask (BD Falcon™). The photo-reactive PVA solution (0.2 mL, 0.3 mg/mL) was placed on the PSt plates and air-dried at room temperature in the dark. The coating region was around 1.0 × 2.0 cm^2. The plates were covered with a photomask and irradiated with UV light (Funa®-UV-Linker FS-1500) at energy of 0.3 J/cm^2 from a distance of 15 cm. After irradiation, the plates were immersed in Milli-Q water and then ultrasonicated to completely remove any unreacted PVA from the non-irradiated areas. After complete washing, a PVA-micropatterned PSt surface was obtained. The plates were sterilized with 70% ethanol solution and used for cell culture. Preparation scheme of PVA-micropatterned PSt surface was shown in Figure 2.3.

2.3.4 AFM observation

The surface topography of the PVA-micropatterned PSt plate was observed by using MFP-3D-BIO™ AFM (Asylum Research). A commercially available cantilever (spring constant: 0.06 N/m; oscillation frequency: 12-24 kHz; DNP, Veeco Probes) with a silicon nitride tip was used to measure the samples (80 × 80 μm^2) in Milli-Q water in contact mode. The step height of the micropatterned PVA layer

was measured by section analysis of the acquired image. Three randomly selected micropatterns were measured to calculate mean and standard deviation.

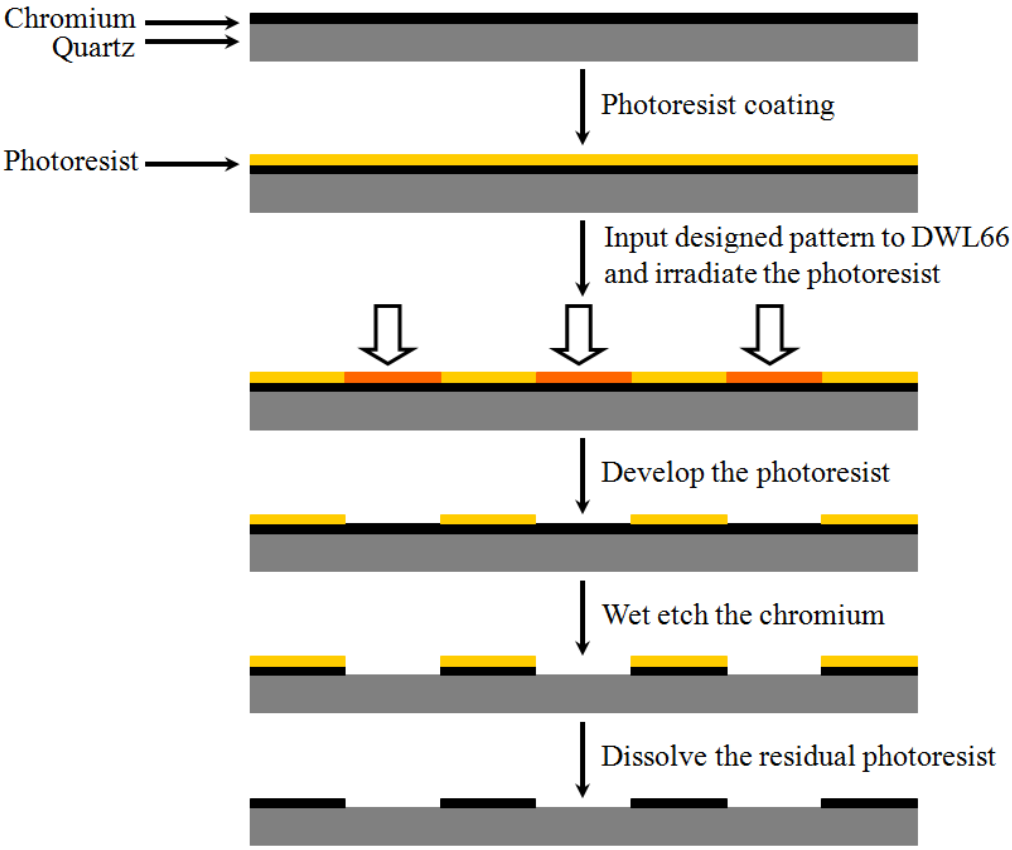

Figure 2.2 Fabrication of photomask using DWL66 laser lithography system.

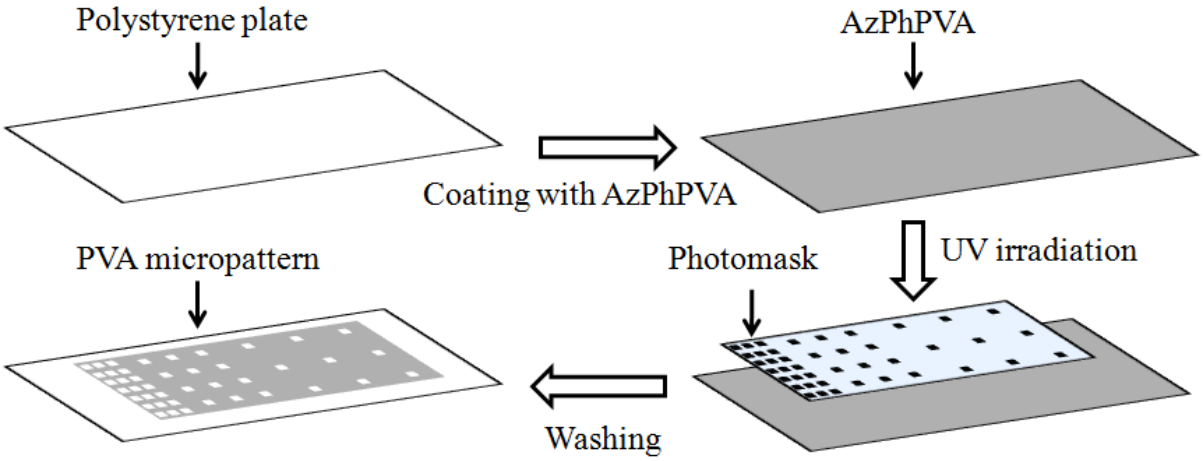

Figure 2.3 Preparation scheme of PVA-micropatterned PSt surface.

2.3.5 Cell culture

Human bone marrow-derived mesenchymal stem cells (MSCs, passage 2) were obtained from Osiris Therapeutics (Columbia, MD). Based on the data sheet from the company, the cells are positive for CD105, CD166, CD29, and CD44; but negative for CD14, CD34, and CD45. The cells were seeded in

cell-culture flasks using growth medium purchased from Lonza (Walkersville, MD). The growth medium contained 440 mL MSC basal medium, 50 mL mesenchymal cell growth supplement, 10 mL 200 mM L-glutamine, and 0.5 mL penicillin/streptomycin mixture. After being subcultured twice, the passage 4 cells were collected by treatment with trypsin/EDTA solution and suspended in a serum medium (control medium) at a density of 1.5×10^4 cells/mL. The serum medium was composed of Dulbecco's Modified Eagle's Medium (DMEM, Sigma) supplemented with 4,500 mg/L glucose, 584 mg/L glutamine, 100 U/mL penicillin, 100 μg/mL streptomycin, 0.1 mM nonessential amino acid, 0.4 mM proline, 50 mg/L ascorbic acid, and 10% fetal bovine serum (FBS).

To seed the cells on the PVA-micropatterned PSt plates, the plates were put in 60 mm cell-culture dishes. Medical silicon frame molds were placed over PVA-micropatterned PSt plates to prevent leakage of cell suspension from the micropatterned areas during cell seeding. The cell suspension (1.0 mL) was added to the silicon frame molds and the cells were cultured for 1 day. After 1 day, MSCs were cultured in control, osteogenic, or chondrogenic media, respectively. The osteogenic medium consisted of DMEM supplemented with 1,000 mg/L glucose, 584 mg/L glutamine, 100 U/mL penicillin, 100 μg/mL streptomycin, 0.1 mM nonessential amino acid, 50 mg/L ascorbic acid, 10% FBS, 100 nM dexamethasone, and 10 mM β-glycerophosphate disodium salt hydrate. The chondrogenic medium consisted of DMEM supplemented with 4500 mg/L glucose, 584 mg/L glutamine, 100 U/mL penicillin, 100 μg/mL streptomycin, 0.1 mM nonessential amino acid, 0.4 mM proline, 50 mg/L ascorbic acid, 100 nM dexamethasone, 10 ng/mL TGF-β3 (Sigma), and 1% ITS+1 (Sigma). The TGF-β3 was thawed and supplemented immediately before use. Each medium was changed every 2-3 days.

2.3.6 Cell distribution and proliferation on PVA-micropatterned PSt surface

After 1 day of culture in control medium, cell adhesion and distribution on the PVA-micropatterned PSt plates were observed with a phase contrast microscope. In order to count the number of cells in each region of the micropattern, the cells were fixed with 4% paraformaldehyde for 10 min at 4 ^{o}C and then the cell nuclei were stained with 4',6-diamidino-2-phenylindole (DAPI, Vector Laboratories, Inc.). For proliferation assay, after 3, 7, and 14 days of culture in osteogenic medium, the cells were fixed with 4% paraformaldehyde for 10 min at 4 ^{o}C and then the cell nuclei were stained with DAPI and counted. At each time point, 3 plates were used to calculate the mean and standard deviation.

2.3.7 Cell viability on PVA-micropatterned PSt surface

After 2 weeks of culture in control medium, cell viability on PVA-micropatterned PSt surface was evaluated using a live/dead assay kit (Cellstain-Double Staining Kit, Dojindo, Tokyo, Japan). The PVA-micropatterned PSt surface was washed twice with PBS and incubated in 2 μM calcein-AM (stain live cells) and 4 μM propidium iodide (PI, stain dead cells) in serum-free DMEM medium for 15 min at 37 ^{o}C. The PVA-micropatterned PSt surface was then washed twice with PBS and observed with a fluorescence microscope.

2.3.8 Alkaline phosphatase staining

Alkaline phosphatase (ALP) activity of the cells after culture in osteogenic medium for 3, 5, 7, and 14 days was assessed as follows. The cultured cells were rinsed with phosphate buffer saline (PBS) three

times and fixed with 4% paraformaldehyde for 10 min at 4 ºC. The fixed cells were soaked in 0.1% naphthol AS-MX phosphate (Sigma) and 0.1% Fast blue RR salt (Sigma) in 56 mM 2-amino-2-methyl-1,3-propanediol (pH 9.9, Sigma) for 10 min at room temperature, washed with PBS, and then observed with an optical microscope.

2.3.9 RNA isolation and real-time PCR

For analyzing gene expression, the MSCs were seeded into cell-culture PSt plates at respective densities of 2.5, 10, 50, and 100×10^3 cells/cm^2 which were corresponded to the cell densities on non-pattern region, Region A, B and C of PVA-micropatterned PSt plate. After culture for 3 and 7 days in osteogenic medium, the cells were washed with PBS, and 1 mL of Isogen reagent (Nippon Gene, Toyama, Japan) was added to each well. Total RNA was extracted following the manufacturer's protocol. 1 μg of total RNA was reversely transcribed into cDNA using a random hexamer primer (Applied Biosystems) in 20 μL reaction. An aliquot (1 μL) of 10-times diluted reaction solution was used for each 25 μL real-time PCR reaction together with 300 nM forward and reverse primers, and 150 nM probes and qPCR Master Mix (Eurogenetic). Primer and probe were for *18S rRNA*, *GAPDH*, *ALP*, and bone sialoprotein (*BSP*). Real-time PCR analysis was performed using the 7500 real-time PCR System (Applied Biosystems). After an initial incubation step of 2 min at 50 ºC and denaturation for 10 min at 95 ºC, 40 cycles of PCR (95 ºC for 15 sec, 60 ºC for 1 min) were performed. *18S rRNA* levels were used as endogenous controls and gene expression levels relative to *GAPDH* were calculated using the comparative Ct method. To calculate the mean and standard deviation, three samples under each condition were measured. The primer and probe sequences (Applied Biosystems) were designed according to previous reports[27-29]. The sequences were shown in Table 2.1.

Table 2.1 Primers and Probes used for real-time PCR analysis.

Gene	Primer 5'→3'	Probe 5'→3'
18S rRNA	(F):GCCGCTAGAGGTGAAATTCTTG	CCGGCGCAAGACGGACCAGA
	(R):CATTCTTGGCAAATGCTTTCG	
GAPDH	(F): ATGGGGAAGGTGAAGGTCG	CGCCCAATACGACCAAATCCGTTGAC
	(R): TAAAAGCAGCCCTGGTGACC	
ALP	(F): GACCCTTGACCCCCACAAT	TGGACTACCTATTGGGTCTCTTCGAGCCA
	(R): GCTCGTACTGCATGTCCCCT	
BSP	(F): TGCCTTGAGCCTGCTTCC	CTCCAGGACTGCCAGAGGAAGCAATCA
	(R):GCAAAATTAAAGCAGTCTTCATTTTG	

2.3.10 Immunocytochemical staining of type II collagen

To check the chondrogenic differentiation of the MSCs cultured in chondrogenic medium, type II collagen was immunocytochemically stained using mouse anti-human type II collagen monoclonal antibody (Neomarkers, Fremont, CA) and Dako Peroxidase K and Dako EnVision+System-HRP (DAB) kit according to the instructions. Briefly, after 14 and 28 days of culture in chondrogenic medium, the cultured cells were rinsed with PBS three times and fixed with 4% paraformaldehyde for 10 min at 4 ºC. The fixed cells were incubated with Proteinase K in Tris-buffered saline (1:50 working dilution, pH 7.4, TBS) for 5 min, and then blocked with peroxidase blocking solution for 5 min and 2% bovine serum albumin (BSA) solution for 30 min. The cells were then incubated with anti-type II collagen antibody (1:100 working dilution) for 1 h. The

peroxidase labeled polymer conjugated to goat anti-mouse immunoglobulins was applied for 30 min followed by incubation with DAB substrate/chromogen solution for 5 min to visualize the bound antibodies. All incubations were at room temperature.

2.3.11 Statistical analysis

A one-way analysis of variance (ANOVA) with Tukey's *post hoc* test for multiple comparisons was used for statistical analysis. A value of $p < 0.05$ was considered statistically significant difference.

2.4 Results

2.4.1 Synthesis of photo-reactive PVA

Photo-reactive PVA was synthesized by coupling the hydroxyl groups of PVA with 4-azidobenzoic acid. The introduction of photoreactive azido groups in AzPhPVA was confirmed by UV and ^{1}H-NMR spectrum. The UV spectra of PVA, 4-azidobenzoic acid, and photo-reactive PVA are shown in Figure 2.4. No special peak appeared in PVA spectrum, whereas the characteristic peak of 4-azidobenzoic acid was 270.6 nm. After azidophenyl groups were introduced into PVA, the characteristic peak shifted to 275.4 nm. Figure 2.5 is the ^{1}H-NMR spectrum of the synthesized photo-reactive PVA. The appearance of peaks assigned to the azidophenyl protons in photo-reactive PVA was around 7.2 and 8.0 ppm. The percentage of the hydroxyl groups in PVA coupled with the azidophenyl groups determined by peak integration was 2.1%.

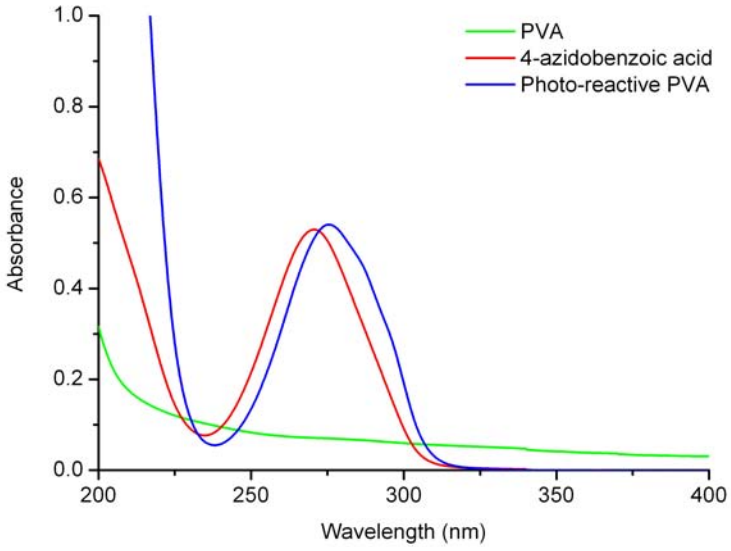

Figure 2.4 UV spectra of PVA, 4-azidobenzoic acid, and photo-reactive PVA.

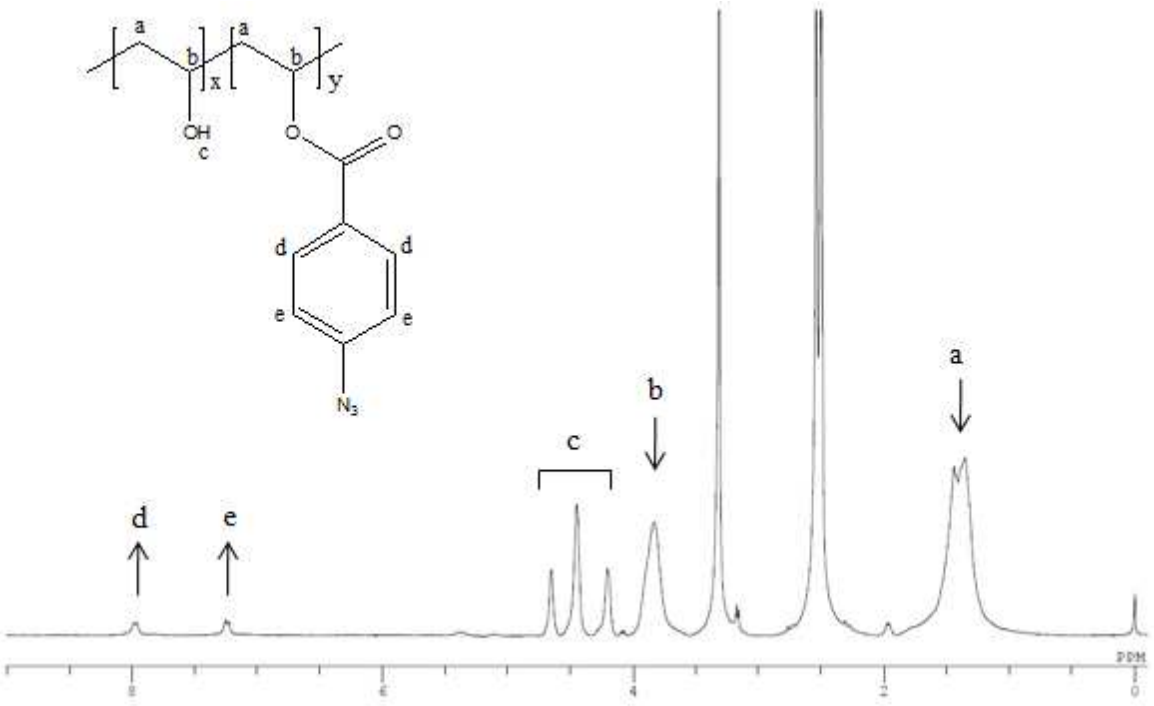

Figure 2.5 ^{1}H-NMR spectrum of the synthesized photo-reactive PVA.

2.4.2 Preparation and characterization of PVA-micropatterned PSt surface

A PSt plate was coated with an aqueous solution of photo-reactive PVA and air-dried in the dark. The cast plate was covered with a photomask and irradiated by UV light. The photomask, consisting of UV-non-transparent dark squares and surrounding UV-transparent domains, had three regions: region A, B, and C. The side length of each dark square was 200 μm and the center-to-center distance between neighboring squares was 400, 1,000, and 1,414 μm for region A, B, and C, respectively (Figure 2.6a). The photo-reactive PVA in the irradiated areas was inter- and intra-molecularly crosslinked and grafted to the PSt surface. The photo-reactive PVA covered by the dark squares that was protected from the UV light remained unreacted. The unreacted photo-reactive PVA was removed by washing with Milli-Q water. Observation with a phase contrast microscope demonstrated the formation of a PVA micropattern on the PSt plate (Figure 2.6). A PVA-grafted region surrounded the PSt squares, reflecting the pattern of UV-transparent parts of the photomask. The PSt squares reflected the UV-non-transparent dark square of the photomask. The PSt squares had the same properties as that of the cell-culture PSt plate and supported cell adhesion. However, the PVA-grafted region inhibited protein adsorption and cell adhesion. The ratio of the surface area of the PSt squares to that of the surrounding PVA-grafted surface in region A, B, and C was 1:4, 1:25, and 1:50, respectively.

The PVA-micropatterned PSt surface in Milli-Q water was observed by AFM. The height and three-dimensional images of the border between PVA and PSt are shown in Figure 2.6b, c. The step height of the micropatterned PVA layer was 50.1 ± 4.1 nm. The AFM images obtained in water reflected the real surface topography of the micropatternd surfaces during cell culture.

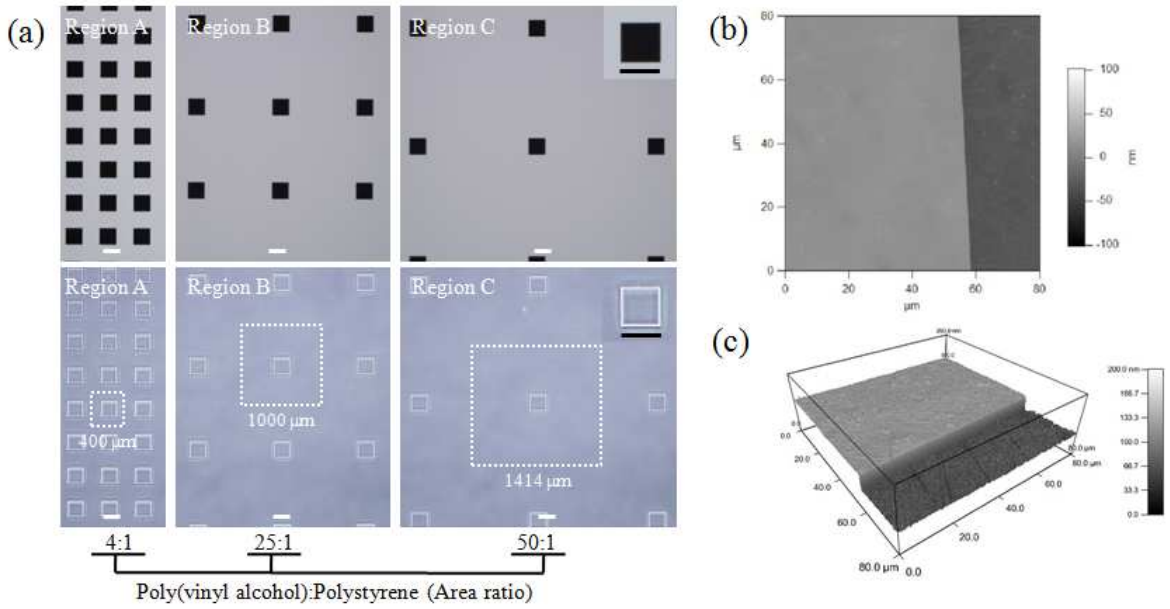

Figure 2.6 Characterization of photomask and PVA-micropatterned PSt surface. (a) Phase contrast micrographs of photomask (upper panel) and the resulting PVA-micropatterned PSt surface (lower panel). The photomask has three regions of A, B, and C. The dark squares are UV-non-transparent and the surrounding bright areas are UV-transparent. The white-dashed squares indicate the hypothetical cell non-adhesive PVA squares that surrounded the central cell-adhesive PSt squares. The numbers under the photomicrographs indicate the area ratio of PVA-grafted surface to polystyrene squares in each region. AFM height (b) and three-dimensional (c) images of the PVA-micropatterned PSt surface measured in Milli-Q water in contact mode. The light gray region is PVA and dark gray region is PSt. Scale bars: 200 μm.

2.4.3 Cell adhesion and distribution on PVA-micropatterned PSt surface

MSCs were seeded on the micropatterned surface. Immediately after cell seeding, the cells distributed evenly on the micropatterned surface (Figure 2.7a). The cell density on the micropatterned surface immediately after cell seeding was $2.5 \pm 0.5 \times 10^3$ cells/cm^2, which could be considered as the seeded cell density. During cell culture, the cells on the PVA-grafted surface moved to the PSt squares because the PVA effectively prevented cell adhesion. From regions A, B, and C, the surface area of each PSt square was constant while the distance between the PSt squares gradually increased. Assuming that all the cells on the PVA-grafted surface moved to the cell-adhesive PSt squares (Figure 2.6a), the cell densities from region A to C should be the same as the surface area ratio of the surrounding PVA-grafted surface to the PSt square. That is, the cell densities from region A to C would theoretically be 4, 25, and 50 times that of the seeded cell density. After 1 day of culture, cell adhesion and distribution were simultaneously regulated on the PVA-micropatterned PSt plate (Figure 2.7b-e). The cells adhered to the bare PSt plate region without patterning and grafting of PVA (non-pattern surface), and PSt squares of regions A, B, and C. The cells spread after 1 day of culture. The cells in the non-pattern region and region A were sparse and those in region C were dense.

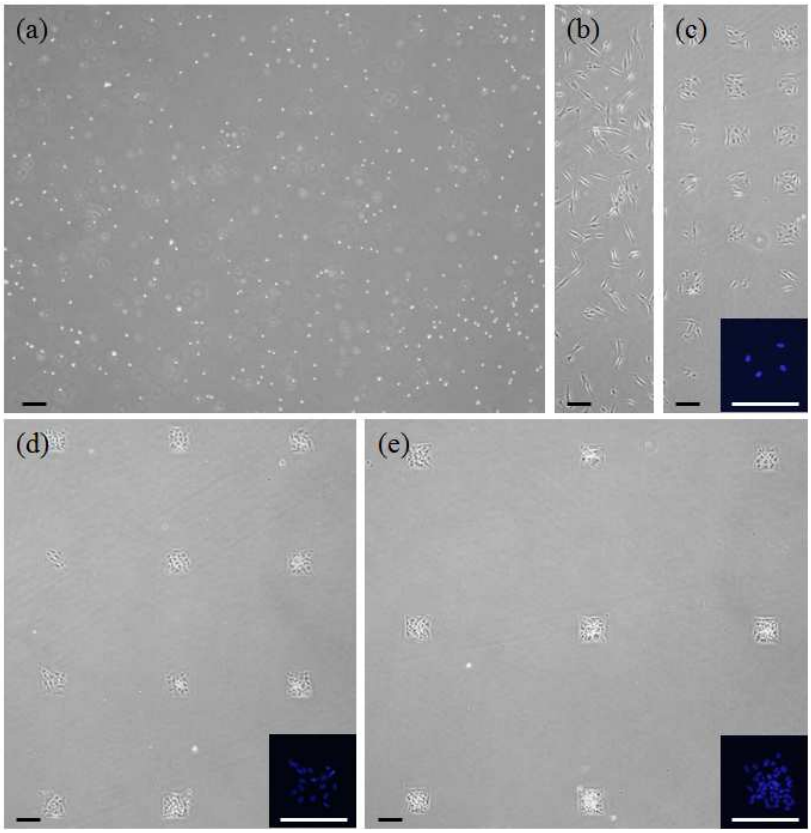

Figure 2.7 Phase contrast micrographs of MSCs cultured on PVA-micropatterned PSt plate for 10 min (a) and for 1 day in non-pattern region (b), region A with low cell density (c), region B with medium cell density (d), and region C with high cell density (e). The insets are representative fluorescent images of the nuclei of MSCs adhered to PSt squares. Scale bars: 200 μm.

The number of cells in each region was counted by staining the cell nuclei with DAPI. The cell density in the non-pattern region and regions A, B, and C was 2.6 ± 0.6, 10.0 ± 2.5, 50.0 ± 15.0, and 112.5 ± 10.0×10^3 cells/cm^2, respectively (Figure 2.8). The ratio of cell density in the non-pattern region and regions A, B, and C to the seeded cell density was 1.0 ± 0.2, 4.0 ± 1.0, 20.0 ± 6.0, and 45.0 ± 4.0, respectively. These results indicate that cell density could be adjusted by controlling the ratio of cell-adhesive and non-adhesive areas and a cell density gradient with a wide range (2.6 to 112.5×10^3 cells/cm^2) was formed on the PVA-micropatterned PSt surface.

2.4.4 Cell proliferation on PVA-micropatterned PSt surface

The proliferation of MSCs on the micropatterned surface during osteogenic culture was evaluated by counting the number of cells. The cells were stained with DAPI and the number of cells in the non-pattern region and regions A, B, and C of the micropatterned surface was counted after 1, 3, 7, and 14 days of culture (Figure 2.9). When the initial cell density was low or medium (non-pattern region, regions A and B), the MSCs proliferated with culture time. However, when the initial cell density was high (region C), the cells proliferated for the first 3 days and then stopped proliferating. These results suggest that low cell density is favorable for MSC proliferation during osteogenic culture.

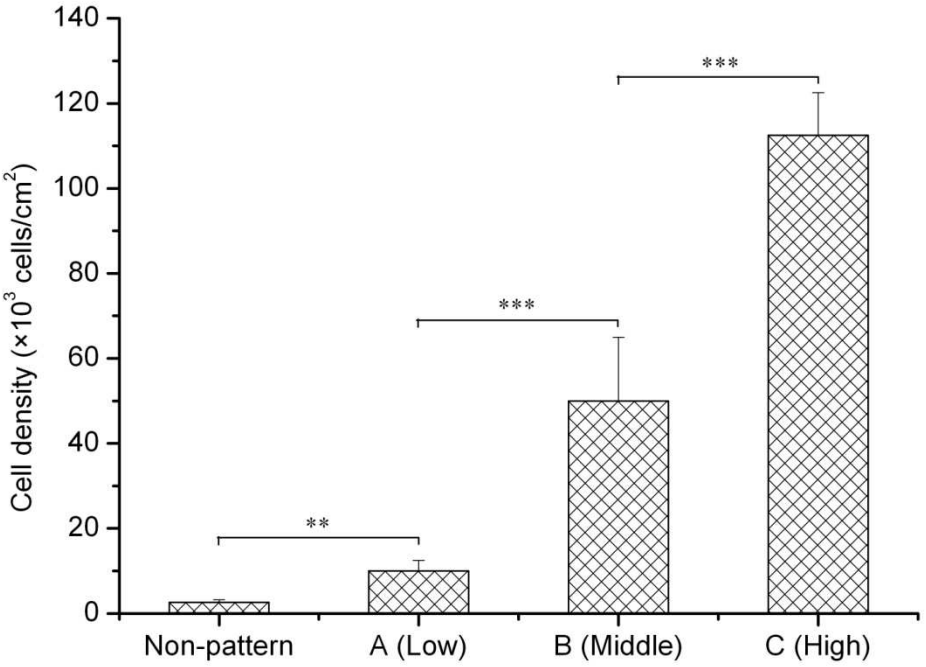

Figure 2.8 Cell density in non-pattern region and regions A, B, and C on PVA-micropatterned PSt plate after 1 day of culture. Non-pattern represents the region without patterning and grafting of PVA. Data represent mean ± SD (n = 3). ** $p < 0.01$ and *** $p < 0.001$.

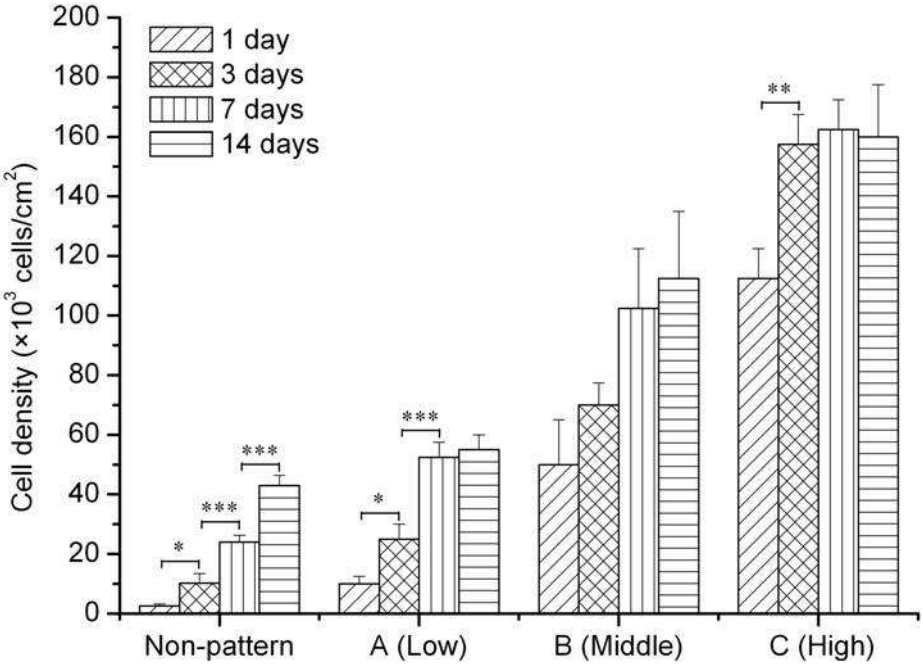

Figure 2.9 Proliferation of MSCs in non-pattern region and regions A, B, and C after culture in osteogenic medium for 1, 3, 7, and 14 days. Data represent mean ± SD (n = 3). * $p < 0.5$, ** $p < 0.01$, and *** $p < 0.001$.

2.4.5 Cell viability on PVA-micropatterned PSt surface

Cell viability was evaluated by live/dead staining after the MSCs were cultured on the

PVA-micropatterned PSt surface for 2 weeks. The results are shown in Figure 2.10. After staining, live cells showed green color while dead cells showed red color. Green living cells were observed on both micropatterned PSt square and non-patterned PSt region. Very few red dead cells can be detected on PVA-micropatterned PSt surface. The results indicate that the MSCs on PVA-micropatterned PSt surface had high viability as those on normal cell-culture PSt surface. The PVA-micropatterned PSt surface can keep the cell viability during long-term cell culture.

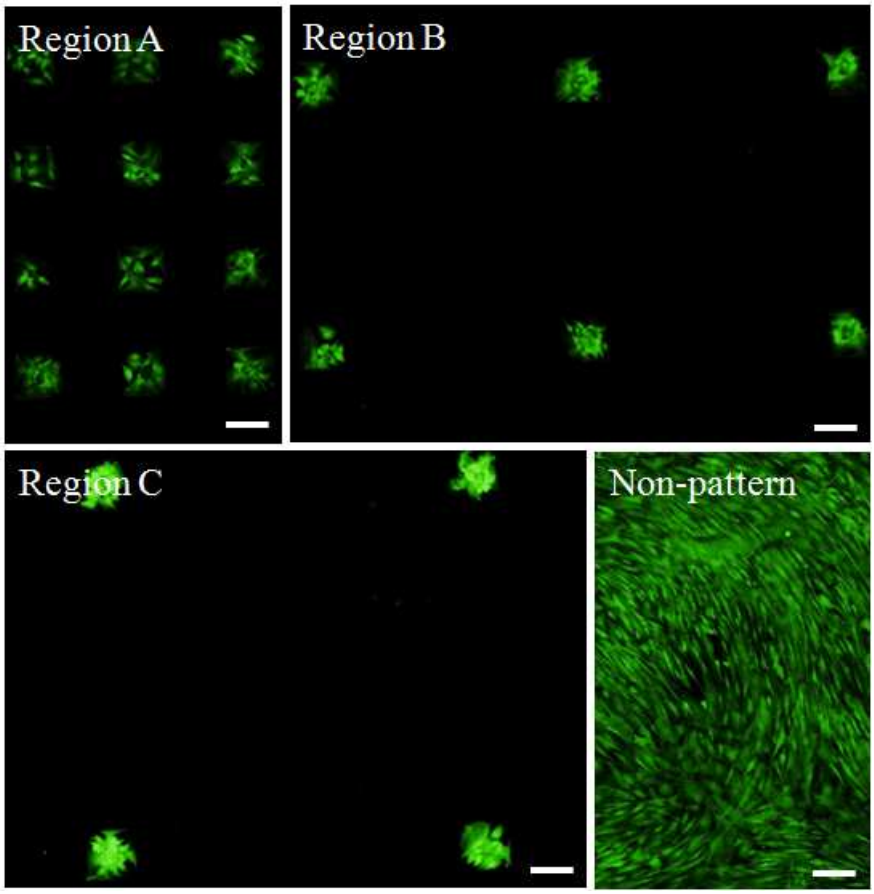

Figure 2.10 Fluorescenct images of Live/dead staining of MSCs cultured on a PVA-micropatterned PSt plate in control medium for 14 days. Scale bars: 200 μm.

2.4.6 Osteogenic differentiation of MSCs on PVA-micropatterned PSt surface

To investigate the effect of cell density gradient on the osteogenic differentiation of MSCs, ALP staining was performed after MSCs were cultured on a PVA-micropatterned PSt surface in osteogenic medium for 3, 5, 7, and 14 days (Figure 2.11). The osteogenic differentiation of MSCs in regions A, B, and C and non-pattern region was compared. The extent of the MSC osteogenesis depended on cell density and culture time as evidenced by ALP staining. At high cell density in region C, MSCs were positively stained after 3 days of culture. At medium cell density in region B, MSCs were only slightly stained after 3 days of culture but positively stained after 5 days of culture. At low cell density in region A and the non-pattern region, MSCs were not positively stained after 3 days and only slightly stained after 5 days of culture but positively stained after 7 days of culture. However, MSCs did not show osteogenic differentiation at any cell density when MSCs on the micropatterned surface were cultured in control medium without osteogenic induction factors.

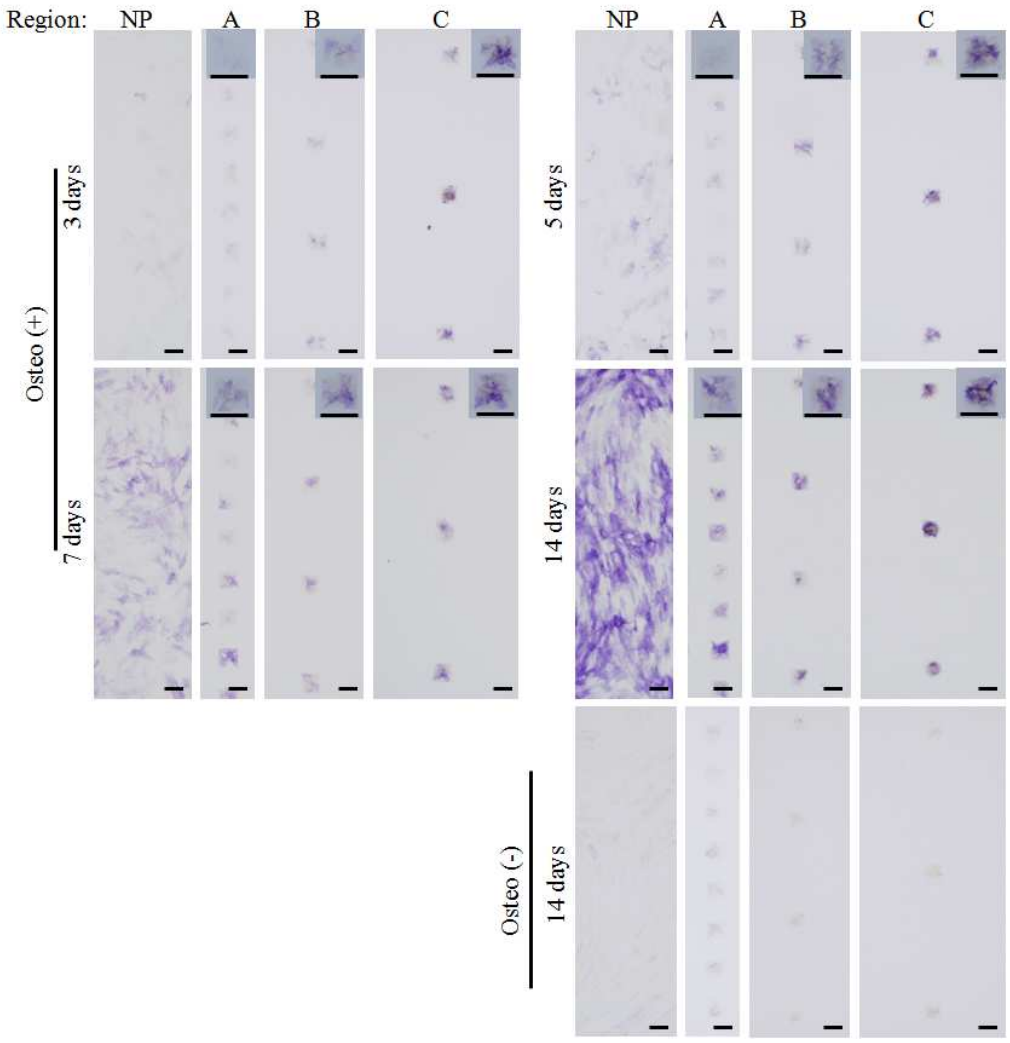

Figure 2.11 Optical micrographs of ALP staining of MSCs cultured on a PVA-micropatterned PSt plate in osteogenic medium for 3, 5, 7, and 14 days and control medium for 14 days. The insets are representative magnification images of MSCs adhered to PSt squares. NP: non-pattern region. Osteo (+) and Osteo (-) represent the presence and absence of osteogenic induction factors, respectively. Scale bars: 200 μm.

The effect of cell density on the expression of genes relative to osteogenic differentiation was checked by real-time PCR. The MSCs were seeded into cell-culture plates and cultured in the osteogenic medium for 3 and 7 days. The seeded cell densities were 2.5, 10, 50, and 100×10^3 cells/cm^2, corresponded to the cell densities on non-pattern region, region A, B and C of PVA-micropatterned PSt plate. The osteogenesis marker genes encoding alkaline phosphatase (*ALP*) and bone sialoprotein (*BSP*) were detected (Figure 2.12). *ALP* is an early osteoblast marker[30] while *BSP* is characteristic of the late stage of osteoblastic differentiation[31]. The MSCs of passage 4 expressed very low level of gene encoding *ALP* and they did not express gene encoding *BSP*. After 3 days of culture, the lowest cell density did not express gene encoding *BSP* and both the *ALP* and *BSP* expression levels increased with the increase of cell densities. However, after 7 days of culture, there was no significant difference in the *ALP* expression levels among different cell densities, whereas the higher cell densities expressed higher *BSP* expression levels than did the lower cell densities.

The staining and gene expression results suggest that high cell density stimulated osteogenic

differentiation more quickly than did low cell density though MSCs at all cell densities eventually underwent osteogenic differentiation.

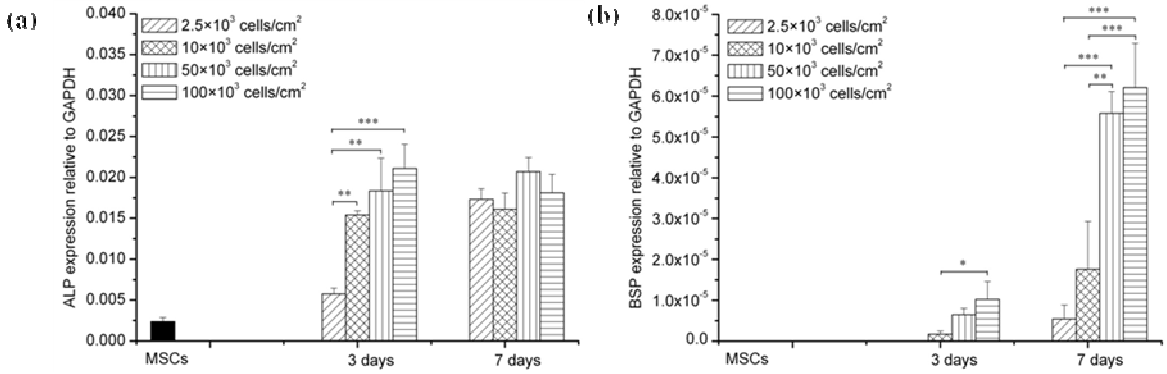

Figure 2.12 Real-time PCR results of mRNA expression of *ALP* (a) and *BSP* (b) genes of MSCs cultured at four different cell densities in cell-culture PSt plates in osteogenic medium for 3 and 7 days. The data are normalized to *GAPDH* and represent mean ± SD (n = 3). * $p < 0.5$; ** $p < 0.01$; and *** $p < 0.001$.

2.4.7 Chondrogenic differentiation of MSCs on PVA-micropatterned PSt surface

The correlation between initial cell density gradient and MSC chondrogenic differentiation was investigated by immunocytochemical staining of type II collagen, which is a specific chondrogenic marker (Figure 2.13). In the presence of chondrogenic induction factors, chondrogenesis of MSCs in regions A, B, and C and the non-pattern region was different due to the difference in initial cell density. Chondrogenesis of MSCs at low cell density in region A and the non-pattern region was not detected even after 4 weeks of chondrogenic culture. The MSCs at medium cell density in region B showed negative staining after 2 weeks of culture, but weak staining after 4 weeks of culture. The staining of MSCs at high cell density in region C was positive and stable after 2 and 4 weeks of culture. In the absence of chondrogenic induction factors, however, the MSCs did not show evidence of chondrogenesis in any region according to type II collagen staining. These results suggest that high cell density is required for chondrogenic differentiation of MSCs.

2.5 Discussion

PVA was chosen as the non-fouling layer because of its superior ability to resist protein adsorption and cell adhesion in aqueous culture medium. To immobilize PVA on cell-culture substrate, photo-reactive azidophenyl groups were coupled with hydroxyl groups in PVA via typical esterification reaction. Upon UV irradiation, the photolyzed azidophenyl groups generated a highly reactive intermediate, phenyl nitrene, which can react with neighboring atoms to form a covalent bond. Therefore, photo-reactive PVA can be expediently grafted to cell-culture substrate using UV light. This simple synthesis method is easy to be adopted by common cell biology laboratory.

A PVA-micropatterned PSt plate was prepared using photo-reactive PVA and UV photolithography. Because this micropatterning method uses photo-generated radical reactions that occur on every organic substrate such as biological matrix and polymeric materials, any special functional groups are not required such as amino, carboxyl, hydroxyl, and thiol groups. Therefore, different molecules can be immobilized by the same method, distinguishing this method from other conventional immobilization methods.

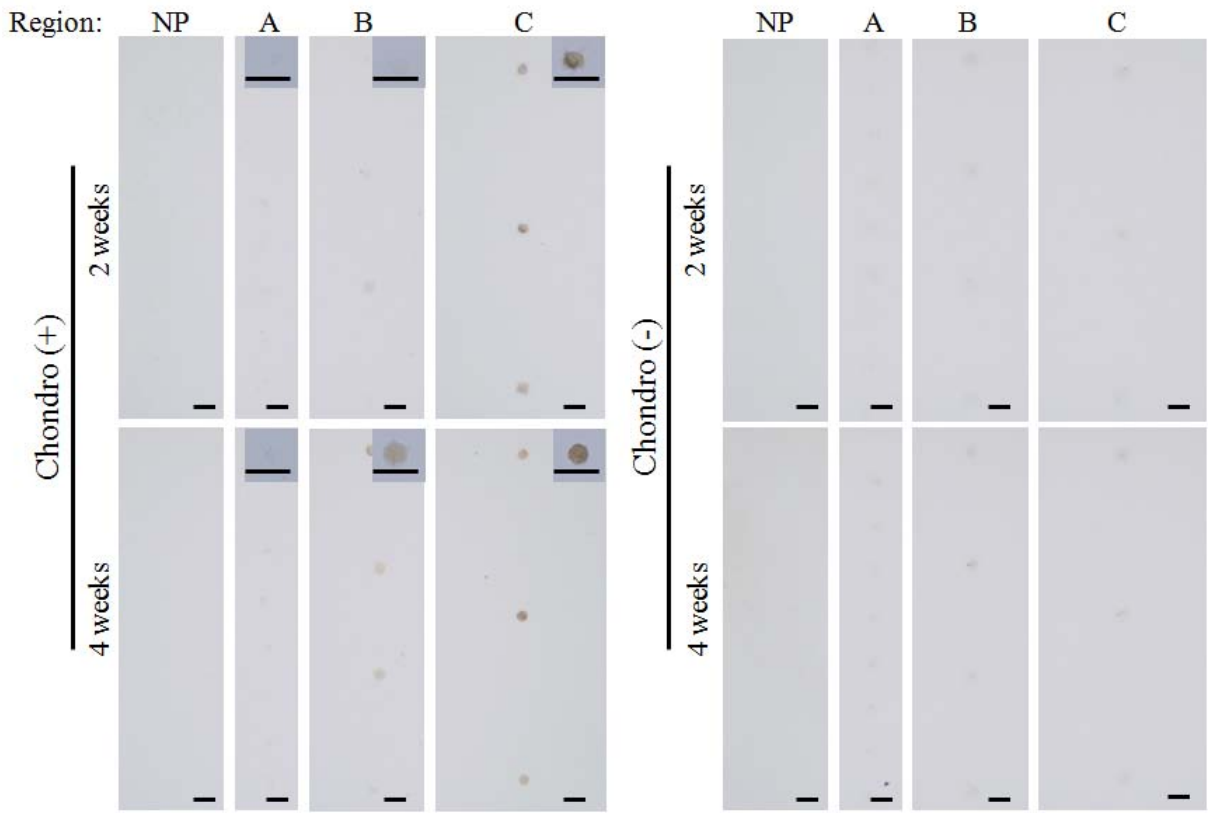

Figure 2.13 Optical micrographs of immunocytochemical staining of type II collagen of MSCs cultured on PVA-micropatterned PSt plate in the presence and absence of chondrogenic induction factors for 2 and 4 weeks. The insets are representative magnification images of MSCs adhered to PSt squares. NP: non-pattern region. Chondro (+) and Chondro (-) represent the presence and absence of chondrogenic induction factors, respectively. Scale bars: 200 μm.

The formation of a cell density gradient with a wide range (2.6 to 112.5×103 cells/cm2) was realized by modulating the area ratio of a central cell-adhesive PSt square and surrounding non cell-adhesive PVA domain. Control over different cell densities on the same plate provided a useful platform to compare the celldensity effect on stem cell functions directly, efficiently, and systematically. For this reason, the osteogenic and chondrogenic differentiation of MSCs on a PVA-micropatterned PSt plate was investigated.

During osteogenic culture, MSCs at a low cell density proliferated continuously while MSCs at a high cell density stopped proliferating after 3 days of culture. This result is consistent with previous reports[32,33]. The cells at low density distributed separately and sparsely on the surface. There was enough space for cell proliferation. The space for cell proliferation decreased as the cell density increased. The MSCs at 112.5×10^3 cells/cm^2 were compactly positioned on the surface and the space available for cell proliferation was very limited. The MSCs showed high viability on PVA-micropatterned PSt surface after 2 weeks culture, which indicated the superiority of micropatterned surface for long-term cell culture. ALP staining indicated that MSCs at a cell density range of 2.6 to 112.5×10^3 cells/cm^2 showed osteogenic differentiation with the synergistic effect of osteogenic induction factors in the culture medium. High cell density initiated osteogenic differentiation more quickly than did low cell density (within 3 days) as demonstrated by staining and gene expression. The possible reason might be that during the initial 3 days, compared with low cell density, incipient high cell density enhanced cell-cell contact, interaction, and thus osteogenic differentiation[20,34]. The cells at low density showed high proliferation capacity other than

osteogenic differentiation. The continuous cell proliferation increased cell density and might induced osteogenic differentiation later. It has been reported that a low plating density of MSCs could facilitate osteogenic differentiation after 1 week of culture[18]. Therefore, the degree of osteogenic differentiation of MSCs was determined by cell density and culture time.

As for the chondrogenic differentiation of MSCs, previous reports showed that higher cell density exhibited more cartilage matrix and cartilage-specific gene expression[35,36]. Our results of the immunocytochemical staining of type II collagen also indicated that high cell density was required for the chondrogenic differentiation of MSCs. Presumably, high cell density prevents the cells from spreading and flattening; thus the chondrogenic genes were upregulated[37].

2.6 Conclusions

Photo-reactive PVA was synthesized by introducing azidophenyl groups in PVA. A PVA-micropatterned PSt plate was prepared by UV photolithography with a photomask. By keeping the area of the central PSt squares constant and gradually increasing the area of the surrounding PVA-grafted surface, a cell density gradient was formed on the micropatterned surface, enabling investigation of the effect of different cell densities on the osteogenic and chondrogenic differentiation of MSCs on a single surface. High cell density induced the osteogenic differentiation of MSCs more quickly than did low cell density, whereas low cell density facilitated cell proliferation. High cell density was necessary to induce the chondrogenic differentiation of MSCs. Therefore, this micropatterning method allowed convenient manipulation of cell distribution in a density gradient manner for the direct and systematic investigation of stem cell functions related to cell density.

2.7 References

1. Pittenger, M. F., Mackay, A. M., Beck, S. C., Jaiswal, R. K., Douglas, R., Mosca, J. D., Moorman, M. A., Simonetti, D. W., Craig, S., Marshak, D. R., Multilineage ptential of ault hman msenchymal sem clls. *Science* **284**, 143-147 (1999).
2. Second, T., Hospital, A., Rat crtilage rpair uing nnophase PLGA/HA cmposite and msenchymal sem clls. *J Bioact Compat Polym* **24**, 83-99 (2009).
3. Danmark, S., Finne-Wistrand, A., Wendel, M., Arvidson, K., Albertsson, A. C., Mustafa, K., Osteogenic dfferentiation by rat bone marrow stromal cells on customized biodegradable polymer scaffolds. *J Bioact Compat Polym* **25**, 207-223 (2010).
4. Discher, D. E., Mooney, D. J., Zandstra, P. W., Growth factors, matrices, and forces combine and control stem cells. *Science* **324**, 1673-1677 (2009).
5. Alberti, K., Davey, R. E., Onishi, K., George, S., Salchert, K., Seib, F. P., Bornhäuser, M., Pompe, T., Nagy, A., Werner, C., Zandstra, P. W., Functional immobilization of signaling proteins enables control of stem cell fate. *Nat Methods* **5**, 645-650 (2008).
6. Marklein, R. A., Burdick, J.,A., Controlling stem cell fate with material design. *Advanced Materials* **22**, 175-89 (2010).
7. Guilak, F., Cohen, D. M., Estes, B. T., Gimble, J. M., Liedtke, W., Chen, C. S., Control of stem cell fate by physical interactions with the extracellular matrix. *Cell Stem Cell* **5**, 17-26 (2009).

8. Watt, F. M., Out of Eden: stem cells and their niches. *Science* **287**, 1427-1430 (2000).
9. Lutolf, M. P., Gilbert, P. M., Blau, H. M., Designing materials to direct stem-cell fate. *Nature* **462**, 433-441 (2009).
10. Hoshiba, T., Kawazoe, N., Tateishi, T., Chen, G., Development of extracellular matrices mimicking stepwise adipogenesis of mesenchymal stem cells. *Adv Mater* **22**, 3042-3047 (2010).
11. Hoshiba, T., Kawazoe, N., Tateishi, T., Chen, G., Development of stepwise osteogenesis-mimicking matrices for the regulation of mesenchymal stem cell functions. *J Biol Chem* **284**, 31164-31173 (2009).
12. Engler, A. J., Sen, S., Sweeney, H. L., Discher, D. E., Matrix elasticity directs stem cell lineage specification. *Cell* **126**, 677-689 (2006).
13. Dalby, M. J., Gadegaard, N., Tare, R., Andar, A., Riehle, M. O., Herzyk, P., Wilkinson, C. D., Oreffo, R. O., The control of human mesenchymal cell differentiation using nanoscale symmetry and disorder. *Nat Mater* **6**, 997-1003 (2007).
14. Benoit, D. S. W., Schwartz, M. P., Durney, A. R., Anseth, K. S., Small functional groups for controlled differentiation of hydrogel-encapsulated human mesenchymal stem cells. *Nat Mater* **7**, 816-823 (2008).
15. Guo, L., Kawazoe, N., Fan, Y., Ito, Y., Tanaka, J., Tateishi, T., Zhang, X., Chen, G., Chondrogenic differentiation of human mesenchymal stem cells on photoreactive polymer-modified surfaces. *Biomaterials* **29**, 23-32 (2008).
16. Lee, I. C., Wang, J. H., Lee, Y. T., Young, T. H., The differentiation of mesenchymal stem cells by mechanical stress or/and co-culture system. *Biochem Biophys Res Commun* **352**, 147-152 (2007).
17. Song, S. J., Jeon, O., Yang, H. S., Han, D. K., Kim, B. S., Effects of culture conditions on osteogenic differentiation in human mesenchymal stem cells. *J Microbiol Biotechnol* **17**, 1113-1119 (2007).
18. McBeath, R., Pirone, D. M., Nelson, C. M., Bhadriraju, K., Chen, C. S., Cell shape, cytoskeletal tension, and RhoA regulate stem cell lineage commitment. *Dev Cell* **6**, 483-495 (2004).
19. Kim, K., Dean, D., Mikos, A. G., Fisher, J. P., Effect of initial cell seeding density on early osteogenic signal expression of rat bone marrow stromal cells cultured on cross-linked poly(propylene fumarate) disks. *Biomacromolecules* **10**, 1810-1817 (2009).
20. Jaiswal, N., Haynesworth, S. E., Caplan, A. I., Bruder, S. P., Osteogenic differentiation of purified, culture-expanded human mesenchymal stem cells in vitro. *J Cell Biochem* **64**, 295-312 (1997).
21. Théry, M., Racine, V., Pépin, A., Piel, M., Chen, Y., Sibarita, J. B., Bornens, M., The extracellular matrix guides the orientation of the cell division axis. *Nat Cell Biol* **7**, 947-953 (2005).
22. Khademhosseini, A., Langer, R., Borenstein, J., Vacanti, J. P., Microscale technologies for tissue engineering and biology. *Proc Natl Acad Sci USA* **103**, 2480-2487 (2006).
23. Barbucci, R., Lamponi, S., Magnani, A., Pasqui, D., Micropatterned surfaces for the control of endothelial cell behaviour. *Biomol Eng* **19**, 161-170 (2002).
24. Chang, W. C., Sretavan, D. W., Novel high-resolution micropatterning for neuron culture using polylysine adsorption on a cell repellant, plasma-polymerized background. *Langmuir* **24**, 13048-13057 (2008).
25. Cheng, X., Wang, Y., Hanein, Y., Böhringer, K. F., Ratner, B. D., Novel cell patterning using microheater-controlled thermoresponsive plasma films. *J Biomed Mater Res A* **70**, 159-168 (2004).
26. Cho, W. K., Kong, B., Park, H. J., Kim, J., Chegal, W., Choi, J. S., Choi, I. S., Long-term stability of cell micropatterns on poly((3-(methacryloylamino)propyl)-dimethyl(3-sulfopropyl)ammonium hydroxide)-patterned silicon oxide surfaces. *Biomaterials* **31**, 9565-9574 (2010).

27. Martin, I., Jakob, M., Schäfer, D., Dick, W., Spagnoli, G., Heberer, M., Quantitative analysis of gene expression in human articular cartilage from normal and osteoarthritic joints. *Osteoarthritis Cartilage* **9**, 112-118 (2001).
28. Guo, L., Kawazoe, N., Hoshiba, T., Tateishi, T., Chen, G., Zhang, X., Osteogenic differentiation of human mesenchymal stem cells on chargeable polymer-modified surfaces. *J Biomed Mater Res A* **87**, 903-912 (2008).
29. Schaefer, J. F., Millham, M. L., De Crombrugghe, B., Buckbinder, L., FGF signaling antagonizes cytokine-mediated repression of Sox9 in SW1353 chondrosarcoma cells. *Osteoarthritis Cartilage* **11**, 233-241 (2003).
30. Aubin, J. E., Osteoprogenitor cell frequency in rat bone marrow stromal populations: role for heterotypic cell-cell interactions in osteoblast differentiation. *J Cell Biochem* **72**, 396-410 (1999).
31. Zur Nieden, N. I., Kempka, G., Ahr, H. J., In vitro differentiation of embryonic stem cells into mineralized osteoblasts. *Differentiation* **71**, 18-27 (2003).
32. Lode, A., Bernhardt, A., Gelinsky, M., Cultivation of human bone marrow stromal cells on three-dimensional scaffolds of mineralized collagen : influence of seeding density on colonization, proliferation and osteogenic differentiation. *J Tissue Eng Regen Med* **2**, 400-407 (2008).
33. Both, S. K., van der Muijsenberg, A. J. C., van Blitterswijk, C. A., de Boer, J., de Bruijn, J. D., A rapid and efficient method for expansion of human mesenchymal stem cells. *Tissue Eng* **13**, 3-9 (2007).
34. Tang, J., Peng, R., Ding, J., The regulation of stem cell differentiation by cell-cell contact on micropatterned material surfaces. *Biomaterials* **31**, 2470-2476 (2010).
35. Koga, H., Muneta, T., Nagase, T., Nimura, A., Ju, Y. J., Mochizuki, T., Sekiya, I., Comparison of mesenchymal tissues-derived stem cells for in vivo chondrogenesis: suitable conditions for cell therapy of cartilage defects in rabbit. *Cell Tissue Res* **333**, 207-215 (2008).
36. Huang, C. Y. C., Reuben, P. M., D'Ippolito, G., Schiller, P. C., Cheung, H. S., Chondrogenesis of human bone marrow-derived mesenchymal stem cells in agarose culture. *Anat Rec A Discov Mol Cell Evol Biol* **278**, 428-436 (2004).
37. Gao, L., McBeath, R., Chen, C. S., Stem cell shape regulates a chondrogenic versus myogenic fate through Rac1 and N-cadherin. *Stem Cells* **28**, 564-572 (2010).

Chapter 3

Manipulation of cell spreading on PVA-micropatterned PSt surface

3.1 Summary

In this chapter, poly(vinyl alcohol) (PVA)-micropatterned polystyrene (PSt) surfaces were prepared using photo-reactive PVA and UV photolithography with a photomask. The micropatterned surface was suitable for single-cell array formation and long-term cell culture due to the nanometer thickness of non-adhesive PVA layer. Different degrees of cell spreading with the same cell shape were established by adjusting the sizes of circular, cell-adhesive PSt micropatterns. Cell spreading and differentiation of human mesenchymal stem cells (MSCs) on the micropatterns were investigated at the single-cell level. The assembly and organization of the cytoskeleton were regulated by the degree of cell spreading. Individual MSCs on large circular micropatterns exhibited a more ordered arrangement of actin filaments than did those on the small circular micropatterns. Furthermore, the differentiation of MSCs was dependent on the degree of cell spreading. Increased cell spreading facilitated the osteogenic differentiation but suppressed the adipogenic differentiation of MSCs.

3.2 Introduction

Stem cells, a reservoir of undifferentiated cells with the capacity for unlimited or prolonged self-renewal, have the potential to produce differentiated and specialized progenies[1]. They hold the key to a number of cellular processes, including development, tissue regeneration, and aging, and the promise of cures for many diseases and injuries. They are a versatile and promising cell source for tissue engineering and regenerative medicine[2].

The inherent plasticity and multi-lineage potential of stem cells have brought about the requirement for strictly controlling cell functions, such as growth, phenotypic expression, and differentiation[3-7]. Traditionally, the fate of stem cells has been regulated by biological factors, such as cytokines and growth factors[8-11]. Recently, more and more evidence has revealed that physical factors also contribute to the overall behaviors and functions of stem cells[12-16]. The area of cell spreading is one such physical factor that has been demonstrated to affect cell behaviors and functions. Bhadriraju and Hansen[17] have reported that the stiffness of hepatocytes is affected by cell spreading. Cell stiffness increases with cell spreading but remains low in

cells with round morphology. Szabo *et al.*[18] have demonstrated the high adipogenic potential of wild-type embryonic stem cells (ESCs) on non-adhesive substrata, where cell spreading is hindered. However, during routine cell culture, the process of cell spreading is often accompanied by a change in cell shape, the area of cell spreading is diverse among cells, and the heterogeneity within a cell population, such as cell-cell interaction, is complex. Therefore, a convenient method for strictly controlling the spreading area of a large number of individual cells with the same shape is extremely desirable for investigating the effect of cell spreading on cell functions.

Micropatterning technology[19] is particularly suitable for this purpose and is already used for investigating the effects of physical parameters on cell behaviors, such as the orientation of the cell division axis[20], the area for cell adhesion[21], left-right asymmetry of cell aggregates[22], cell polarization[23-25], proliferation[26], apoptosis[27], and differentiation[28]. However, one of the main obstacles in applying cell micropatterning technologies is that few of them are compatible with long-term cell culture. Extended culture time is normally required because many cell functions, such as differentiation, need a long time to respond to external stimuli.

In this chapter, we prepared poly(vinyl alcohol) (PVA)-micropatterned polystyrene (PSt) surfaces using UV photolithography with a photomask. This method is simple and reproducible. The micropatterned surfaces were used to culture human mesenchymal stem cells (MSCs), form a stable cell array at the single-cell level for long-term cell culture, and compare the effect of cell spreading on the adipogenic and osteogenic differentiation of individual MSCs.

3.3 Materials and methods

3.3.1 Synthesis of azidophenyl-derivatized PVA

Azidophenyl-derivatized PVA (AzPhPVA) was synthesized by coupling the hydroxyl groups of PVA to 4-azidobenzoic acid as previously described in Chapter 2.3.1.

3.3.2 Fabrication of photomask

The photomask was prepared using DWL66 laser lithography system as previously described in Chapter 2.3.2.

3.3.3 Micropatterning of PVA with a photomask

A PSt plate (2.0 × 2.0 cm^2) was cut from a tissue-culture PSt flask (BD Falcon™). The photo-reactive PVA solution (0.15 mL, 0.3 mg/mL) was placed on the PSt plate and air-dried in the dark at room temperature. The coating region was around 1.5 × 1.0 cm^2. The preparation method was previously described in Chapter 2.3.3 and shown in Figure 3.1. The plates were sterilized with 70% ethanol solution and used for cell culture.

3.3.4 AFM observation

The surface topography of the PVA-micropatterned PSt plate was observed using MFP-3D-BIO™

AFM (Asylum Research). A commercially available cantilever (spring constant: 0.06 N/m; oscillation frequency: 12-24 kHz; DNP, Veeco Probes) with a silicon nitride tip was used to measure the samples (90 × 90 μm^2) in Milli-Q water in contact mode. The diameter and thickness of the circular micropattern were measured by section analysis of the acquired image. Three randomly selected micropatterns were measured to calculate the mean and standard deviation.

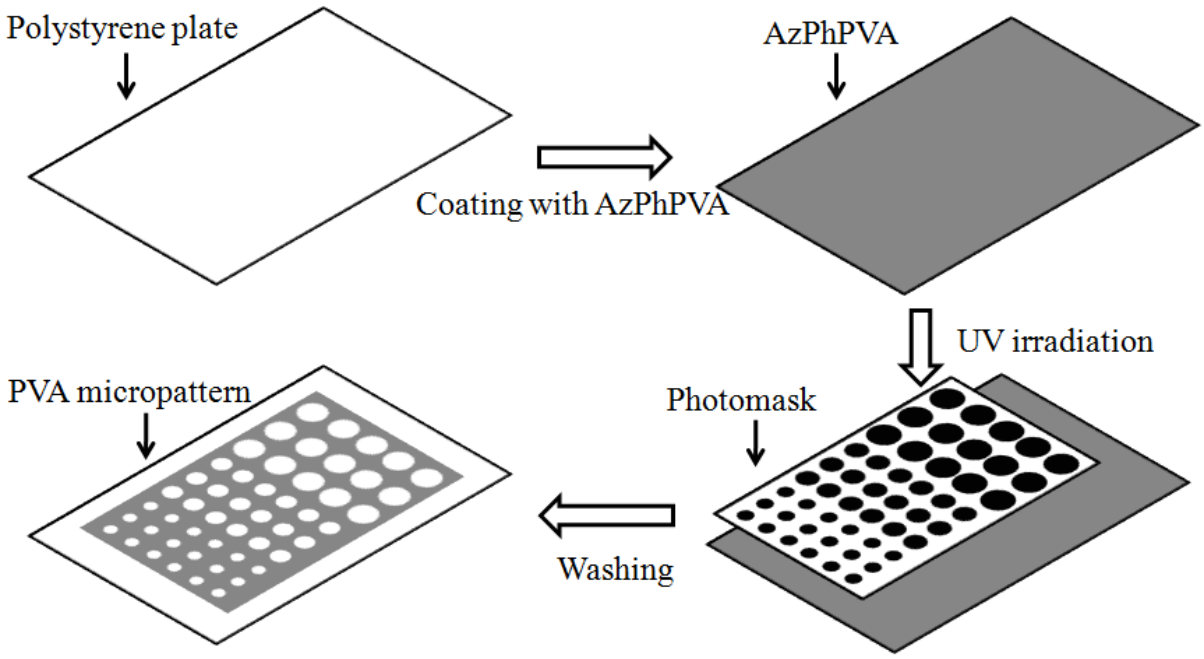

Figure 3.1 Preparation scheme of PVA-micropatterned PSt surface.

3.3.5 Cell culture

Human bone marrow-derived mesenchymal stem cells (MSCs) were obtained from Osiris Therapeutics (Columbia, MD) at passage 2. The cells were subcultured twice as previously described in Chapter 2.3.4 and used at passage 4.

The micropatterned PSt plates were placed in 6-well cell culture plates, and a glass ring (diameter: 15 mm; height: 10 mm) was placed over each PVA-micropatterned PSt plate. 3 mL control medium was added to each well, and then the cell suspension (0.36 mL, 1.5×10^4 cells/mL) was placed inside the glass ring (seeding density: 3.0×10^3 cells/cm^2). The compositions of control medium were previously described in Chapter 2.3.4.

After 6 h, the glass rings were removed, and the control medium was replaced with adipogenic or osteogenic medium. The adipogenic medium consisted of DMEM supplemented with 4500 mg/L glucose, 584 mg/L glutamine, 100 U/mL penicillin, 100 μg/mL streptomycin, 0.1 mM nonessential amino acids, 0.4 mM proline, 50 mg/L ascorbic acid, 10% FBS, 1 μM dexamethasone, 0.5 mM methyl-isobutylxanthine, 10 μg/mL insulin, and 100 μM indomethacin. The compositions of osteogenic medium were previously described in Chapter 2.3.4. The adipogenic and osteogenic media were changed every 3 days.

3.3.6 F-actin staining

After incubation for 6 h in control medium, the cultured cells were fixed with 4%

paraformaldehyde for 10 min at 4 ^{O}C, permeabilized with 0.2% Triton X-100 for 2 min, and blocked with 1% BSA solution for 30 min at room temperature. The F-actin and nuclei of cells were stained with Alexa Fluor® 488 phalloidin (Invitrogen) for 20 min and 4', 6-diamidino-2-phenylindole (DAPI, Vector Laboratories, Inc.) for 10 min, respectively. Fluorescence photographs of stained MSCs were captured by an Olympus BX51 microscope with a DP-70 CCD camera (Olympus, Tokyo, Japan).

3.3.7 Oil Red O staining

After incubation in adipogenic medium for 7 days, the cultured cells were fixed with 4% paraformaldehyde for 10 min at 4 ^{O}C, incubated in 60% isopropanol for 5 min, and then stained with fresh Oil Red O solution for 5 min. The nucleus was counterstained with 2 μg/mL DAPI solution for 10 min (Dojindo). The Oil Red O solution was prepared by mixing three parts stock solution (0.3% in isopropanol) with two parts Milli-Q water and filtering through a 0.2 μm filter. Photomicrographs were captured by an optical microscope with a DP-70 CCD camera (Olympus, Tokyo, Japan).

The probability of MSC adipogenesis at different cell spreading areas was studied by calculating the percentage of MSCs that committed to an adipocyte lineage. MSCs containing lipid vacuoles positively stained by Oil Red O were considered to be adipocytes, and only single cells on each circular micropattern (as confirmed by nuclear staining) were counted. Three samples were used to calculate the mean and standard deviation.

3.3.8 Alkaline phosphatase staining

Cellular ALP activity was assessed after culture for 7 and 21 days in osteogenic medium. The cultured cells were rinsed three times with PBS and fixed with 4% paraformaldehyde for 10 min at 4 ^{O}C. The fixed cells were soaked in 0.1% naphthol AS-MX phosphate (Sigma) and 0.1% fast red violet LB salt (Sigma) in 56 mM 2-amino-2-methyl-1,3-propanediol (pH 9.9, Sigma) for 10 min at room temperature, washed with PBS, and then observed by an optical microscope with a DP-70 CCD camera (Olympus, Tokyo, Japan).

The probability of MSC osteogenesis at different cell spreading areas was studied by calculating the percentage of MSCs that committed to an osteoblast lineage. MSCs positively stained were considered to be osteoblasts, and only single cells on each circular micropattern (as confirmed by nuclear staining) were counted. Three samples were used to calculate the mean and standard deviation.

3.3.9 Statistical analysis

A one-way analysis of variance (ANOVA) with Tukey's post hoc test for multiple comparisons was used for statistical analysis. A value of $p < 0.05$ was considered to be a statistically significant difference.

3.4 Results

3.4.1 Preparation and observation of PVA-micropatterned PSt surfaces

The AzPhPVA-coated plate was covered with a photomask and irradiated with UV light. The

photomask had three different circular micropatterns with diameters of 40, 60, and 80 μm (Figures 3.2). These circular micropatterns were UV blocking, and the underlying AzPhPVA was protected from UV light, unreacted during UV irradiation, and washed away by Milli-Q water after UV irradiation. However, the AzPhPVA under the surrounding UV transparent domains was exposed to UV light, inter- and intra-molecularly crosslinked, and grafted to the PSt surface. Therefore, three different circular PSt micropatterns were formed and surrounded by PVA domains (Figures 3.2). The circular PSt micropatterns promoted cell adhesion, whereas the surrounding PVA domains inhibited cell adhesion.

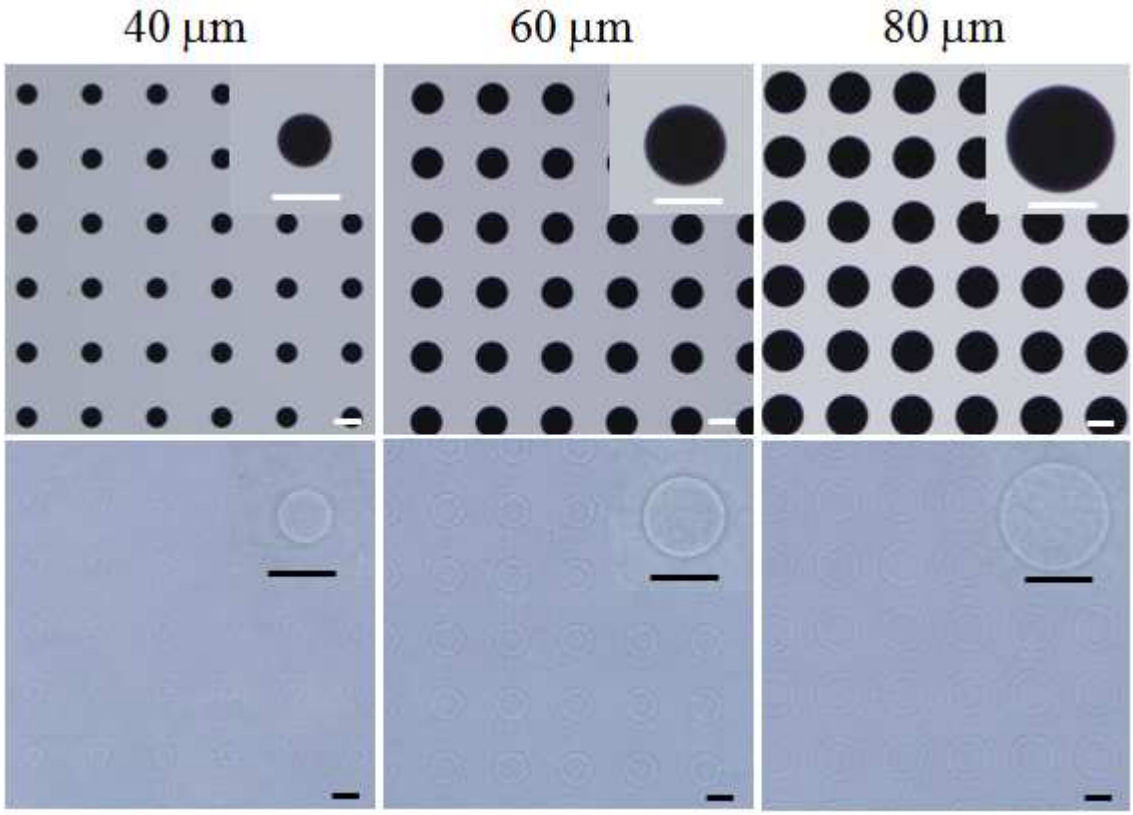

Figure 3.2 Phase contrast micrographs of the photomask (upper panel) and PVA-micropatterned PSt surface (lower panel). Three types of circular PSt micropatterns with different diameters were formed and surrounded by PVA domains. Scale bars: 50 μm.

To measure the diameter of each circular PSt micropattern, the PVA-micropatterned PSt surfaces were observed by AFM in Milli-Q water in contact mode. The three-dimensional images of the three circular PSt micropatterns are shown in Figure 3.3. The diameter and thickness of the circle were analyzed by section analysis of the acquired images (Table 3.1). The diameters of the circular micropatterns formed from the 40-, 60-, and 80-μm-diameter photomask micropatterns were 39.24 ± 0.50, 59.86 ± 0.43, and 79.84 ± 0.61 μm, respectively. The circular PSt micropatterns had almost the same diameters as the designed photomask micropatterns. The thickness of the PVA layer was ranged from 51.4 to 53.6 nm. Therefore, circular PSt micropatterns with different diameters were formed, and their structures could be controlled by designing the micropatterns of a photomask.

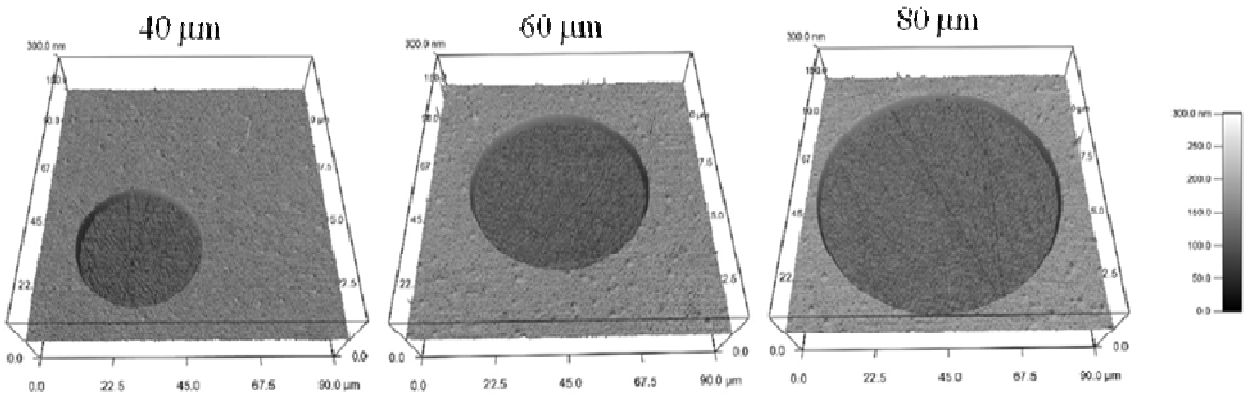

Figure 3.3 Three-dimensional AFM images of the three types of circular PSt micropatterns with different diameters measured in Milli-Q water in contact mode.

Table 3.1 The designed diameter of the circle on the photomask and the measured diameter and thickness of the prepared circular micropatterns, as determined by AFM section analysis. Data represent mean ± SD (n = 3).

Designed diameter (μm)	Measured diameter (μm)	Measured thickness (nm)
40	39.24 ± 0.50	51.4 ± 1.9
60	59.86 ± 0.43	53.6 ± 2.8
80	79.84 ± 0.61	52.9 ± 3.0

3.4.2 Cell adhesion and spreading

The micropatterned surfaces were used for the culture of MSCs in control medium. After 6 h of culture, MSCs only adhered to cell-adhesive circular PSt micropatterns, and MSCs on non-adhesive PVA regions were removed by a medium change. About 85% of circular micropatterns were occupied by a single cell, as confirmed by cell nuclear staining using DAPI. Therefore, the heterogeneity of the cell population in routine cell culture could be reduced, and the behaviors and functions of MSCs could be studied at a single-cell level.

As shown in Figure 3.4, F-actin staining revealed that the spreading of MSCs followed the underlying circular PSt micropatterns and was confined by the surrounding non-adhesive PVA domains, whereas MSCs spread freely on bare PSt surfaces (non-pattern). Interestingly, the assembly and organization of the actin structure of MSCs were affected by the degree of cell spreading. Circular MSCs with the largest degree of spreading (80 μm) mainly assembled actin in the radial and concentric directions of the circle. However, such organization of the actin structure weakened as the degree of cell spreading decreased. On the smallest circle (40 μm), MSCs predominately assembled actin along their edges, between the adhesive PSt and non-adhesive PVA. The MSCs cultured on the bare PSt plate did not exhibit any regular organization.

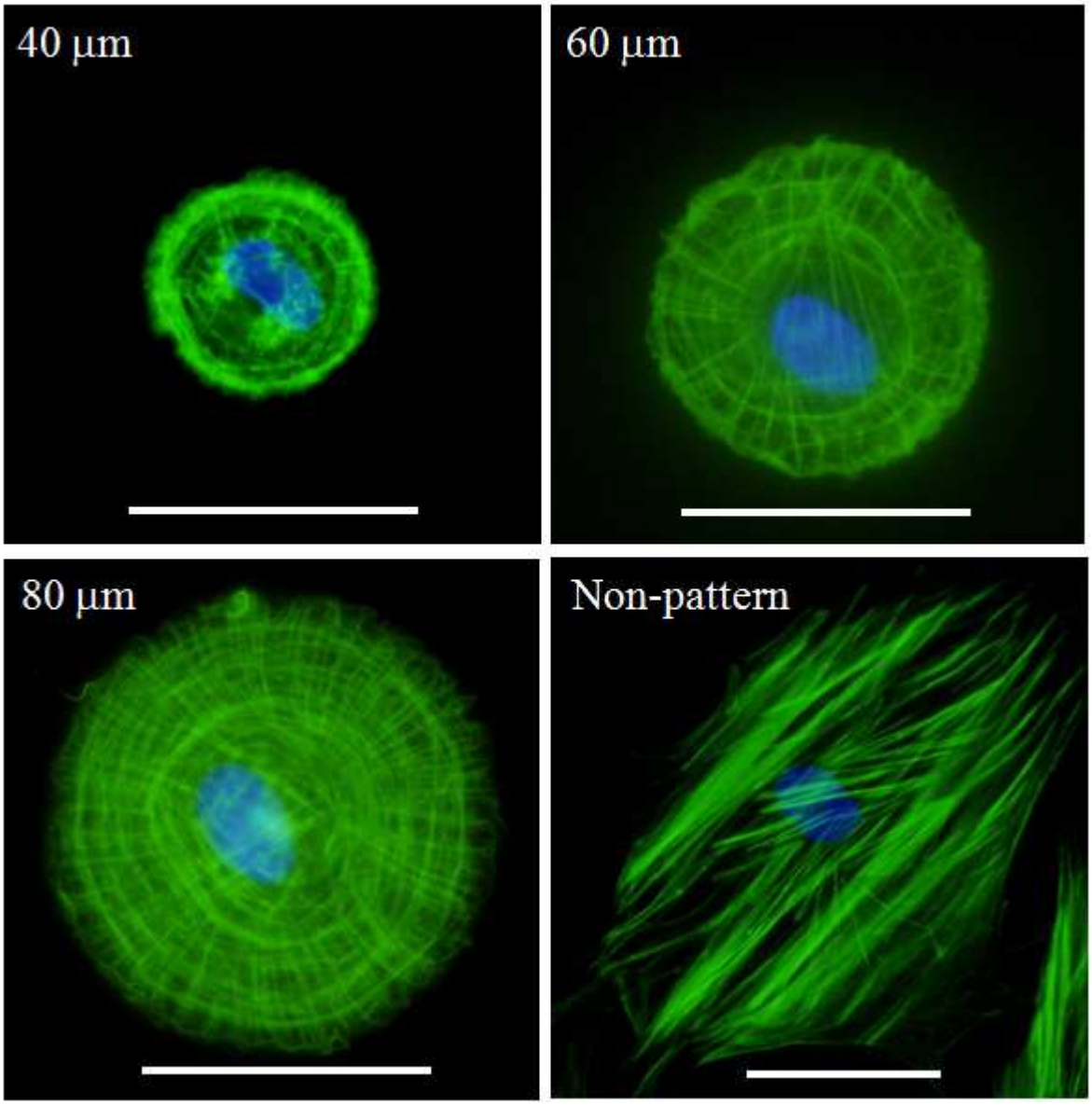

Figure 3.4 Fluorescent images of MSCs with different spreading areas stained for F-actin (green) and nuclei (blue) after culture in control medium for 6 h. "Non-pattern" indicates a bare PSt surface without micropatterning and grafting of PVA. Scale bars: 50 μm.

3.4.3 Adipogenic differentiation of MSCs with different cell spreading areas

MSCs were cultured on the micropatterns in adipogenic medium for 7 days. Some MSCs on micropatterns committed to adipocytes that contained lipid vacuoles. Lipid vacuoles were stained with Oil Red O, a specific marker for adipogenic differentiation. Representative optical photographs of positively stained cells with different cell spreading areas are shown in Figure 3.5.

The probabilities that MSCs with different degrees of cell spreading committed to adipocytes were evaluated. The cells containing lipid vacuoles positively stained by Oil Red O were considered to be adipocytes, and only single cells on each circular micropattern were counted. The results show that the probability of MSC adipogenesis was dependent on the degree of cell spreading (Figure 3.6). The percentages of MSCs undergoing adipogenic differentiation were 45.3 ± 3.4%, 26.3 ± 3.4%, and 14.7 ± 4.2%

for 40- to 80-μm circles and 12.4 ± 2.0% for the bare PSt surface (non-pattern). Therefore, the probability of adipogenic differentiation of MSCs decreased as the degree of cell spreading increased.

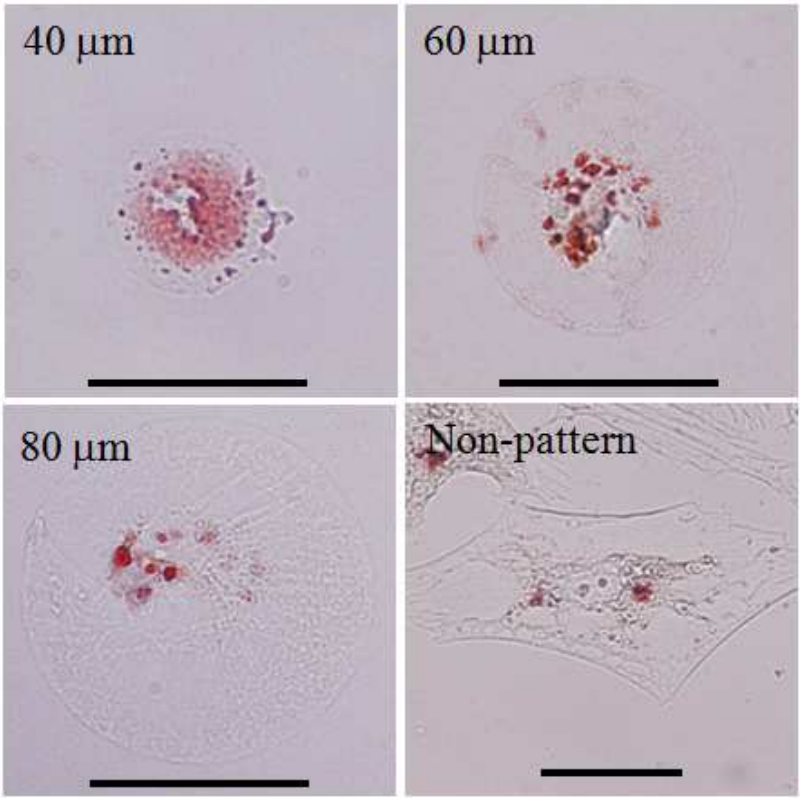

Figure 3.5 Representative optical photographs of MSCs with different spreading areas stained by Oil Red O after culture in adipogenic medium for 7 days. Scale bars: 50 μm.

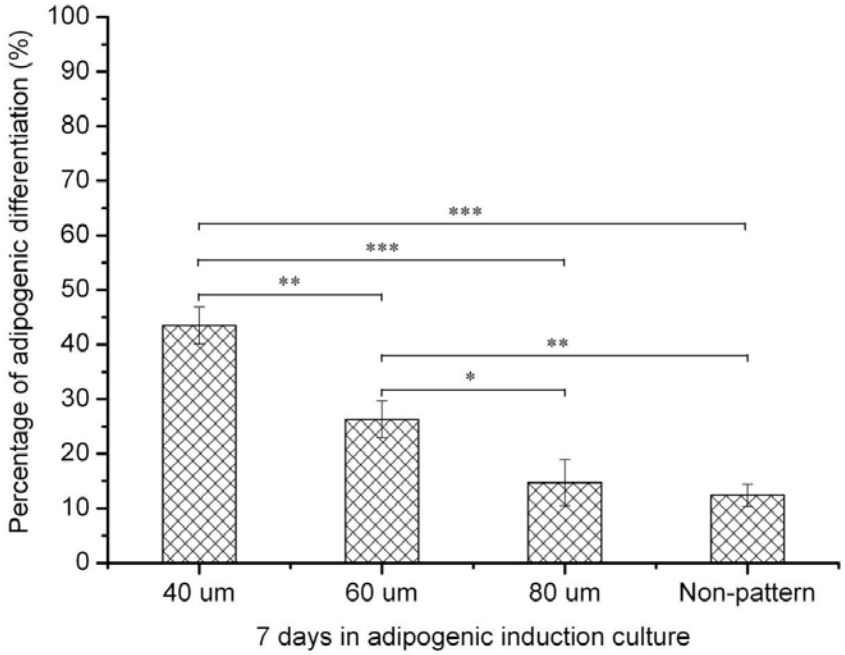

Figure 3.6 The percentage of adipogenic differentiation of MSCs with different spreading areas. Data represent mean ± SD (n = 3). * $p < 0.05$, ** $p < 0.01$, and *** $p < 0.001$.

3.4.4 Osteogenic differentiation of MSCs with different cell spreading areas

MSCs were cultured on the micropatterns in osteogenic induction medium for 7 and 21 days. The cells that were constrained on the micropatterns did not spread out from the micropatterns, even after 21 days of culture, while a confluent cell layer already formed on the bare PSt surface (Figure 3.7). This result indicates that the micropatterned surfaces were stable and useful for long-term cell culture and assessment.

Osteogenic differentiation was evaluated by ALP staining, a marker for osteogenesis. Representative optical photographs of positively stained cells are shown in Figure 3.8. The probabilities that MSCs with different degrees of cell spreading committed to osteoblasts are shown in Figure 3.9. The percentages of MSCs undergoing osteogenic differentiation were 13.0 ± 2.2%, 28.3 ± 3.0%, and 41.2 ± 1.9% on micropatterns with 40- to 80-μm circles and 54.6 ± 4.2% on the bare PSt surface (non-pattern) after 7 days of osteogenic culture. The probability of osteogenic differentiation of MSCs increased as the degree of cell spreading was enhanced. After osteogenic culture for 21 days, the percentages of MSCs undergoing osteogenic differentiation were 17.5 ± 3.5%, 40.2 ± 3.8%, and 53.9 ±5.4 % on the micropatterns with 40- to 80-μm circles and 86.0 ± 3.0% on the bare PSt surface (non-pattern). Although the trend of the probability of osteogenic differentiation at 21 days was similar to that at 7 days, more cells underwent osteogenic differentiation after long-term culture. These results indicate that cell spreading facilitated osteogenic differentiation of MSCs, and long-term cell culture on the micropatterned surfaces was realized.

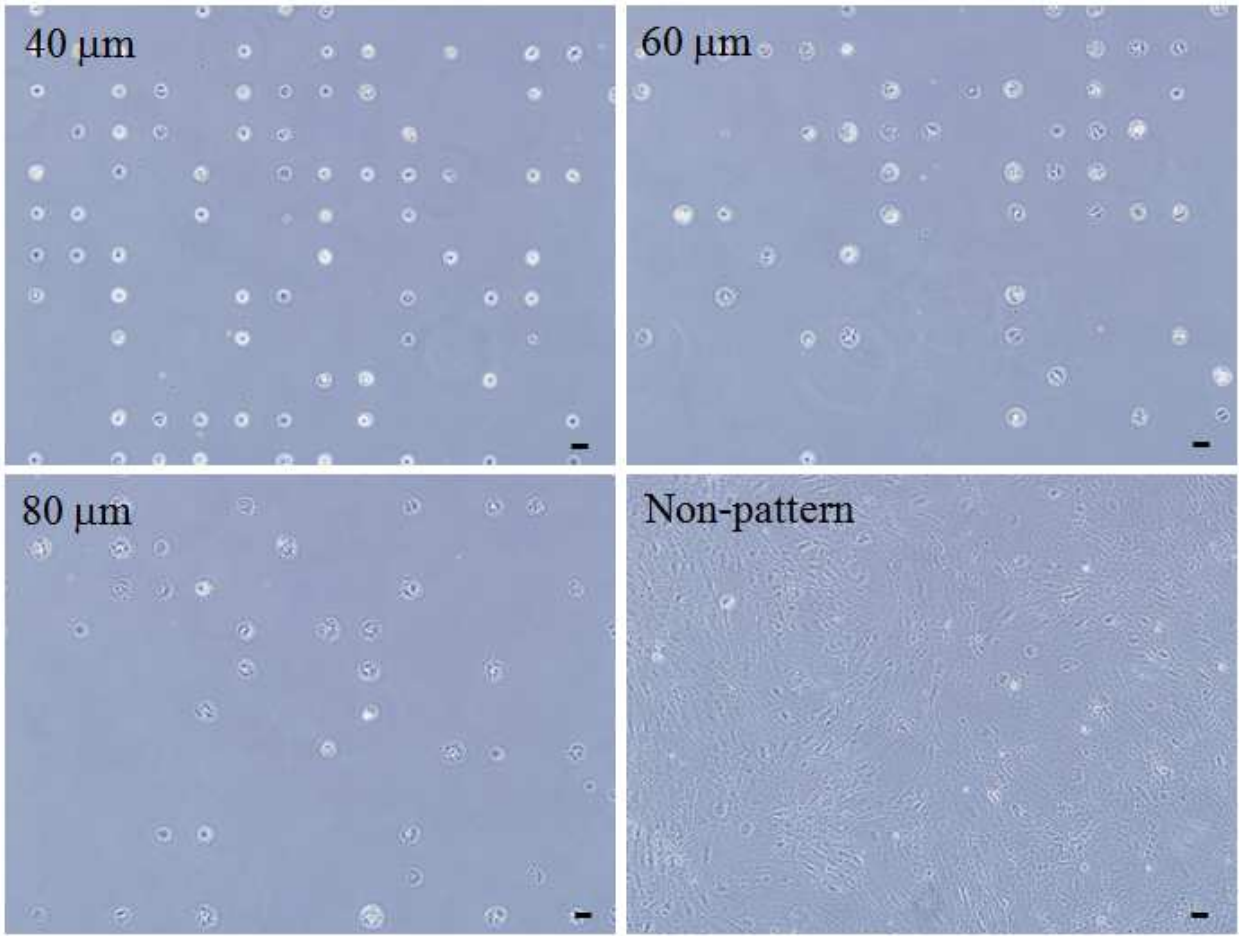

Figure 3.7 Phase contrast photographs of MSCs after culture on micropatterned surfaces in osteogenic medium for 21 days. Scale bars: 50 μm.

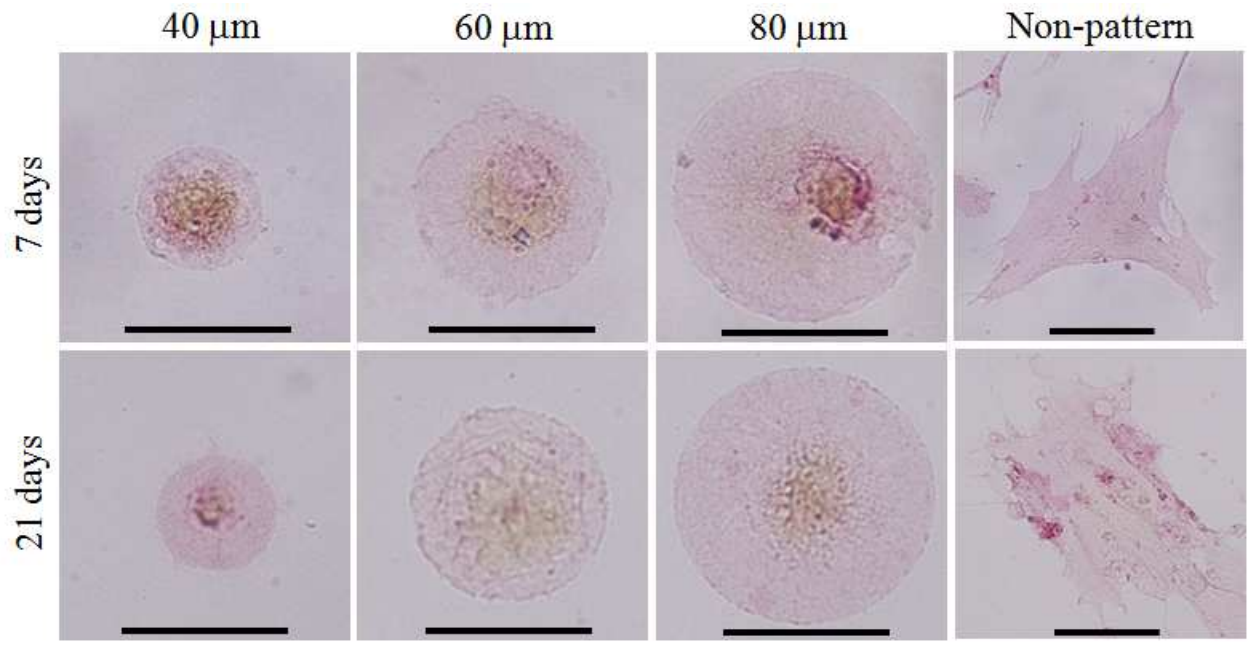

Figure 3.8 Representative optical photographs of ALP staining of MSCs with different spreading areas after culture in osteogenic medium for 7 and 21 days. Scale bars: 50 μm.

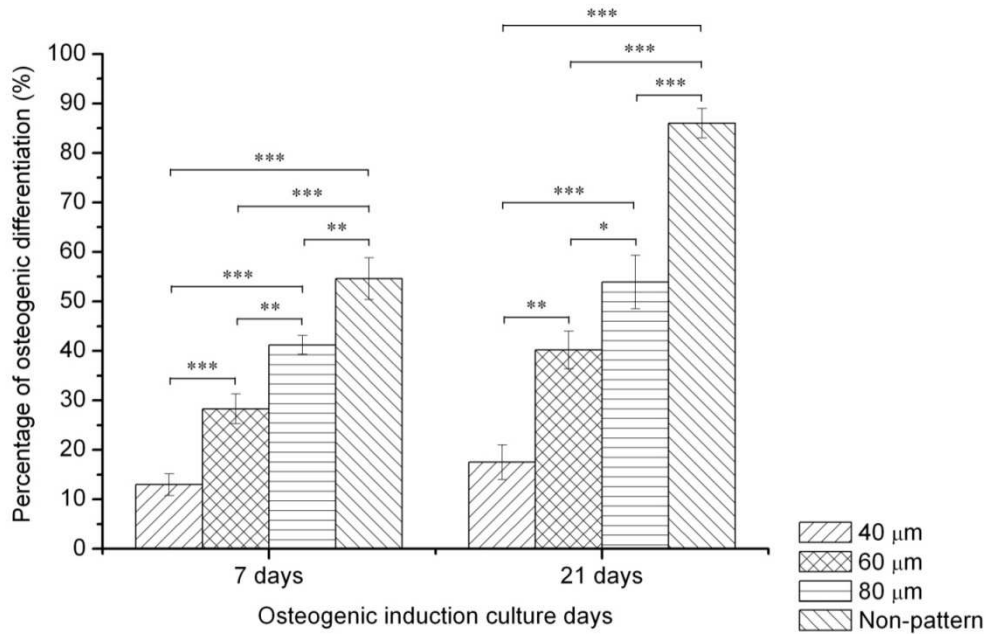

Figure 3.9 The percentage of osteogenic differentiation of MSCs with different spreading areas after culture in osteogenic medium for 7 and 21 days. Data represent mean ± SD (n = 3). ∗ $p < 0.05$, ∗∗ $p < 0.01$, and ∗∗∗ $p < 0.001$. Scale bars: 50 μm.

3.5 Discussion

In this study, different degrees of cell spreading with the same cell shape were controlled using micropatterning technology, and the effect of different cell spreading area on the differentiation of MSCs was investigated on a micropatterned surface at the single-cell level.

Although many methods have been adopted to construct micropatterned surfaces for cell culture[29], few of them would be compatible with long-term cell culture (especially longer than 2 weeks), mainly because of the unstable non-fouling layer. Here, photo-reactive PVA was micropatterned on cell-culture PSt surfaces using photolithography. Because PVA molecules were intra- and inter-molecularly crosslinked and covalently grafted to the PSt surface, PVA-micropattern on PSt surface is stable during long-term cell culture. The thickness of non-adhesive PVA layer within nanometer scale is important for preventing protein adsorption and cell adhesion and for trapping single cell in PSt circle. Arima *et al.*[30] have reported that highly hydrated PVA layer with the thickness around 53.3 nm effectively resists serum proteins adsorption. The thickness of our micropatterned PVA layer is ranged from 51.4 to 53.6 nm. Therefore, long-term stability of this micropatterned surface in aqueous culture medium is probably due to the suitable thickness and hydration of PVA layer. On the other hand, the thickness of PVA layer was controlled at nanometer scale to capture the single cell by means of different surface chemistry other than topography. The cell adhesion result showed that ~85% of circular PSt domain was occupied by single cell. Otherwise, the topography of PVA layer with micrometer scale thickness is similar to micro-well structure. Multi-layer cells are likely to be trapped in such PVA micro-well. It has been reported that micro-well structures were adopted to prepare multi-layer cell spheroids[31,32]. Consequently, nanometer thick PVA-micropattern on PSt surface is compatible with single-cell array formation and long-term cell culture.

With the advantage of micropatterns, cell adhesion, shape, and spreading were regulated at the single-cell level. Hence, the complexity of cell-cell interactions and the heterogeneity of the cell population during routine cell culture were significantly reduced[33]. The behaviors and functions of individual MSCs could be investigated and compared at specific conditions with a fixed shape but varied spreading areas. The actin structure of MSCs was affected by the degree of cell spreading. Well-organized stress fibers appeared in MSCs that adhered to the large circular micropatterns. In contrast, MSCs confined to small circular micropatterns assembled thicker actin filaments at the edge than in the interior, a phenomenon suggesting that cells were maximizing their spreading. It has been reported that actin structures play an important role in the differentiation of MSCs[34-36]. Thus, the different actin arrangements suggest a tight relationship among cell spreading, the cytoskeletal network, and stem cell functions.

The long-term effects of different degrees of cell spreading on the differentiation of isolated individual MSCs without direct cell-cell interactions were directly compared on the same PVA-micropatterned PSt surface. This way, uncertain factors arising from separate cell cultures and heterogeneity of cell population in common cell culture were greatly reduced. The differentiation of MSCs strongly depended on the degree of cell spreading. However, osteogenic and adipogenic differentiation of MSCs exhibited opposite correlations. Namely, cell spreading promoted osteogenic differentiation but suppressed adipogenic differentiation of MSCs. This result is consistent with other reports[14,37], which also suggests that cell spreading favors osteogenic differentiation but inhibits adipogenic differentiation of MSCs. The reason may be that cytoskeletal contractility was enhanced with increased cell spreading[38,39], and high contractility favors osteogenesis, whereas lower contractility enhanced the adipogenesis of MSCs[40,41].

3.6 Conclusions

Different degrees of cell spreading with the same cell shape were established on PVA-micropatterned PSt surfaces. The thickness of PVA micropattern at nanometer scale played a crucial role in controlling cell micropattern at the single-cell level and in applying to long-term culture. The

assembly and organization of actin filaments depended on the degree of cell spreading. MSCs on larger circular micropatterns exhibited a more highly ordered actin structure, whereas MSCs on small circular micropatterns mainly aligned actin fibers along the edge between cell-adhesive PSt and non-adhesive PVA. The distinct degree of cell spreading also had an effect on the differentiation of MSCs. Osteogenic differentiation of MSCs increased with increased cell spreading. In contrast, adipogenic differentiation of MSCs decreased with increased cell spreading. This micropatterning technique provides a convenient method to directly compare stem cell functions for both short- and long-term cell culture.

3.7 References

1. Watt, F. M., Out of Eden: stem cells and their niches. *Science* **287**, 1427-1430 (2000).
2. Lutolf, M. P., Gilbert, P. M., Blau, H. M., Designing materials to direct stem-cell fate. *Nature* **462**, 433-441 (2009).
3. Guo, L., Kawazoe, N., Hoshiba, T., Tateishi, T., Chen, G., Zhang, X., Osteogenic differentiation of human mesenchymal stem cells on chargeable polymer-modified surfaces. *J Biomed Mater Res A* **87**, 903-912 (2008).
4. Guo, L., Kawazoe, N., Fan, Y., Ito, Y., Tanaka, J., Tateishi, T., Zhang, X., Chen, G., Chondrogenic differentiation of human mesenchymal stem cells on photoreactive polymer-modified surfaces. *Biomaterials* **29**, 23-32 (2008).
5. Guilak, F., Cohen, D. M., Estes, B. T., Gimble, J. M., Liedtke, W., Chen, C. S., Control of stem cell fate by physical interactions with the extracellular matrix. *Cell Stem Cell* **5**, 17-26 (2009).
6. Hoshiba, T., Kawazoe, N., Tateishi, T., Chen, G., Development of extracellular matrices mimicking stepwise adipogenesis of mesenchymal stem cells. *Adv Mater* **22**, 3042-3047 (2010).
7. Hoshiba, T., Kawazoe, N., Tateishi, T., Chen, G., Development of stepwise osteogenesis-mimicking matrices for the regulation of mesenchymal stem cell functions. *J Biol Chem* **284**, 31164-31173 (2009).
8. Jaiswal, N., Haynesworth, S. E., Caplan, A. I., Bruder, S. P., Osteogenic differentiation of purified, culture-expanded human mesenchymal stem cells in vitro. *J Cell Biochem* **64**, 295-312 (1997).
9. Pittenger, M. F., Mackay, A. M., Beck, S. C., Jaiswal, R. K., Douglas, R., Mosca, J. D., Moorman, M. A., Simonetti, D. W., Craig, S., Marshak, D. R., Multilineage potential of adult human mesenchymal stem cells. *Science* **284**, 143-147 (1999).
10. Alberti, K., Davey, R. E., Onishi, K., George, S., Salchert, K., Seib, F. P., Bornhäuser, M., Pompe, T., Nagy, A., Werner, C., Zandstra, P. W., Functional immobilization of signaling proteins enables control of stem cell fate. *Nat Methods* **5**, 645-650 (2008).
11. Doran, M. R., Markway, B. D., Aird, I. A., Rowlands, A. S., George, P. A., Nielsen, L. K., Cooper-White, J. J., Surface-bound stem cell factor and the promotion of hematopoietic cell expansion. *Biomaterials* **30**, 4047-4052 (2009).
12. Engler, A. J., Sen, S., Sweeney, H. L., Discher, D. E., Matrix elasticity directs stem cell lineage specification. *Cell* **126**, 677-689 (2006).
13. Dalby, M. J., Gadegaard, N., Tare, R., Andar, A., Riehle, M. O., Herzyk, P., Wilkinson, C. D., Oreffo, R. O., The control of human mesenchymal cell differentiation using nanoscale symmetry and disorder. *Nat Mater* **6**, 997-1003 (2007).

14. McBeath, R., Pirone, D. M., Nelson, C. M., Bhadriraju, K., Chen, C. S., Cell shape, cytoskeletal tension, and RhoA regulate stem cell lineage commitment. *Dev Cell* **6**, 483-495 (2004).
15. Peerani, R., Rao, B. M., Bauwens, C., Yin, T., Wood, G. A., Nagy, A., Kumacheva, E., Zandstra, P. W., Niche-mediated control of human embryonic stem cell self-renewal and differentiation. *EMBO J* **26**, 4744-4755 (2007).
16. Connelly, J. T., Gautrot, J. E., Trappmann, B., Tan, D. W., Donati, G., Huck, W. T., Watt, F. M., Actin and serum response factor transduce physical cues from the microenvironment to regulate epidermal stem cell fate decisions. *Nat Cell Biol* **12**, 711-718 (2010).
17. Bhadriraju, K., Hansen, L. K., Extracellular matrix- and cytoskeleton-dependent changes in cell shape and stiffness. *Exp Cell Res* **278**, 92-100 (2002).
18. Szabo, E., Feng, T., Dziak, E., Opas, M., Cell adhesion and spreading affect adipogenesis from embryonic stem cells: the role of calreticulin. *Stem Cells* **27**, 2092-2102 (2009).
19. Chen, G., Kawazoe, N., Fan, Y., Ito, Y., Tateishi, T., Grid pattern of nanothick microgel network. *Langmuir* **23**, 5864-5867 (2007).
20. Théry, M., Racine, V., Pépin, A., Piel, M., Chen, Y., Sibarita, J. B., Bornens, M., The extracellular matrix guides the orientation of the cell division axis. *Nat Cell Biol* **7**, 947-953 (2005).
21. Yan, C., Sun, J., Ding, J., Critical areas of cell adhesion on micropatterned surfaces. *Biomaterials* **32**, 3931-3938 (2011).
22. Wan, L. Q., Ronaldson, K., Park, M., Taylor, G., Zhang, Y., Gimble, J. M., Vunjak-Novakovic, G., Micropatterned mammalian cells exhibit phenotype-specific left-right asymmetry. *Proc Natl Acad Sci USA* **108**, 12295-12300 (2011).
23. Chan, E. W. L., Yousaf, M. N., A photo-electroactive surface strategy for immobilizing ligands in patterns and gradients for studies of cell polarization. *Mol Biosyst* **4**, 746-753 (2008).
24. Théry, M., Racine, V., Piel, M., Pépin, A., Dimitrov, A., Chen, Y., Sibarita, J. B., Bornens, M., Anisotropy of cell adhesive microenvironment governs cell internal organization and orientation of polarity. *Proc Natl Acad Sci USA* **103**, 19771-19776 (2006).
25. Gautrot, J. E., Trappmann, B., Oceguera-Yanez, F., Connelly, J., He, X., Watt, F. M., Huck, W. T., Exploiting the superior protein resistance of polymer brushes to control single cell adhesion and polarisation at the micron scale. *Biomaterials* **31**, 5030-5041 (2010).
26. Thakar, R. G., Cheng, Q., Patel, S., Chu, J., Nasir, M., Liepmann, D., Komvopoulos, K., Li, S., Cell-shape regulation of smooth muscle cell proliferation. *Biophys J* **96**, 3423-3432 (2009).
27. Chen, C. S., Mrksich, M., Huang, S., Whitesides, G. M., Ingber, D. E., Geometric control of cell life and death. *Science* **276**, 1425-1428 (1997).
28. Wan, L. Q., Kang, S. M., Eng, G., Grayson, W. L., Lu, X. L., Huo, B., Gimble, J., Guo, X. E., Mow, V. C., Vunjak-Novakovic, G., Geometric control of human stem cell morphology and differentiation. *Integr Biol* **2**, 346-353 (2010).
29. Falconnet, D., Csucs, G., Grandin, H. M., Textor, M., Surface engineering approaches to micropattern surfaces for cell-based assays. *Biomaterials* **27**, 3044-3063 (2006).
30. Arima, Y., Kawagoe, M., Furuta, M., Toda, M., Iwata, H., Effect of swelling of poly(vinyl alcohol) layers on complement activation. *Biomaterials* **31**, 6926-6933 (2010).
31. Choi, Y. Y., Chung, B. G., Lee, D. H., Khademhosseini, A., Kim, J. H., Lee, S. H., Controlled-size embryoid body formation in concave microwell arrays. *Biomaterials* **31**, 4296-4303 (2010).

32. Karp, J. M., Yeh, J., Eng, G., Fukuda, J., Blumling, J., Suh, K. Y., Cheng, J., Mahdavi, A., Borenstein, J., Langer, R., Khademhosseini, A., Controlling size, shape and homogeneity of embryoid bodies using poly(ethylene glycol) microwells. *Lab Chip* **7**, 786-794 (2007).
33. Singhvi, R., Kumar, A., Lopez, G. P., Stephanopoulos, G. N., Wang, D. I., Whitesides, G. M., Ingber, D. E., Engineering cell shape and function. *Science* **264**, 696-698 (1994).
34. Tay, C. Y., Yu, H., Pal, M., Leong, W. S., Tan, N. S., Ng, K. W., Leong, D. T., Tan, L. P., Micropatterned matrix directs differentiation of human mesenchymal stem cells towards myocardial lineage. *Exp Cell Res* **316**, 1159-1168 (2010).
35. Rodríguez, J. P., González, M., Ríos, S., Cambiazo, V., Cytoskeletal organization of human mesenchymal stem cells (MSC) changes during their osteogenic differentiation. *J Cell Biochem* **93**, 721-731 (2004).
36. Yourek, G., Hussain, M. A., Mao, J. J., Cytoskeletal changes of mesenchymal stem cells during differentiation. *ASAIO J* **53**, 219-228 (2007).
37. Gao, L., McBeath, R., Chen, C. S., Stem cell shape regulates a chondrogenic versus myogenic fate through Rac1 and N-cadherin. *Stem Cells* **28**, 564-572 (2010).
38. Roca-Cusachs, P., Alcaraz, J., Sunyer, R., Samitier, J., Farré, R., Navajas, D., Micropatterning of single endothelial cell shape reveals a tight coupling between nuclear volume in G1 and proliferation. *Biophys J* **94**, 4984-4995 (2008).
39. Théry, M., Pépin, A., Dressaire, E., Chen, Y., Bornens, M., Cell distribution of stress fibres in response to the geometry of the adhesive environment. *Cell Motility Cytoskeleton* **63**, 341-355 (2006).
40. Kilian, K. A., Bugarija, B., Lahn, B. T., Mrksich, M., Geometric cues for directing the differentiation of mesenchymal stem cells. *Proc Natl Acad Sci USA* **107**, 4872-4877 (2010).
41. Ruiz, S. A., Chen, C. S., Emergence of patterned stem cell differentiation within multicellular structures. *Stem Cells* **26**, 2921-2927 (2008).

Chapter 4

Manipulation of cell shape and its effect on adipogenic differentiation of MSCs

4.1 Summary

In this chapter, poly(vinyl alcohol) (PVA) micropatterns on cell-culture polystyrene (PSt) plates were prepared using UV photolithography. Cell-adhesive PSt geometries of triangle, square, pentagon, hexagon, and circle were surrounded by cell non-adhesive PVA to manipulate cell shapes. These different geometries had the same small surface areas for cell spreading. Human mesenchymal stem cells (MSCs) were cultured on the micropatterned surface and the effect of cell shape on the adipogenic differentiation was investigated. MSCs adhered to the geometric micropatterns and formed arrays of single cell with different shapes. The distribution patterns of actin filaments were similar among these cell shapes and remolded during adipogenesis. The adipogenic differentiation potential of MSCs was similar on the small size triangular, square, pentagonal, hexagonal, and circular geometries according to lipid vacuoles staining.

4.2 Introduction

Manipulation of cell functions, especially among stem cells, has an important role in the fields of tissue engineering and regenerative medicine[1]. Various types of stem cells, such as embryonic stem cells, induced pluripotent stem cells, and mesenchymal stem cells have been established and isolated for the purpose of regenerating and repairing defects in various tissues and organs. Differentiation of stem cells into cells of a specific lineage is critical to reconstructing a tissue or organ. How to manipulate stem cell functions, such as proliferation and differentiation, remains a great challenge to researchers looking to regenerate functional tissues and organs[2].

There are many clues found *in vivo* that indicate what aspects of a cell and its environment dictate the functions of that cell[3,4]. The *in vivo* microenvironments surrounding cells regulate cell migration, adhesion, proliferation, differentiation, and extracellular matrix (ECM) secretion. Factors found in the microenvironment that influence cell functions are both biochemical and physical. In recent years, along with biochemical factors[5], physical cues have been reported to play very important roles in the manipulation

of cell functions[6]. These physical cues include size, shape, morphology, electrostatic properties, mechanical properties, roughness and topography. With recently-developed surface control and modification technologies, various surfaces with controlled surface characteristics have been created to study the effects of these physical elements[7,8,9,10,11,12]. Micropatterning technology is particularly useful for investigating the effects of physical parameters on cell behaviors. Micropatterned substrates have been adapted to study the orientation of the cell division axis[13], cell migration[14], cytoskeleton assembly[15], cell proliferation[16,17], and cell polarization[18,19]. Cellular functions such as adhesion, spreading, proliferation, differentiation and apoptosis can be affected by the size of the cell adhesion area[20,21]. When mesenchymal stem cells (MSCs) are cultured in single form in a mixture medium of adipogenic and osteogenic induction, MSCs prefer to differentiate to adipocytes on small square island (1,024 μm^2) but to osteoblasts on large square island (10,000 μm^2)[9], whereas intermediate cell size (2,500 μm^2) shows little bias in directing cell differentiation towards either osteogenic or adipogenic fates[22]. Interestingly, at such intermediate size, the geometry of the cell adhesion area can direct the differentiation of MSCs. The rectangle with high aspect ratio and the star shape lead to preferential osteogenesis. In contrast, the square with low aspect ratio and flower shape favor adipogenesis. However, it is not clear whether different geometries with a small surface area have effect on the adipogenesis of MSCs in adipogenic medium alone.

Therefore, in this chapter, single cell culture was carried out on different geometric micropatterns with the same surface area that was in the small range for cell spreading. We used photo-reactive poly(vinyl alcohol) (PVA) to prepare micropatterns on a cell-culture polystyrene (PSt) plate by photolithography. This micropatterning protocol is simple because non-adhesive photo-reactive PVA can be easily micropatterned on the PSt surface by UV irradiation and the micropatterned surface can be directly used for cell culture without further coating of ECM proteins to support cell adhesion. Additionally, the micropatterned surface is transparent and hence compatible with routine imaging technique. At the single-cell level, the spread and shape of cell were defined and thus the heterogeneity among individual cells was reduced. The geometries of regular triangle, pentagon, hexagon, square, and circle were chosen to minimize the asymmetrical concentration of actin filaments along the long edge as observed in cells with rectangular and elliptical shapes[16,22]. The shapes of individual human MSCs were manipulated on such geometric micropatterns. The symmetry and area of different cell shapes were similar, whereas the roundness of them gradually increased from triangular to circular shape. The effect of these distinct cell shapes on the adipogenic differentiation of MSCs was then compared.

4.3 Materials and methods

4.3.1 Synthesis of azidophenyl-derivatized PVA

Azidophenyl-derivatized poly(vinyl alcohol) (AzPhPVA) was synthesized by coupling the hydroxyl groups of PVA to 4-azidobenzoic acid as previously described in Chapter 2.3.1.

4.3.2 Fabrication of photomask

The photomask was prepared using DWL66 laser lithography system as previously described in Chapter 2.3.2.

4.3.3 Micropatterning of PVA with a photomask

A PSt plate (2.5 × 2.5 cm^2) was cut from a tissue-culture PSt flask (BD Falcon™). The AzPhPVA solution (0.15 mL, 0.3 mg/mL) was placed on the PSt plate and air-dried in the dark at room temperature. The coating region was around 1.5 × 1.0 cm^2. The preparation method was previously described in Chapter 2.3.3 and shown in Figure 4.1. The plates were sterilized with 70% ethanol solution and used for cell culture.

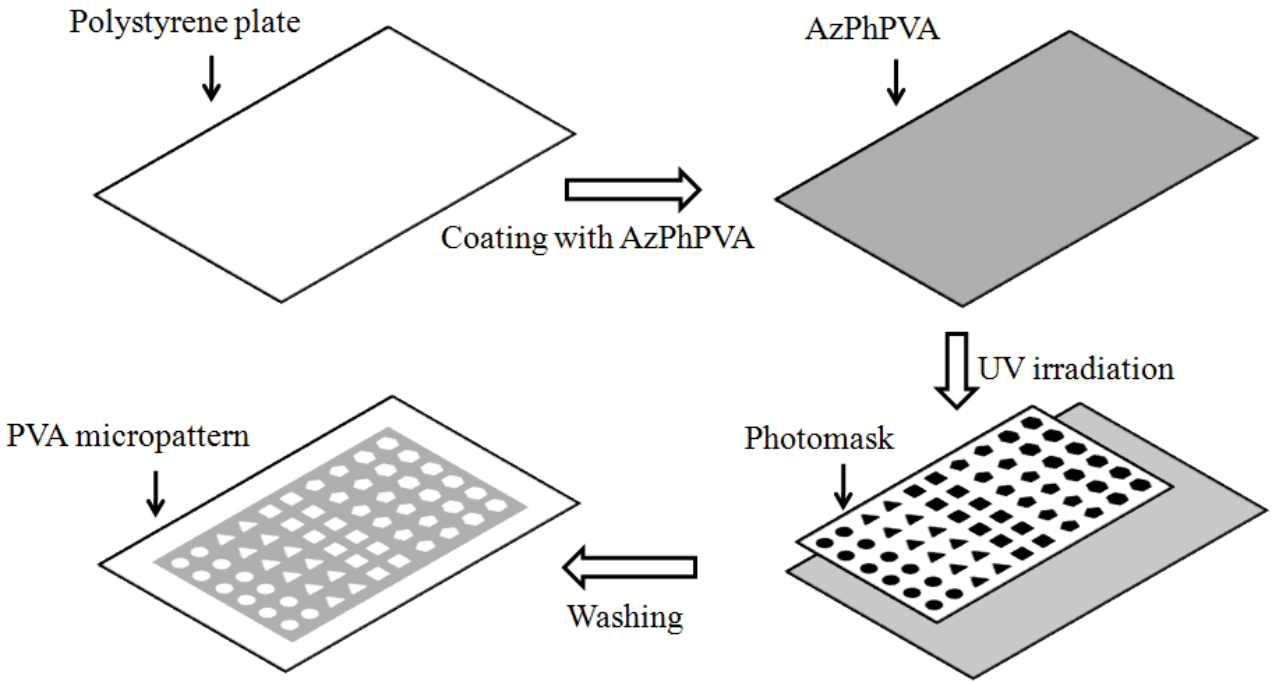

Figure 4.1 Preparation scheme of PVA-micropatterned PSt surface.

4.3.4 AFM observation

The surface topography of the PVA-micropatterned PSt plate was observed using MFP-3D-BIO™ AFM (Asylum Research). A commercially available cantilever (spring constant: 0.06 N/m; oscillation frequency: 12-24 kHz; DNP, Veeco Probes) with a silicon nitride tip was used to measure the samples (60 × 60 μm^2) in Milli-Q water in contact mode. The diameter and thickness of the circular micropattern were measured by section analysis of the acquired image. Three randomly selected micropatterns were measured to calculate the mean and standard deviation.

4.3.5 Cell culture

Human bone marrow-derived mesenchymal stem cells (MSCs) were obtained from Osiris Therapeutics (Columbia, MD) at passage 2. The cells were subcultured twice as previously described in Chapter 2.3.4 and used at passage 4.

The micropatterned PSt plates were placed in 6-well cell culture plates, and a glass ring (diameter: 15 mm; height: 10 mm) was placed over each PVA-micropatterned PSt plate. 3 mL control medium was added to each well, and then the cell suspension (0.36 mL, 1.5×10^4 cells/mL) was placed inside the glass ring (seeding density: 3.0 × 10^3 cells/cm^2). The compositions of control medium were previously described in Chapter 2.3.4.

After 6 h, the glass rings were removed, and the control medium was replaced with adipogenic or osteogenic medium. The compositions of adipogenic medium were previously described in Chapter 3.3.4. The adipogenic medium was changed every 3 days.

4.3.6 F-actin staining

After incubation for 6 h in control medium and 7 days in adipogenic medium, the cultured cells were fixed with 4% paraformaldehyde for 10 min at 4 ^{O}C, permeabilized with 0.2% Triton X-100 for 2 min, and blocked with 1% BSA solution for 30 min at room temperature. The F-actin and nuclei of cells were stained with Alexa Fluor® 488 phalloidin (Invitrogen) for 20 min and 4', 6-diamidino-2-phenylindole (DAPI, Vector Laboratories, Inc.) for 10 min, respectively. Fluorescence photographs of the stained MSCs were captured by an Olympus BX51 microscope with a DP-70 CCD camera (Olympus, Tokyo, Japan).

4.3.7 Oil Red O and Nile Red staining

After incubation in adipogenic medium for 7 days, the cultured cells were fixed with 4% paraformaldehyde for 10 min at 4 ^{O}C, incubated in 60% isopropanol for 5 min, and then stained with fresh Oil Red O solution for 5 min. The nucleus was counterstained with 2 μg/mL DAPI solution (Dojindo) for 10 min. The Oil Red O solution was prepared by mixing three parts stock solution (0.3% in isopropanol) with two parts Milli-Q water and filtering through a 0.2 μm filter. Photomicrographs were captured by an optical microscope with a DP-70 CCD camera (Olympus, Tokyo, Japan).

Alternatively, the F-actin of cultured cells was stained as previously described in Chapter 4.3.6. The lipid vacuoles were stained with 0.1 μg/mL Nile Red solution (Fluka) and the nuclei of the cells were counterstained with 2 μg/mL Hoechst solution (Dojindo) for 10 min, respectively. Fluorescence photographs of the stained MSCs were captured by an Olympus BX51 microscope with a DP-70 CCD camera (Olympus, Tokyo, Japan).

The probability of adipogenesis of MSCs with different cell shapes was studied by calculating the percentage of MSCs that committed to an adipocyte lineage. The MSCs containing lipid vacuoles that were positively stained by Oil Red O were considered as adipocytes, and only single cells from each geometric micropattern, as confirmed by nuclei staining, were counted. For each cell shape, three samples were used to calculate the mean and standard deviation.

4.3.8 Area of positively stained lipid vacuoles

To compare the variability in the extent of adipogenic differentiation among different cell shapes, the area of positively stained lipid vacuoles by Oil Red O was calculated using ImageJ software (freely available at www.nih.gov). The colorful optical images were converted to 8-bit grayscale images. And then the threshold images were obtained using Adjust/Threshold settings. The area of positively stained lipid vacuoles was calculated using Particles Analyze. 24 cells were used to calculate the mean and standard deviation.

4.3.9 Statistical analysis

A one-way analysis of variance (ANOVA) with Tukey's *post hoc* test for multiple comparisons was

used for statistical analysis. A value of $p < 0.05$ was considered to be a statistically significant difference.

4.4 Results

4.4.1 Preparation and observation of PVA-micropatterned PSt surfaces

An aqueous solution of AzPhPVA was coated on a PSt plate and air-dried in the dark. The cast plate was covered with a photomask and photoirradiated by UV light. The photomasks had five geometric micropatterns: triangles, squares, pentagons, hexagons and circles (Figure 4.2). These geometric micropatterns were UV non-transparent and the surrounding domains were UV transparent. The AzPhPVA under the UV transparent domains was inter- and intra-molecularly crosslinked and grafted to the PSt surface, whereas the AzPhPVA covered by UV non-transparent geometric micropatterns was unreacted, and later removed by washing with Milli-Q water. Observation with a phase contrast microscope demonstrated that five types of PSt geometric micropatterns were formed and encircled by PVA domains. The PSt geometric micropatterns had the same properties as the cell-culture PSt plate, which supports cell adhesion, whereas the surrounding PVA domains inhibit protein adsorption and cell adhesion.

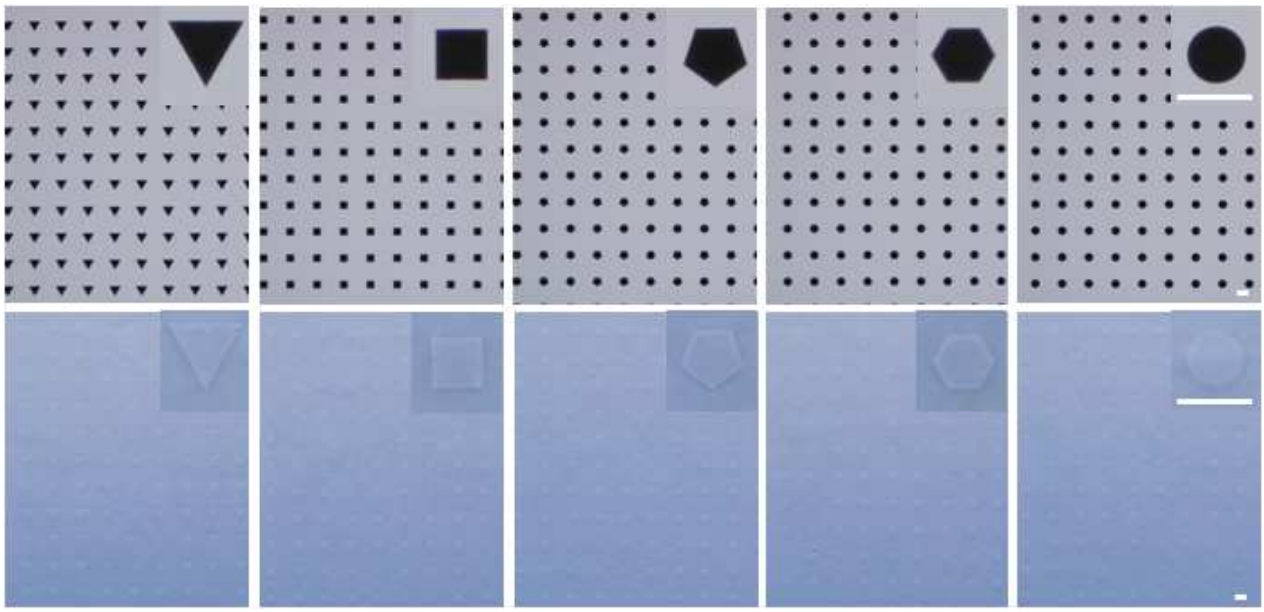

Figure 4.2 Phase contrast micrographs of a photomask (upper panel) and a PVA-micropatterned PSt surface (lower panel). The photomask has five types of geometric micropatterns: triangles, squares, pentagons, hexagons, and circles. The dark geometric micropatterns are UV non-transparent, and the surrounding bright areas are UV transparent. Scale bars: 50 μm.

To calculate the surface area of each type of PSt geometric micropattern, the PVA-micropatterned PSt surface was observed by AFM in Milli-Q water in contact mode. The height images of five types of PSt geometric micropatterns are shown in Figure 4.3. The side length (triangle, square, pentagon, and hexagon) or diameter (circle) of the shapes were analyzed by section analysis of the acquired images, and the surface area of each PSt geometric micropattern was calculated (Table 4.1). The side lengths were 50.9 ± 0.3, 33.8 ± 0.2, 25.7 ± 0.3, and 21.0 ± 0.3 μm for the triangle, square, pentagon, and hexagon, respectively. The diameter of the circle was 38.4 ± 0.5 μm. The surface area of each was 1122.6 ± 13.4, 1140.9 ± 16.5, 1138.5 ± 28.7,

1148.5 ± 33.9, and 1158.1 ± 32.3 μm^2 for the triangular, square, pentagonal, hexagonal, and circular micropatterns, respectively. The thickness of the grafted PVA layer was 51.3-55.3 nm. The micropatterns reflected those of the designed photomask, and there was no significant difference in surface area among the different PSt geometric micropatterns. Therefore, from the triangular to the circular micropattern, the symmetry and surface areas of the shapes were almost the same, with only the roundness gradually increasing as the geometry of the shape changed.

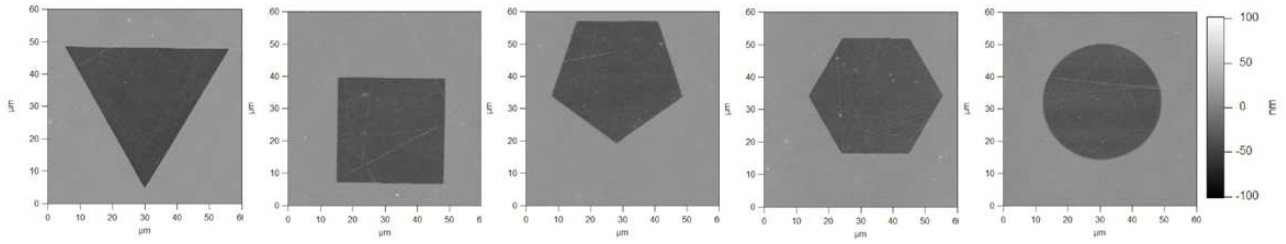

Figure 4.3 AFM height images of five types of PSt geometric micropatterns measured in Milli-Q water in contact mode.

Table 4.1 Designed size and area of the photomask micropatterns and the measured size, area, and thickness of the geometric micropatterns. Data represent mean ± SD (n = 3).

	Designed Side/Diameter (μm)	Measured Side/Diameter (μm)	Designed Surface area (μm^2)	Measured Surface area (μm^2)	Depth (nm)
Triangle	51.2	50.9 ± 0.3	1134.2	1122.6 ± 13.4	55.3 ± 3.0
Square	33.7	33.8 ± 0.2	1133.7	1140.9 ± 16.5	54.7 ± 3.1
Pentagon	25.7	25.7 ± 0.3	1134.6	1138.5 ± 28.7	54.5 ± 3.0
Hexagon	20.9	21.0 ± 0.3	1134.9	1148.5 ± 33.9	52.8 ± 1.8
Circle	38.0	38.4 ± 0.5	1134.1	1158.1 ± 32.3	51.3 ± 1.6

4.4.2 Cell adhesion and shape

The adhesion and distribution of MSCs on the micropatterned surface after culture in control medium for 6 hours is shown in Figure 4.4. MSCs only adhered to the cell-adhesive PSt region. MSCs seeded on the non-adhesive PVA regions did not adhere and were removed by medium change. MSCs spread following the underlying geometric micropatterns and were confined by the surrounding non-adhesive PVA domains. However, when MSCs were cultured on the non-pattern region without grafting of PVA, cells spread freely. In this way, different cell shapes were manipulated on the same PSt plate.

The MSC nuclei were stained by DAPI to visualize the adhesion of single cells on the micropattern. About 90% of the geometric micropattern domains were occupied by a single cell. Therefore, stem cell functions related to cell shape could be investigated at the single cell level while excluding the effect of cell-cell interactions and cell density.

The F-actin of MSCs was stained to examine the effects of different cell shapes on actin organization. As shown in Figure 4.5, the cell shapes of MSCs were almost the same as geometries of the micropatterns. The MSCs cultured on micropatterns predominately assembled actin filaments along the peripheral edges of the micropatterns, indicating that cells were sensing their peripheral microenvironment and maximizing their spreading. However, the MSCs cultured on the bare PSt plate had strong actin filaments and stress fibers at peripheral and central regions.

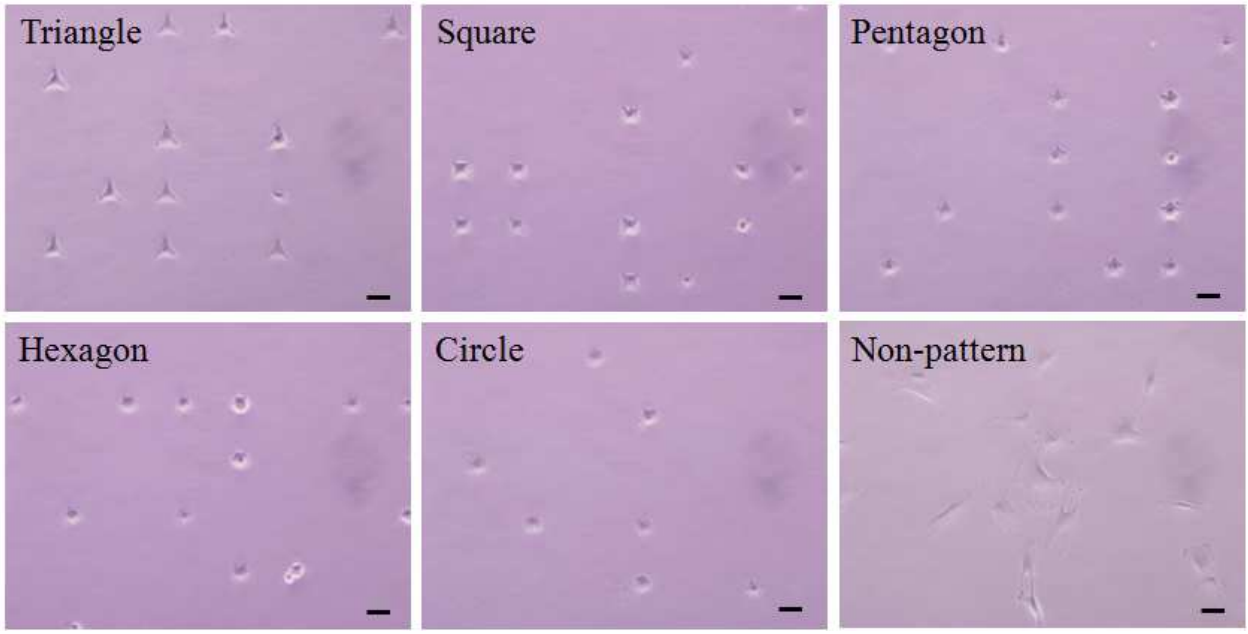

Figure 4.4 Phase contrast photographs of MSCs after culture on micropatterns in control medium for 6 h. Scale bars: 50 μm.

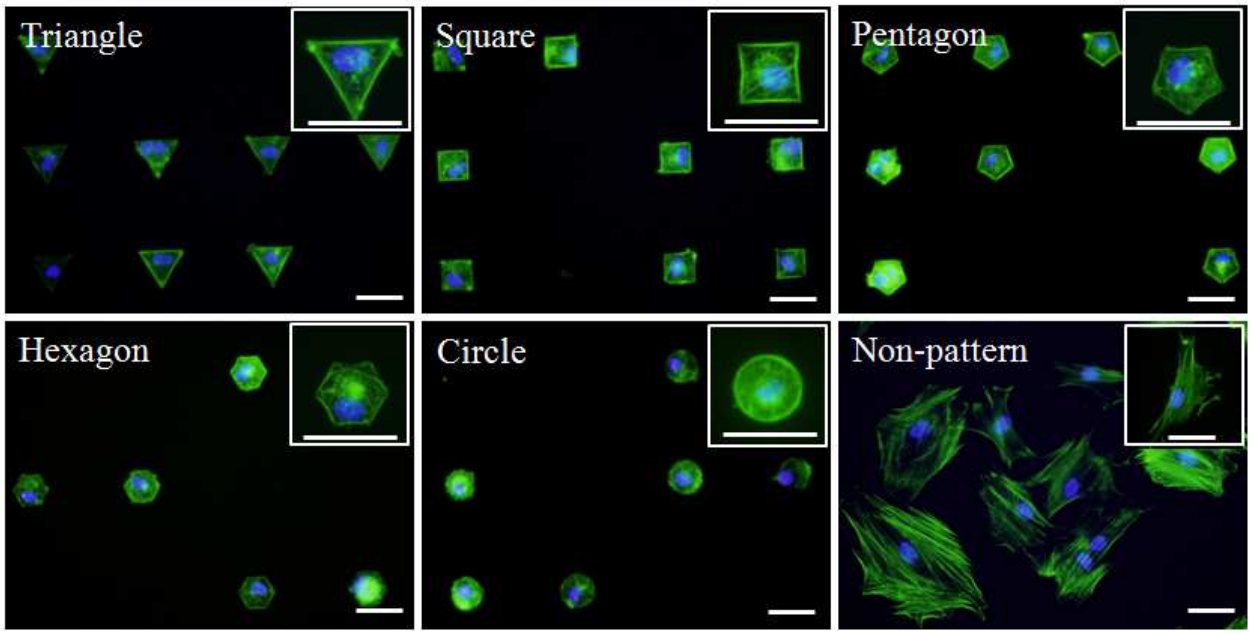

Figure 4.5 Fluorescent images of MSCs with different cell shapes stained for F-actin (green) and nuclei (blue) after culture in control medium for 6 h. Scale bars: 50 μm.

4.4.3 Adipogenic differentiation of MSCs with different shapes

MSCs were cultured on micropatterns and non-patterned PSt surface in adipogenic medium for 7 days. Cells on the five types of micropatterns still remained alive and kept the same shapes as cells incubated for initial 6 hours in control medium. Lipid vacuoles were observed in some of the cells as indicated by black arrow (Figure 4.6), and were stained by Oil Red O. Representative optical photographs of positively stained cells of different shapes are shown in Figure 4.7. Because lipid vacuoles are specific markers for adipogenic

differentiation of MSCs, these results suggest that MSCs of all five shapes can become adipocytes.

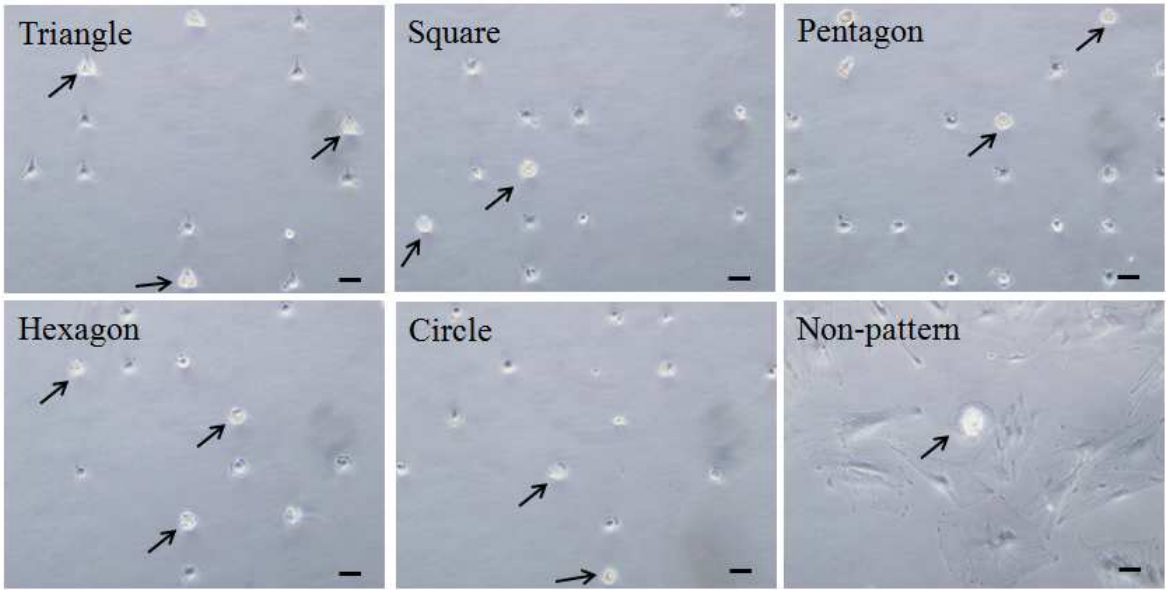

Figure 4.6 Representative optical photographs of MSCs with different spreading areas stained by Oil Red O after culture in adipogenic medium for 7 days. Black arrows indicate the cells containing lipid vacuoles. Scale bars: 50 μm.

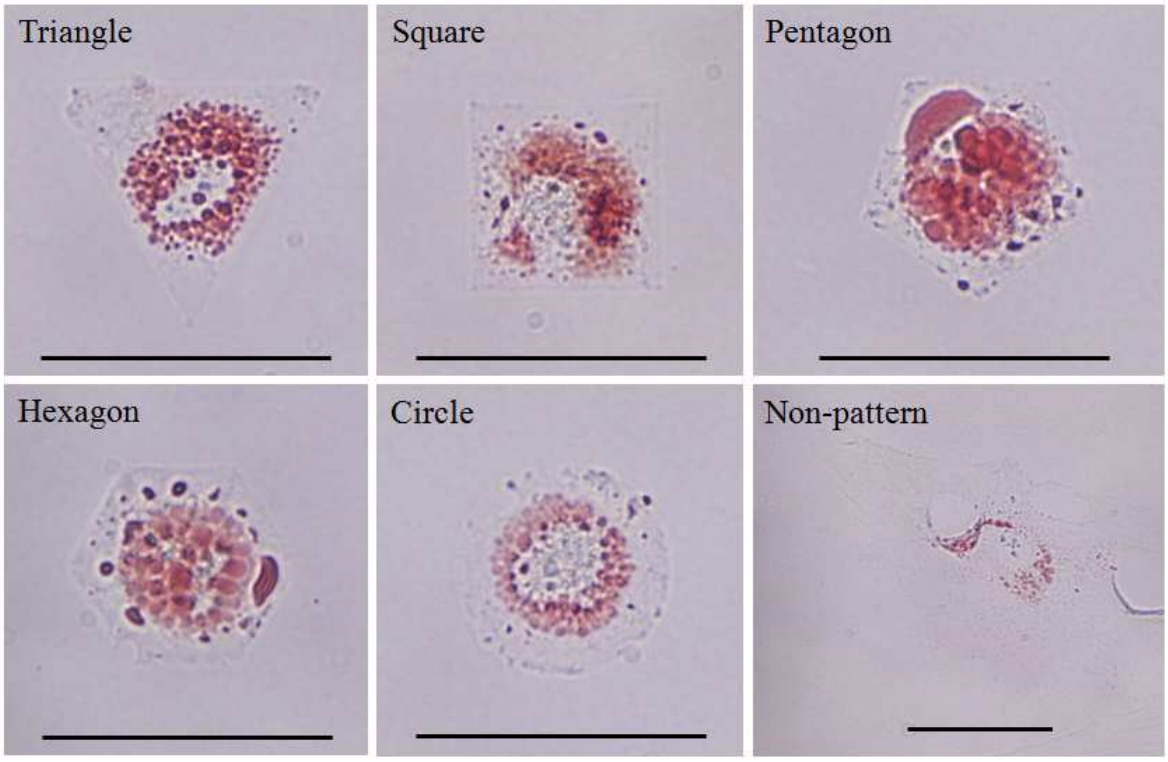

Figure 4.7 Representative optical photographs of MSCs with different cellular shapes stained by Oil Red O after culture in adipogenic induction medium for 7 days. Scale bars: 50 μm.

The influence of different cell shapes on the probability of MSC adipogenesis was studied by calculating the percentage of MSCs that committed to an adipocyte lineage. Cells containing lipid vacuoles that were positively stained by Oil Red O were considered as adipocytes, and only single cells from each

shape were counted. The results are shown in Figure 4.8. The percentage of adipogenic differentiation of MSCs was 35.7 ± 1.4%, 33.9 ± 5.5%, 35.8 ± 4.7%, 43.0 ± 2.5%, and 42.9 ± 6.3% on the triangular, square, pentagonal, hexagonal, and circular micropatterns, respectively. Although the MSCs with hexagonal and circular shapes showed slightly higher potential for adipogenesis, there was no significant difference among different cell shapes. However, the percentage of adipogenic differentiation of MSCs on a non-patterned surface was significantly lower than on the micropatterns, which is consistent with the report that a smaller spreading area favors the adipogenic differentiation of MSCs[9].

Moreover, the extent of adipogenesis of individual cells among different cell shapes was compared by analyzing the area of positively stained lipid vacuoles using ImageJ software. The method was illustrated in Figure 4.9. The colorful optical images were first converted to 8-bit grayscale images. And then the threshold images were obtained using Adjust/Threshold settings. The area of positively stained lipid vacuoles was automatically calculated using Particles Analyze of ImageJ. The result of Figure 4.10 showed that the area was 306.4 ± 63.7, 323.9 ± 95.2, 310.9 ± 85.9, 301.5 ± 57.2, and 291.2 ± 81.7 μm^2 in the triangular, square, pentagonal, hexagonal, and circular shapes, respectively. Therefore, not only the probability but also was the extent of adipogenic differentiation similar among these different cellular shapes.

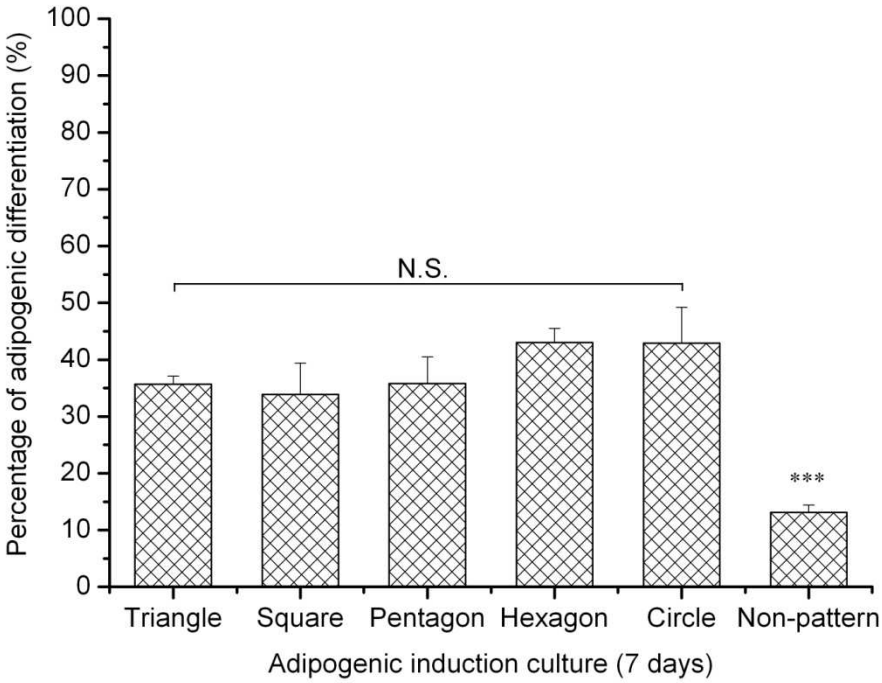

Figure 4.8 The percentage of adipogenic differentiation of MSCs with different cell shapes after culture on micropatterns in adipogenic medium for 7 days. Data represent the mean ± SD (n = 3). N. S. indicates that there is no significant difference. *** indicates $p < 0.001$ compared with all other groups.

Finally, to check for the cytoskeletal changes in the MSCs during adipogenic differentiation, the lipid vacuoles, F-actin, and nuclei of the MSCs were stained by Nile Red, phalloidin and Hoechst, respectively. The representative fluorescence images of the MSCs that showed adipogenesis are shown in Figure 4.11. Compared with the F-actin of MSCs incubated in control medium for 6 hours, the organization and assembly of F-actin weakened in cells of all five shapes after 7 days culture in adipogenic medium, particularly the actin filaments at the edges between the adhesive PSt and the non-adhesive PVA.

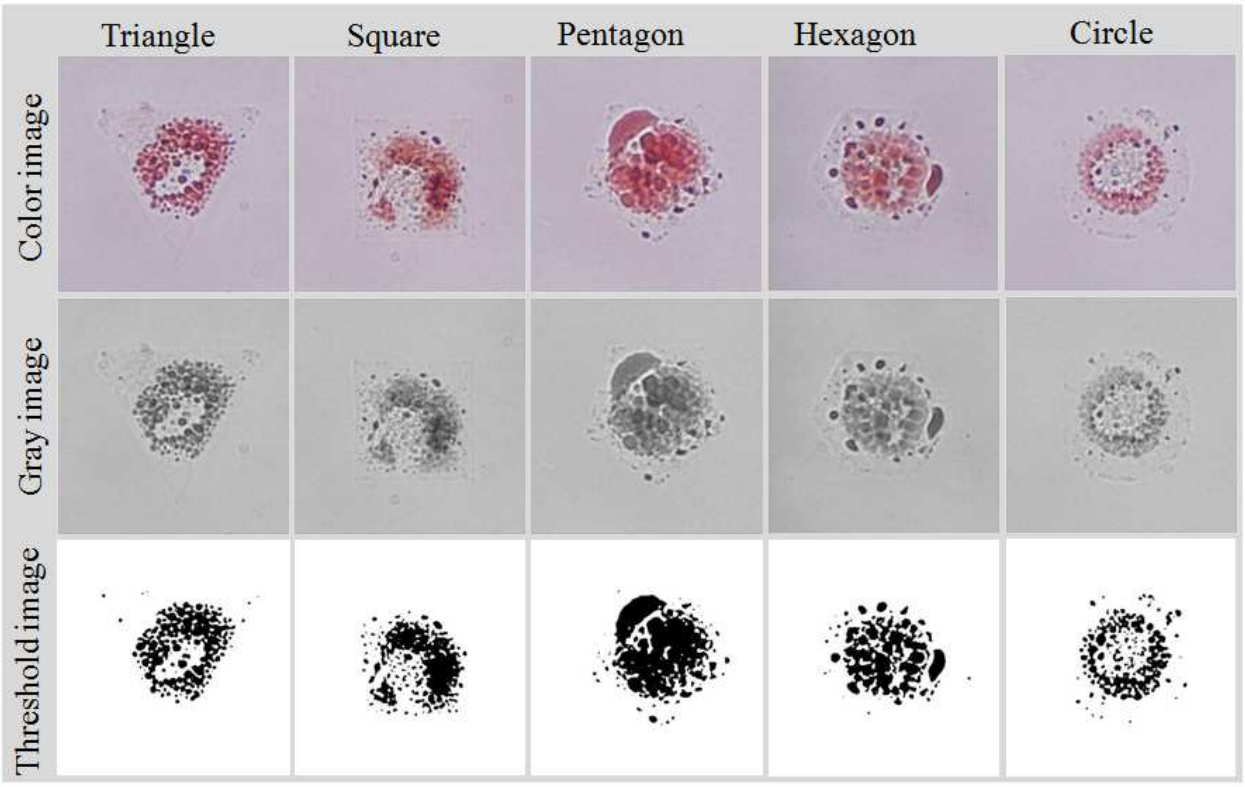

Figure 4.9 The surface area of positively stained lipid vacuoles was analyzed using Particles Analyze of ImageJ software.

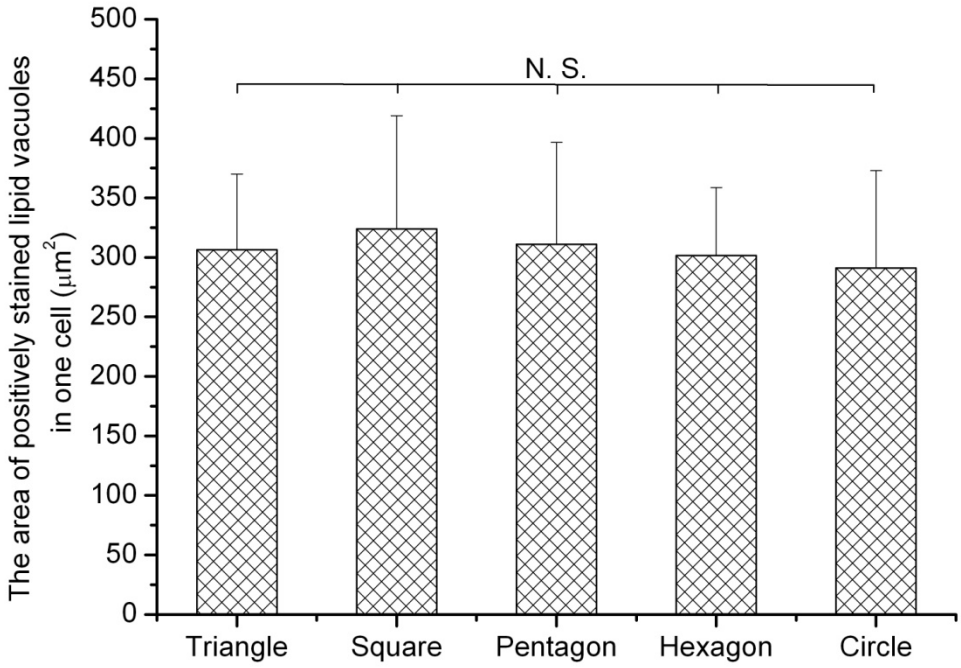

Figure 4.10 The area of positively stained lipid vacuoles in single cell. Data represent the mean ± SD (n = 24). N.S. indicates that there is no significant difference.

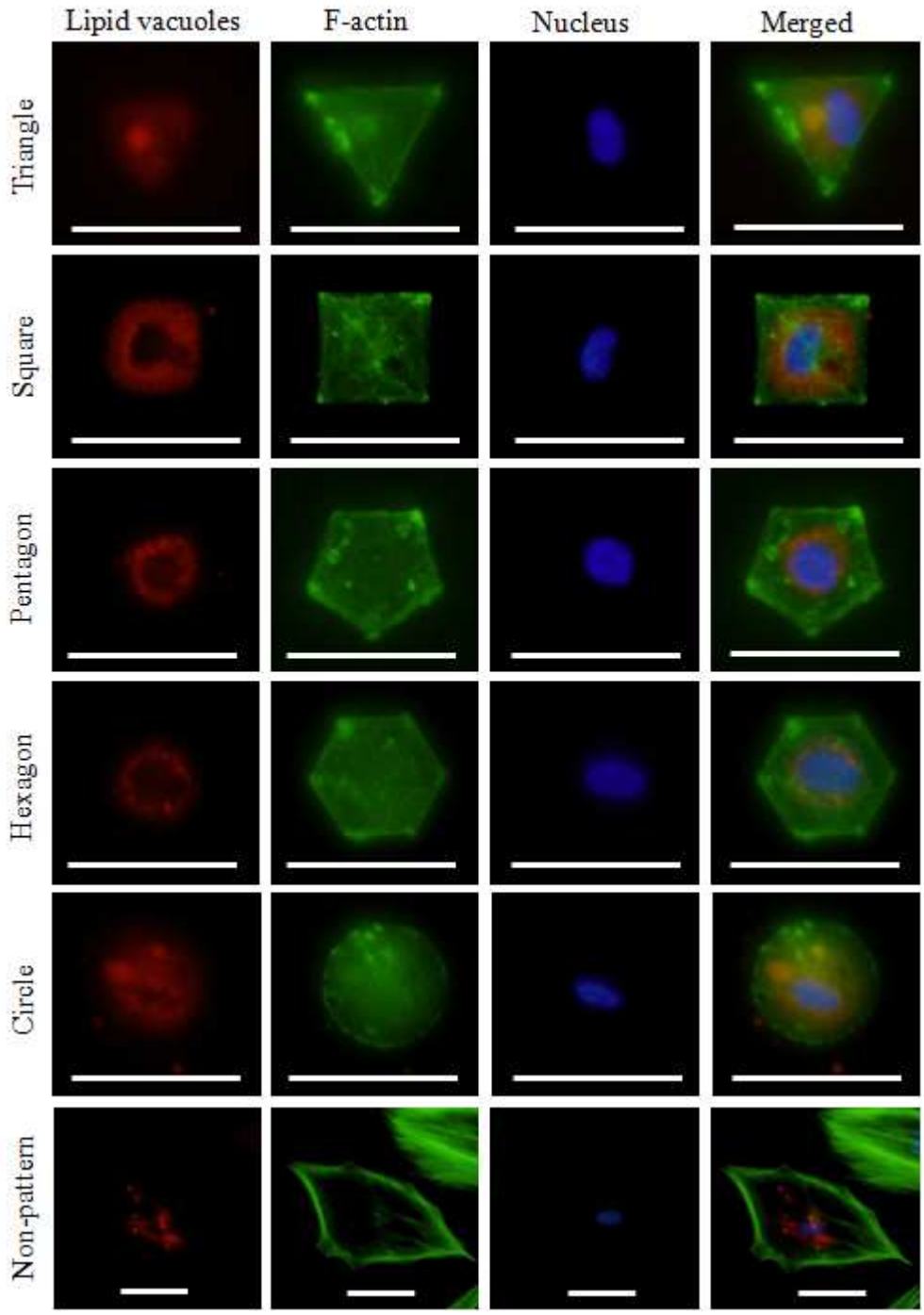

Figure 4.11 Representative fluorescent images of MSCs with different cell shapes stained for lipid vacuoles (red), F-actin (green), and nuclei (blue) after culture in adipogenic medium for 7 days. Scale bars: 50 μm.

4.5 Discussion

There are many methods that can be used to make micropatterned structures for cell culture[23]. The most frequently used method is based on the micro-contact printing of alkylthiols on gold-coated surfaces. In micro-contact printing, cell adhesion factors such as fibronectin, laminin, and arginine-glycine-aspartic acid (RGD) are normally coated on the hydrophobic regions to promote cell adhesion and the formation of cell

patterns. However, the influence of the coated cell adhesion factors cannot be excluded from the results. To avoid this, photo-reactive PVA can be directly micropatterned on cell-culture PSt plates by the present method. The micropatterned surfaces can be used for cell culture without any additional treatment, and the transparency of PSt plates facilitates the direct observation of cells on the micropatterns.

The five types of geometric micropatterns (triangle, square, pentagon, hexagon, and circle) had varying degrees of roundness, but all were symmetrical and small for cell spreading. Based on the formation of lipid vacuole result, no significant difference in the adipogenic differentiation of MSCs was detected among these five geometric micropatterns. However, MSCs showed significantly higher potential for adipogenic differentiation on these micropatterns than on the non-patterned PSt surface. Cell spreading was suppressed by the micropatterns, which have some positive effect on the adipogenic differentiation of MSCs. The result that constraining MSCs in symmetrically small micropatterns favors adipogenic differentiation of MSCs is similar to the results reported by Chen *et al*[9].

However, the effect of different geometries on the adipogenic differentiation of MSCs was not evident in this study. In a recent report, Luo *et al*.[24] indicated that the rate of adipogenic differentiation of MSC aggregates could be affected by different geometric micropatterns. Their work highlighted the geometric effect on the differentiation of MSCs at the multiple-cell level. However, the cell number, shape, and cell-cell contact within each geometric micropattern were heterogeneous. In contrast, in this study, the cell shape cues for the differentiation of MSCs at single-cell level without cell-cell contact were investigated. The apparent conflicting results actually revealed the diversity and complexity of cell differentiation at single- and multiple-levels.

It has been reported that cytoskeletal organization in cells is important to the commitment of MSCs[25,26]. Generally, the assembly of cytoskeleton correlates with intracellular contractility. Large cell spreading and increased contractility favor osteogenic differentiation, while small cell spreading and low contractility favor adipogenic differentiation. In this study, MSCs cultured on triangular, square, pentagonal, hexagonal and circular micropatterns in control medium showed similar patterns of actin filaments. Although actin filaments were thicker and denser at the edges than in the interior regions of the micropatterns, asymmetrical concentrations of actin filaments were not shown in either edge of all the geometries and no predominated alignment of the actin filaments emerged inside the micropattern geometry (Figure 4.5). After culture in adipogenic medium for one week, the actin cytoskeleton underwent remodeling and the differentiated cells showed faint actin filaments (Figure 4.11). The similarity and symmetry of cytoskeletal structures may implicate the similar low level of intracellular contractility in the cells cultured on the five micropatterns and might partially cause the parallel potential of adipogenic differentiation of MSCs on the micropatterns. Another possibility is that the global low contractility in cell was dominated by same small cell size rather than different cell shapes. As different geometries of intermediate size can influence cell differentiation[22], it would be valuable to investigate the threshold size where the geometric effect would be overwhelmed by size effect. However, the possibility that the slight geometric effects which might be reflected in protein and gene expression level were overshadowed by morphological phenotype cannot be completely excluded, which is deserved to be further investigated.

4.6 Conclusions

In summary, we have presented a photolithographic method to make micropatterns with different geometries using photo-reactive PVA. The photo-reactive PVA was micropatterned on a PSt cell-culture plate,

and micropatterns with triangular, square, pentagonal, hexagonal, and circular geometries, yet with the same small surface area for cell spreading, were formed. Human MSCs adhered to the PSt geometric micropatterns and single cell arrays with different shapes (triangles, squares, pentagons, hexagons, and circles) were obtained. The effect of cell shape on the adipogenic differentiation of MSCs was compared. The actin cytoskeletal structures were remolded during differentiation and adipogenic differentiation levels of MSCs were similar on these different geometric micropatterns with same small surface area. This simple micropatterning technique using photo-reactive molecules will be useful for creating micropatterns of arbitrary design on an organic surface and cell functions can be directly and systematically compared on a single surface without external factors resulting from separate cell culture and coating method.

4.7 References

1. Griffith, L. G., Tissue engineering--current challenges and expanding opportunities. *Science* **295**, 1009-1014 (2002).
2. Lutolf, M. P., Gilbert, P. M., Blau, H. M., Designing materials to direct stem-cell fate. *Nature* **462**, 433-441 (2009).
3. Watt, F. M., Out of Eden: stem cells and their niches. *Science* **287**, 1427-1430 (2000).
4. Discher, D. E., Mooney, D. J., Zandstra, P. W., Growth factors, matrices, and forces combine and control stem cells. *Science* **324**, 1673-1677 (2009).
5. Pittenger, M. F., Mackay, A. M., Beck, S. C., Jaiswal, R. K., Douglas, R., Mosca, J. D., Moorman, M. A., Simonetti, D. W., Craig, S., Marshak, D. R., Multilineage potential of adult human mesenchymal stem cells. *Science* **284**, 143-147 (1999).
6. Guilak, F., Cohen, D. M., Estes, B. T., Gimble, J. M., Liedtke, W., Chen, C. S., Control of stem cell fate by physical interactions with the extracellular matrix. *Cell Stem Cell* **5**, 17-26 (2009).
7. Engler, A. J., Sen, S., Sweeney, H. L., Discher, D. E., Matrix elasticity directs stem cell lineage specification. *Cell* **126**, 677-689 (2006).
8. Dalby, M. J., Gadegaard, N., Tare, R., Andar, A., Riehle, M. O., Herzyk, P., Wilkinson, C. D., Oreffo, R. O., The control of human mesenchymal cell differentiation using nanoscale symmetry and disorder. *Nat Mater* **6**, 997-1003 (2007).
9. McBeath, R., Pirone, D. M., Nelson, C. M., Bhadriraju, K., Chen, C.S. Cell shape, cytoskeletal tension, and RhoA regulate stem cell lineage commitment. *Dev Cell* **6**, 483-495 (2004).
10. Peerani, R., Rao, B. M., Bauwens, C., Yin, T., Wood, G. A., Nagy, A., Kumacheva, E., Zandstra, P. W., Niche-mediated control of human embryonic stem cell self-renewal and differentiation. *EMBO J* **26**, 4744-4755 (2007).
11. Connelly, J. T., Gautrot, J. E., Trappmann, B., Tan, D. W., Donati, G., Huck, W. T., Watt, F. M., Actin and serum response factor transduce physical cues from the microenvironment to regulate epidermal stem cell fate decisions. *Nat Cell Biol* **12**, 711-718 (2010).
12. Guo, L., Kawazoe, N., Fan, Y., Ito, Y., Tanaka, J., Tateishi, T., Zhang, X., Chen, G., Chondrogenic differentiation of human mesenchymal stem cells on photoreactive polymer-modified surfaces. *Biomaterials* **29**, 23-32 (2008).
13. Théry, M., Racine, V., Pépin, A., Piel, M., Chen, Y., Sibarita, J. B., Bornens, M., The extracellular matrix guides the orientation of the cell division axis. *Nat Cell Biol* **7**, 947-953 (2005).

14. Jiang, X., Bruzewicz, D. A., Wong, A. P., Piel, M., Whitesides, G. M., Directing cell migration with asymmetric micropatterns. *Proc Natl Acad Sci USA* **102**, 975-978 (2005).
15. Cheng, Q., Li, S., Komvopoulos, K., Plasma-assisted surface chemical patterning for single-cell culture. *Biomaterials* **30**, 4203-4210 (2009).
16. Roca-Cusachs, P., Alcaraz, J., Sunyer, R., Samitier, J., Farré, R., Navajas, D., Micropatterning of single endothelial cell shape reveals a tight coupling between nuclear volume in G1 and proliferation. *Biophys J* **94**, 4984-4995 (2008).
17. Thakar, R. G., Cheng, Q., Patel, S., Chu, J., Nasir, M., Liepmann, D., Komvopoulos, K., Li, S., Cell-shape regulation of smooth muscle cell proliferation. *Biophys J* **96**, 3423-3432 (2009).
18. Gautrot, J. E., Trappmann, B., Oceguera-Yanez, F., Connelly, J., He, X., Watt, F. M., Huck, W. T., Exploiting the superior protein resistance of polymer brushes to control single cell adhesion and polarisation at the micron scale. *Biomaterials* **31**, 5030-5041 (2010).
19. Théry, M., Racine, V., Piel, M., Pépin, A., Dimitrov, A., Chen, Y., Sibarita, J. B., Bornens, M., Anisotropy of cell adhesive microenvironment governs cell internal organization and orientation of polarity. *Proc Natl Acad Sci USA* **103**, 19771-19776 (2006).
20. Singhvi, R., Kumar, A., Lopez, G. P., Stephanopoulos, G. N., Wang, D. I., Whitesides, G. M., Ingber, D. E., Engineering cell shape and function. *Science* **264**, 696-698 (1994).
21. Chen, C. S., Mrksich, M., Huang, S., Whitesides, G. M., Ingber, D. E., Geometric control of cell life and death. *Science* **276**, 1425-1428 (1997).
22. Kilian, K. A., Bugarija, B., Lahn, B. T., Mrksich, M. Geometric cues for directing the differentiation of mesenchymal stem cells. *Proc Natl Acad Sci USA* **107**, 4872-4877 (2010).
23. Falconnet, D., Csucs, G., Grandin, H. M., Textor, M., Surface engineering approaches to micropattern surfaces for cell-based assays. *Biomaterials* **27**, 3044-3063 (2006).
24. Luo, W., Jones, S. R., Yousaf, M. N., Geometric control of stem cell differentiation rate on surfaces. *Langmuir* **24**, 12129-12133 (2008).
25. Yourek, G., Hussain, M. A., Mao, J. J., Cytoskeletal changes of mesenchymal stem cells during differentiation. *ASAIO J* **53**, 219-228 (2007).
26. Rodríguez, J. P., González, M., Ríos, S., Cambiazo, V., Cytoskeletal organization of human mesenchymal stem cells (MSC) changes during their osteogenic differentiation. *J Cell Biochem* **93**, 721-731 (2004).

Chapter 5

Preparation of micropattern of negatively charged polymer and its effect on MSCs functions

5.1 Summary

In this chapter, the micropatterning method was used to investigate the electrostatic effect derived from different chemical groups on the functions of individual and multiple human mesenchymal stem cells (MSCs). Differently sized circular micropatterns of negatively charged poly(acrylic acid) (PAAc) and neutral polystyrene (PSt) were created using UV photolithography. The PAAc and PSt micropatterns showed different effects on actin cytoskeleton organization and adipogenic differentiation of MSCs. The assembly and distribution of actin filaments for individual MSCs correlated with the degree of cell spreading as well as the surface charge of the underlying substrates. The degree of MSC adipogenesis was evaluated by comparing the percentage of PAAc and PSt micropatterns that contained Oil Red O stained cells. The adipogenic differentiation at the single-cell level was enhanced on the PAAc micropatterns and decreased as the diameter of the circular micropattern increased. The adipogenic differentiation at the multiple-cell level was stronger on PAAc micropatterns and was independent of the diameter of the circular micropattern.

5.2 Introduction

Stem cells are versatile and promising cell sauces for tissue engineering and regenerative medicine due to their inherent plasticity and multi-lineages potential[1-6]. *In vitro*, suitable biomaterials are used to propagate stem cells to obtain sufficient cell quantities for cell transplantation[7]. Alternatively, porous scaffolds are provided for stem cells as a temporary support to regenerate required tissue implants[8]. *In vivo*, appropriate carriers or scaffolds are loaded with stem cells to protect them from hostile microenvironment and to delivery them to target site[9]. All these applications highlight the important roles of cell-material interactions on controlling over the functions of stem cells.

The surface chemistry is one of the critical factors of material's properties because it alters the surface's energy, wettability, and charge. For examples, polylysine modified surfaces are positively charged and suitable for neural cells adhesion[10,11]. And foreign-body responses are regulated by different cationic

polymer coatings[12]. Allen *et al.* synthesized a group of copolymers consisted of varied ratios of *N*-isopropylacrylamide (NIPAAm) and *N-tert*-butylacrylamide (NtBAAm). The different combinations of NIPAAm and NtBAAm monomers altered the surface hydrophobicity of copolymers and thus modulated the attachment of HeLa cells[13]. Brodbeck *et al.* reported that macrophage apoptosis was increased *in vivo* on hydrophilic and anionic surfaces[14]. As a high-throughput screen method, the combinatorial library of chemistry microarrays has also been developed to rapidly interrogate the interactions between biomaterials chemistry and cells[15-17]. For example, Anderson *et al.*[18] synthesized a series of biopolymers from diverse combinations of acrylate and methacrylate monomers and then simultaneously characterize over 1,700 human embryonic stem cells-biopolymers interactions.

By using different surface modification methods, various chemical groups were immobilized onto surfaces and their effects on the differentiation of mesenchymal stem cells (MSCs) have been investigated. These results indicated that the methyl group maintained the phenotype of MSCs[19], the amino, thiol, and phosphate groups promoted the osteogenesis[19-22], and the carboxyl and hydroxyl groups facilitated the chondrogenesis[19,20,23]. Additionally, the carboxyl coated gels of intermediate and lowest stiffness were in favor of myogneic and neurogenic differentiation, respectively[24]. Although these works discerned the respective effect of different chemical groups on the MSC's differentiation, the results were derived from responses across multiple-cell populations cultured under conventional conditions. Under these conditions, cells freely spread and divide in all directions, resulting in an inherent variability in cell spreading, shape, and behavior; therefore, results are sometimes controversial. The high cell-to-cell variation of the overall population highlights the importance of single-cell analyses regarding the effects of surface chemistry.

In this study, we developed a method to prepare micropatterned surfaces with different surface chemistries. Negatively charged poly(acrylic acid) (PAAc) micropatterns and neutral polystyrene (PSt) micropatterns were prepared using photolithography. The micropatterns were used to study single-cell and multiple-cell cultures of MSCs, and they allowed for the control of shape and spreading of the MSCs. Using this method, the electrostatic effect on the functions of individual and multiple MSCs was investigated.

5.3 Materials and methods

5.3.1 Synthesis of azidophenyl-derivatized PAAc

Azidophenyl-derivatized poly(acrylic acid) (AzPhPAAc) was synthesized by coupling the carboxyl groups of PAAc with 4-azidoaniline, as shown in Figure 5.1. PAAc (Sigma-Aldrich, Mw=450,000, 1.0 mmol on monomer unit), 4-azidoaniline hydrochloride (Sigma-Aldrich, 0.1 mmol), and 1-ethyl-3-(3-dimethylamino propyl) carbodiimide hydrochloride (WSC, Wako Pure Chemical Industries Ltd., 6.0 mmol) were dissolved in deionized water (110 mL). The pH of the solution was adjusted to 7.0 by adding NaOH or HCl solution. After being stirred at 4 ^{O}C for 48 h, the reaction solution was dialyzed against Milli-Q water through a seamless cellulose tube (cutoff Mw=12,000) until the absence of azidoaniline in the washing solution was confirmed by UV spectroscopy. The dialyzed AzPhPVA was freeze-dried and stored at -4 ^{O}C in the dark.

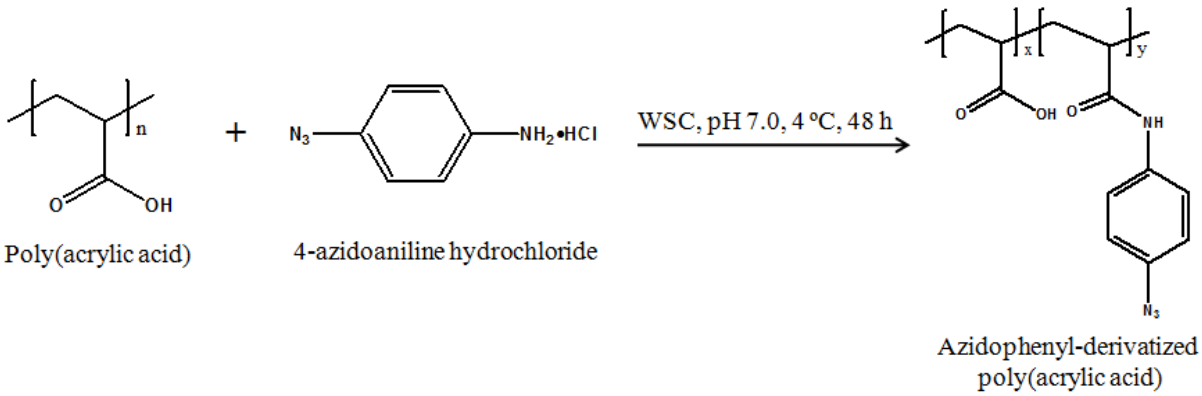

Figure 5.1 The chemical equation for the synthesis of azidophenyl-derivatized poly(acrylic acid).

5.3.2 Synthesis of azidophenyl-derivatized PVA

Azidophenyl-derivatized poly(vinyl alcohol) (AzPhPVA) was synthesized by coupling the hydroxyl groups of PVA to 4-azidobenzoic acid as previously described in Chapter 2.3.1.

5.3.3 Fabrication of photomask

The photomask was prepared using DWL66 laser lithography system as previously described in Chapter 2.3.2.

5.3.4 Preparation of PVA-PAAc- and PVA-micropatterned PSt surfaces with a photomask

A PSt plate (2.5 × 2.5 cm^2) was cut from a tissue-culture PSt flask (BD Falcon™). The AzPhPAAc solution (0.15 mL, 0.2 mg/mL) was placed on the PSt plate and air-dried in the dark at room temperature. The coating region was around 1.5 × 1.0 cm^2. The plates were irradiated with UV light (Funa®-UV-Linker FS-1500) at energy of 0.5 J/cm^2 from a distance of 15 cm without using a photomask. After irradiation, the plates were immersed in diluted alkaline solution (pH 10) and ultrasonicated to completely remove any unreacted PAAc. Subsequently the AzPhPVA solution (0.15 mL, 0.5 mg/mL) was placed on the PAAc-grafted plate and air-dried in the dark at room temperature. The plates were then covered with a photomask and irradiated with UV light at energy of 0.3 J/cm^2 from a distance of 15 cm. After irradiation, the plates were immersed in Milli-Q water and then ultrasonicated to completely remove any unreacted PVA from the non-irradiated areas. After complete washing, a PVA-PAAc-micropatterned PSt surface was obtained. Preparation scheme of PVA-PAAc-micropatterned PSt surface was shown in Figure 5.2. To visualize the circular PAAc micropatterns, the PVA-PAAc-micropatterned PSt surface was stained with 1% Brilliant Green solution for 10 sec.

The preparation of PVA-micropatterned PSt surfaces was previously described in Chapter 3.3.3.

The PVA-PAAc- and PVA-micropatterned PSt plates were sterilized with 70% ethanol and used for cell culture.

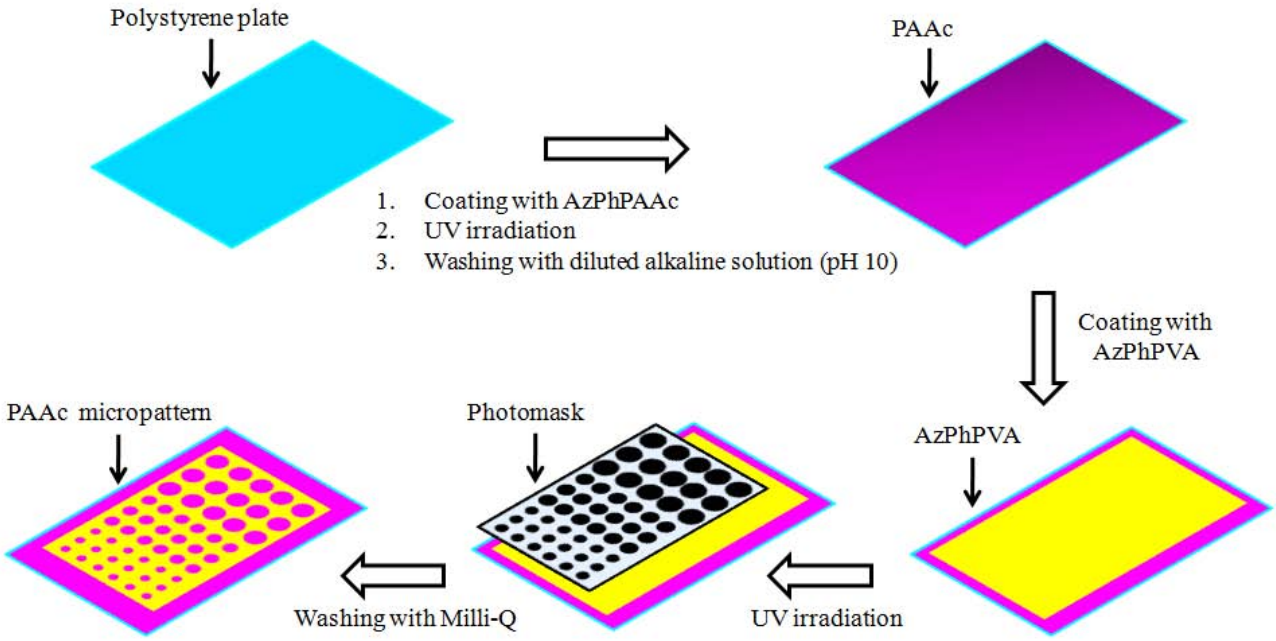

Figure 5.2 Preparation scheme of PVA-PAAc-micropatterned PSt surface.

5.3.5 AFM observation

The surface topography of the PVA-PAAc- and PVA-micropatterned PSt plate was observed using MFP-3D-BIO^{TM} AFM (Asylum Research). A commercially available cantilever (spring constant: 0.06 N/m; oscillation frequency: 12-24 kHz; DNP, Veeco Probes) with a silicon nitride tip was used to measure the samples (90 × 90 μm^2) in Milli-Q water in contact mode. The diameter of circular PAAc and PSt micropatterns and step height of surrounding PVA layer was measured by section analysis of the acquired images. Three randomly selected micropatterns were measured to calculate the mean and standard deviation.

5.3.6 Cell culture

Human bone marrow-derived mesenchymal stem cells (MSCs) were obtained from Osiris Therapeutics (Columbia, MD) at passage 2. The cells were subcultured twice as previously described in Chapter 2.3.4 and used at passage 4.

The PVA-PAAc- and PVA-micropatterned PSt plates were placed in 6-well cell culture plates, and a glass ring (diameter: 15 mm; height: 10 mm) was placed over each plate. 3 mL control medium were added to each well, and then the cell suspension (0.3 mL, 3.0 × 10^4 cells/mL) was placed inside the glass ring (seeding density: 5.0×10^3 cells/cm^2). The compositions of control medium were previously described in Chapter 2.3.4.

The glass rings were removed after 6 h and the control medium was replaced with adipogenic medium after 24 h. The compositions of adipogenic medium were previously described in Chapter 3.3.4. The adipogenic medium was changed every 3 days.

5.3.7 F-actin staining

After incubation for 6 h in control medium, the cultured cells were fixed with 4%

paraformaldehyde for 10 min at 4 ^{O}C, permeabilized with 0.2% Triton X-100 for 2 min, and blocked with 1% BSA solution for 30 min at room temperature. The F-actin and nuclei of cells were stained with Alexa Fluor® 488 phalloidin (Invitrogen) for 20 min and 4', 6-diamidino-2-phenylindole (DAPI, Vector Laboratories, Inc.) for 10 min, respectively. Fluorescence photographs of the stained MSCs were captured by an Olympus BX51 microscope with a DP-70 CCD camera (Olympus, Tokyo, Japan).

5.3.8 Single-cell percentage on PVA-PAAc- and PVA-micropatterned PSt surfaces

After 6 and 24 h of culture in control medium and 7 days of culture in adipogenic medium, the cells were fixed with 4% paraformaldehyde for 10 min at 4 ºC and then the cell nuclei were stained with 4', 6-diamidino-2-phenylindole (DAPI, Vector Laboratories, Inc.). The respective number of circular PAAc and PSt dots occupied by single cells and multiple cells was counted after the cell nuclei were stained. The formula (1) was used to calculate the single-cell percentage. At each time point, three plates were used to calculate the mean and standard deviation.

$$\text{Single cell}\,\% = \frac{N_{\text{Single cell dot}}}{N_{\text{Total cell dot}}} \quad (1)$$

$N_{\text{Single cell dot}}$: The number of circular PAAc or PSt dots occupied by a single cell; $N_{\text{Total cell dot}}$: The total number of circular PAAc or PSt dots occupied by either a single cell or multiple cells.

5.3.9 Oil Red O staining

After incubation in adipogenic medium for 7 days, the cultured cells were fixed with 4% paraformaldehyde for 10 min at 4 ^{O}C, incubated in 60% isopropanol for 5 min, and then stained with fresh Oil Red O for 5 min. The nucleus was counterstained with 2 μg/mL DAPI solution for 10 min (Dojindo). The Oil Red O solution was prepared by mixing three parts stock solution (0.3% in isopropanol) with two parts Milli-Q water and filtering through a 0.2 μm filter. Photomicrographs were captured by an optical microscope with a DP-70 CCD camera (Olympus, Tokyo, Japan).

The probability of MSC adipogenesis on the PVA-PAAc- and PVA-micropatterned PSt surfaces was studied by calculating the percentage of MSCs that committed to an adipocyte lineage as shown in formula (2) and (3). Cells containing lipid vacuoles positively stained by Oil Red O were considered to be adipocytes. Both single and multiple cells on each circular micropattern (as confirmed by nuclear staining) were counted. Three samples were used to calculate the mean and standard deviation.

$$\text{Adipogenesis of single cell}\,\% = \frac{N_{\text{Stained single cell dot}}}{N_{\text{Total single cell dot}}} \quad (2)$$

$N_{\text{Stained single cell dot}}$: The number of circular PAAc or PSt dots occupied by a positively stained single cell; $N_{\text{Total single cell dot}}$: The total number of circular PAAc or PSt dots occupied by a single cell.

$$\text{Adipogenesis of multiple cells}\,\% = \frac{N_{\text{Stained multiple cells dot}}}{N_{\text{Total multiple cells dot}}} \quad (3)$$

$N_{\text{Stained multiple cells dot}}$: The number of circular PAAc or PSt dots occupied by positively stained multiple cells; $N_{\text{Total multiple cells dot}}$: The total number of circular PAAc or PSt dots occupied by multiple cells.

5.3.10 Statistical analysis

A one-way analysis of variance (ANOVA) with Tukey's *post hoc* test for multiple comparisons was used for statistical analysis. A value of $p < 0.05$ was considered to be a statistically significant difference.

5.4 Results

5.4.1 Preparation and observation of PVA-PAAc- and PVA-micropatterned PSt surfaces

Photo-reactive AzPhPAAc was grafted to the surface of cell-culture PSt plate using UV irradiation without a photomask. To prepare the PAAc micropatterns, the PAAc-grafted PSt plate was coated with photo-reactive AzPhPVA and dried. The AzPhPVA-coated PAAc-grafted PSt was covered with a photomask and irradiated with UV light (Figure 5.2). The photomask had three different circular micropatterns with diameters of 40, 60, and 80 μm. These circular micropatterns were not transparent under UV light so that the underlying AzPhPVA did not react during UV irradiation and was washed away by Milli-Q water after UV irradiation. The AzPhPVA below the surrounding transparent regions was exposed to UV light, inter- and intra-molecularly crosslinked, and immobilized to the underlying PAAc-grafted PSt surface. Therefore, three differently sized circular micropatterns of PAAc were formed and surrounded by PVA, which can effectively prevent cell adhesion. PVA-micropatterned PSt surface was prepared as previously described in Chapter 3.3.3.

Photomicroscopic images of the PVA-PAAc-micropatterned and PVA-micropatterned PSt surfaces are shown in Figure 5.3. The micropatterns were clearly displayed when viewed using an optical microscope. The PVA-PAAc-micropatterned PSt surface was stained with Brilliant Green solution to show the PAAc micropatterns. The basic dye interacted electrostatically with the negatively charged PAAc, and the circular PAAc micropatterns were visualized by a dark green color under optical microscopy (Figure 5.3). During the staining process, the dye permeated through the overlying PVA layer to the PAAc layer below, causing the surrounding light green color. PVA-PAAc-micropatterned and PVA-micropatterned PSt surfaces were also observed with AFM in Milli-Q water in contact mode and section images of the boundary between PVA and PAAc/PSt are shown in Figure 3. The diameter of micropatterned circles and the step height were analyzed by section analysis of the acquired images (Table 5.1). The diameters of circular PAAc and PSt micropatterns were same as the designed diameters on photomask. The step height of surrounding PVA layer was ~50 and ~105 nm on PAAc and PSt, indicating that cell non-adhesive PVA sufficiently covered the underlying PAAc and PSt. These results confirmed the formation of the PAAc and PSt micropatterns.

5.4.2 Cell adhesion, spreading, and proliferation

Human MSCs were cultured on the PVA-PAAc- and PVA-micropatterned PSt surfaces. After culturing for 6 h in the control medium, the MSCs only adhered to the circular PAAc and PSt micropatterns; the MSCs on the non-adhesive PVA regions were removed by changing the medium (Figure 5.5). These results confirmed that the MSCs were confined within the circular micropatterns on the micropatterned surfaces.

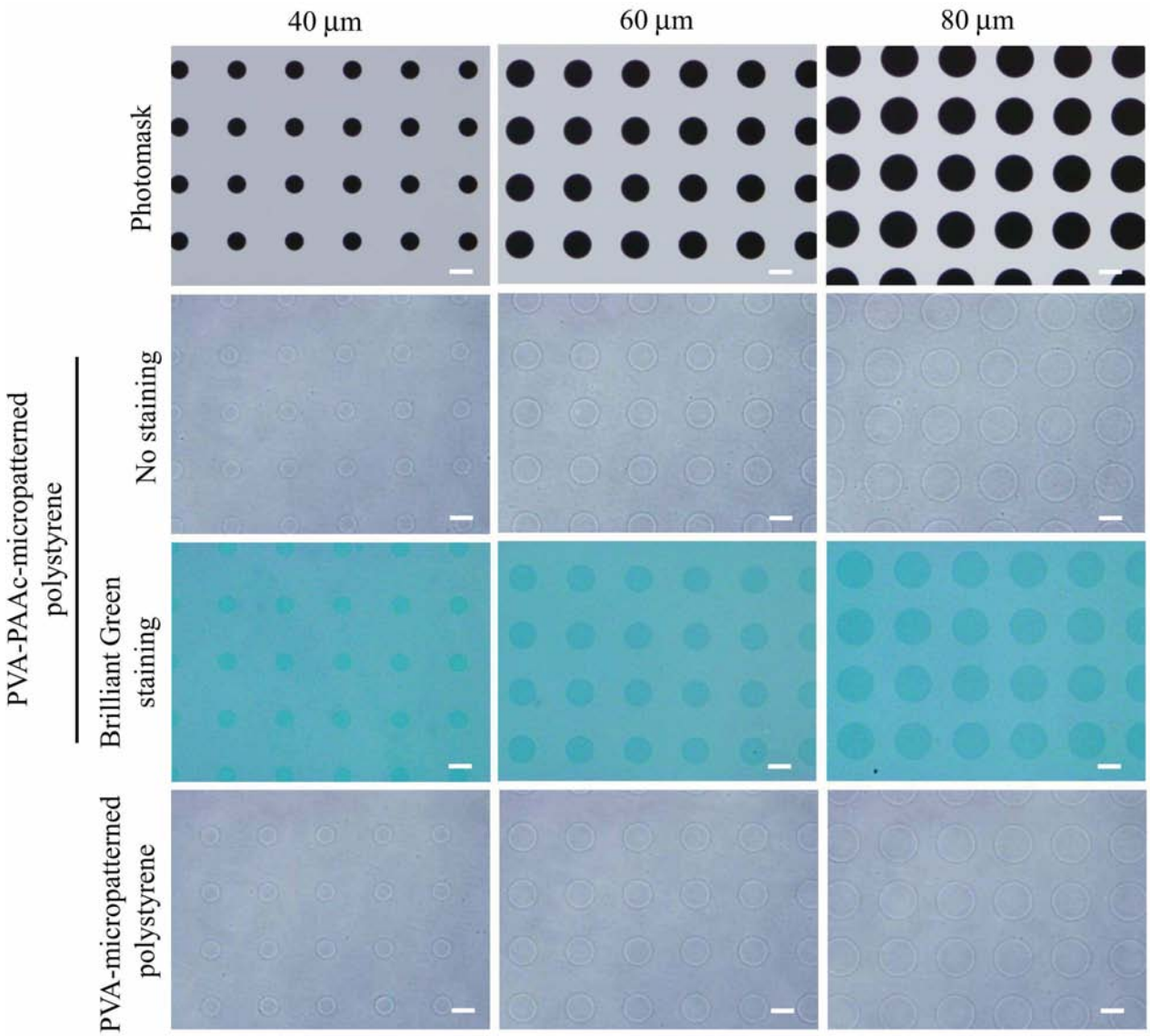

Figure 5.3 Photographs of the photomask and the PVA-PAAc-micropatterned and PVA-micropatterned PSt surfaces. Three types of circular micropatterns with diameters of 40, 60, and 80 μm were fabricated and surrounded by regions of PVA. The PVA-PAAc-micropatterned PSt surface was stained with Brilliant Green solution. Scale bars: 50 μm.

Table 5.1 The diameters of circular PAAc and PSt micropatterns and step height of surrounding PVA layer, as determined by AFM section analysis. Data represent mean ± SD (n = 3).

Designed diameter	Circular diameter (μm)		Step height of PVA (nm)	
(μm)	PVA-PAAc	PVA-PSt	PVA-PAAc	PVA-PSt
40	39.10 ± 0.53	39.14 ± 0.56		
60	58.65 ± 0.35	59.00 ± 0.63	52.0 ± 6.6	105.8 ± 8.1
80	78.90 ± 0.36	79.19 ± 0.27		

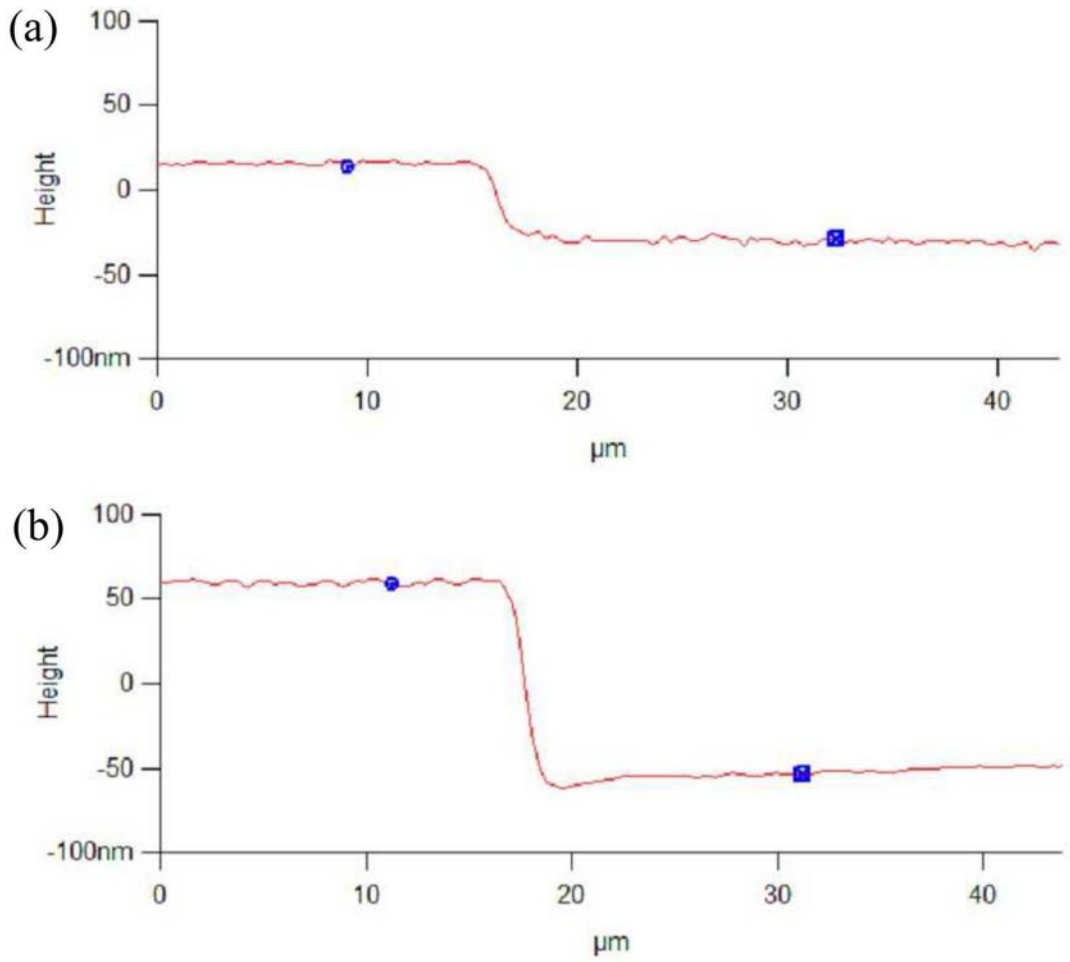

Figure 5.4 Representative AFM section images of step height of surrounding PVA layer on circular PAAc (a) and PSt micropattern (b). The blue circular dots indicate PVA surface. The blue square dots in (a) and (b) indicate PAAc and PSt surfaces, respectively.

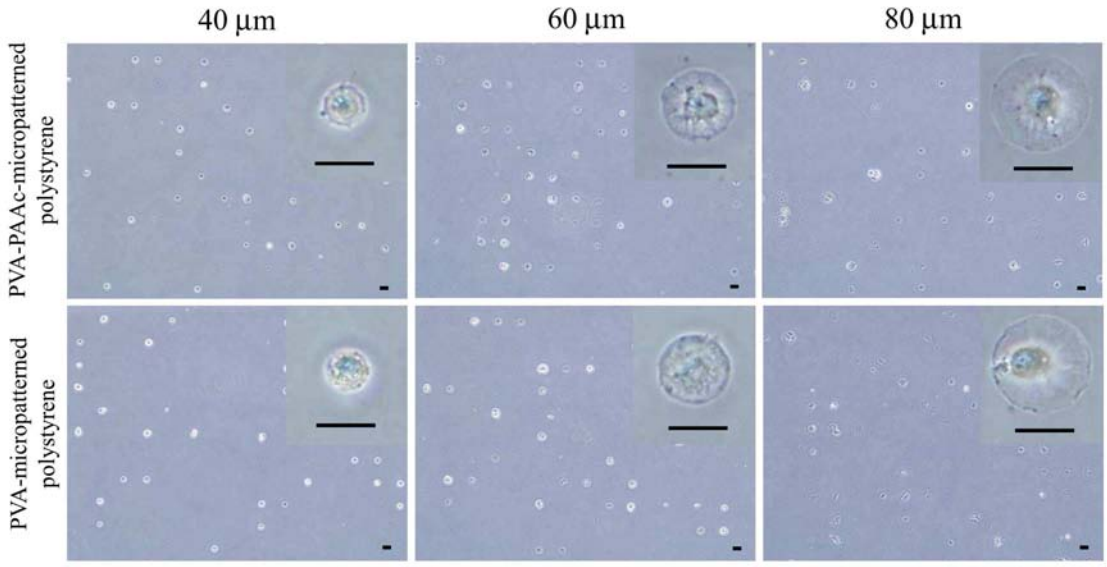

Figure 5.5 Phase contrast photographs of the MSCs after culturing for 6 h on the PVA-PAAc- and PVA-micropatterned PSt surfaces in the control medium. The inserts are enlarged photographs. Scale bars: 50 μm.

As shown in Figure 5.6, F-actin staining revealed that the spreading of MSCs followed the underlying circular PAAc and PSt micropatterns and that the surrounding non-adhesive PVA regions confined the spreading. Interestingly, the assembly and organization of the actin filaments of the MSCs were affected by the degree of cell spreading and the surface charge. On 40 μm micropatterns, the distribution of actin filaments was homogeneous on the negatively charged PAAc circles, whereas the circular MSCs primarily organized actin filaments along the periphery of cell on the neutral PSt circles. The organization of the actin structure became more ordered as the degree of cell spreading increased (60 μm micropatterns). As the cell spreading further enlarged (80 μm micropatterns), the radial and concentric arrangement of actin filaments appeared on both PAAc and PSt circles.

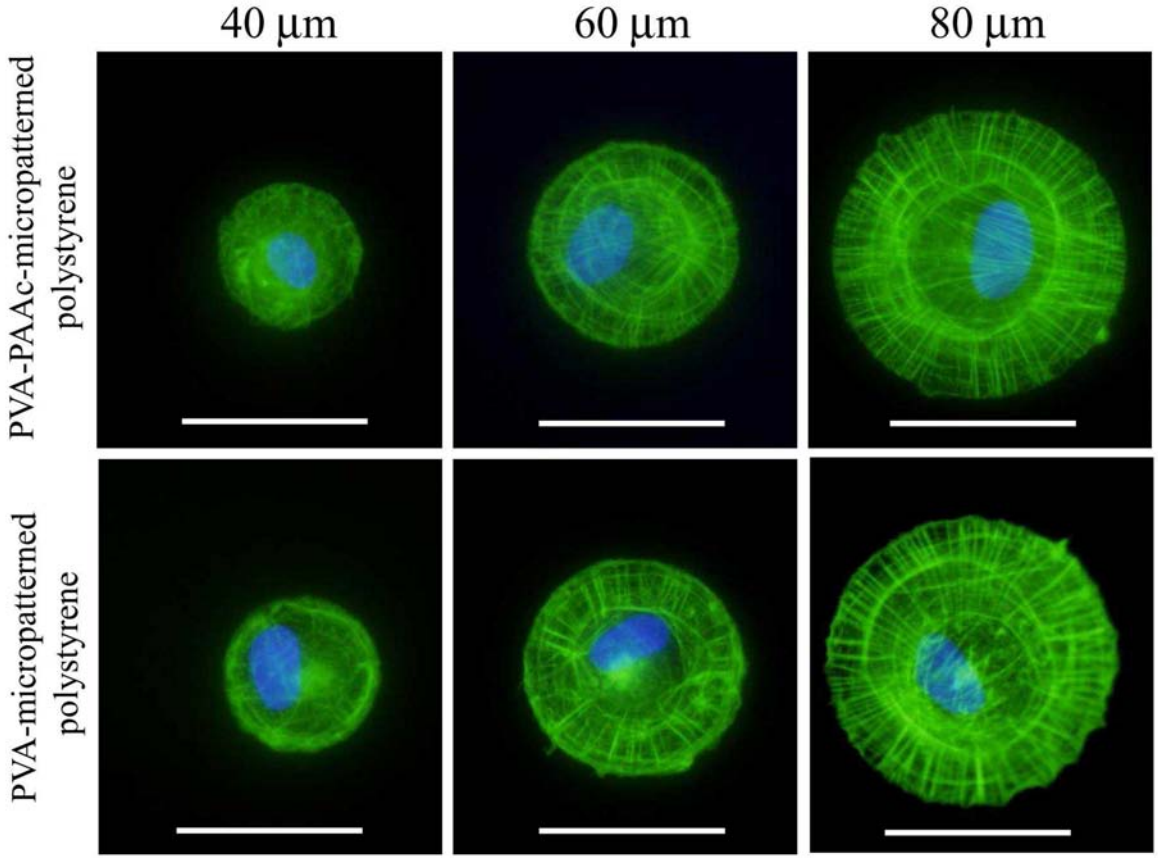

Figure 5.6 Fluorescent images of individual MSCs with different spreading areas on the PVA-PAAc- and PVA-micropatterned PSt surfaces for F-actin (green) and nuclei (blue) after culturing for 6 h in the control medium. Scale bars: 50 μm.

The proliferation of MSCs was investigated by counting the percentage of circular PAAc and PSt micropatterns that contained only a single cell during cell culture. The results are shown in Figure 5.7. After culturing for 6 h in the control medium, the percentage of the micropatterns containing only a single cell was lower on the PAAc micropatterned surfaces than on the PSt micropatterned surfaces. The percentages after 24 h culture were similar to those after culturing for 6 h in the control medium. The proliferation of the MSCs on the PAAc and PSt micropatterns was not obvious and was independent of the circular size after 24 h. However, the MSCs divided and proliferated during the adipogenic culture period as the percentage of single cells decreased after culturing for 7 d in the adipogenic medium. The degree of decrement was almost the same for the PAAc and PSt micropatterns, indicating that PAAc and PSt showed no difference on cell proliferation. However, the proliferation of the MSCs increased as the circular diameter was increased,

regardless of the charge properties of the substrates.

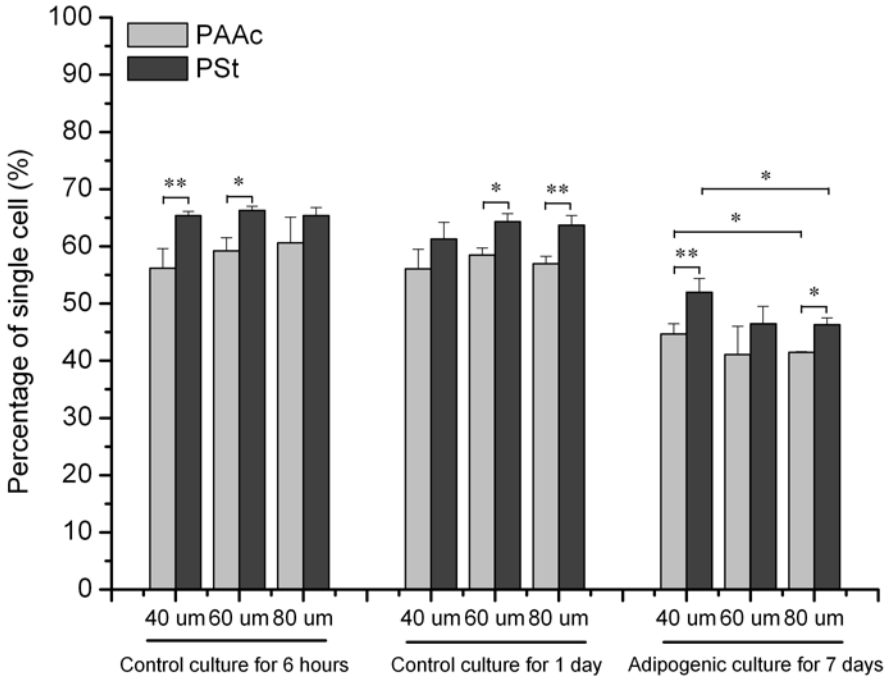

Figure 5.7 Single-cell percentage on the PVA-PAAc- and PVA-micropatterned PSt surfaces after culturing in the control medium for 6 and 24 h, and after culturing in the adipogenic medium for 7 days. Data represent mean ± SD (n = 3). * p<0.5 and ** p<0.01.* *p*<0.5 and ** *p*<0.01.

5.4.3 Adipogenic differentiation of MSCs

The MSCs were cultured on the PVA-PAAc- and PVA-micropatterned PSt surfaces in the adipogenic medium for 7 days. As shown in Figure 5.8, the MSCs were confined within the micropatterns, indicating that the PVA-PAAc- and PVA-micropatterned PSt surfaces were suitable for long-term cell culture. Some MSCs on the micropatterns differentiated into adipocytes containing lipid vacuoles. Lipid vacuoles were stained with Oil Red O, a specific marker for adipogenic differentiation. Figure 5.9 shows representative optical photomicrographs of the positively stained cells with different cell spreading areas on the PAAc and PSt micropatterns. Neither the PAAc nor the PSt micropatterns supported the adipogenesis of MSCs in the control medium without adding adipogenic inductive factors.

The effects of surface charge and circular diameter on the probability that the MSCs would differentiate to adipocytes were evaluated. The cells containing lipid vacuoles that were positively stained by Oil Red O were considered to be adipocytes. Single cells and multiple cells on each circular micropattern were counted. The results showed that the probability of the adipogenesis of the MSC was dependent on the surface charge and circular diameter (Figure 5.10). At the single-cell level, the adipogenesis of the MSCs was enhanced on the negatively charged PAAc micropatterns when the circular diameter was small (40 and 60 μm micropatterns). By contrast, the adipogenesis of the MSCs was similar between the negatively charged PAAc and the neutral PSt micropatterns when the circular diameter was large (80 μm micropatterns). Moreover, the percentage of differentiated MSCs decreased as the circular diameter increased; this trend was independent of surface charge. At the multiple-cell level, the negatively charged PAAc micropatterns promoted the adipogenesis of the MSCs when compared to the neutral PSt micropatterns. However, the effect of the circular diameter was not evident in the adipogenesis of groups of multiple MSCs.

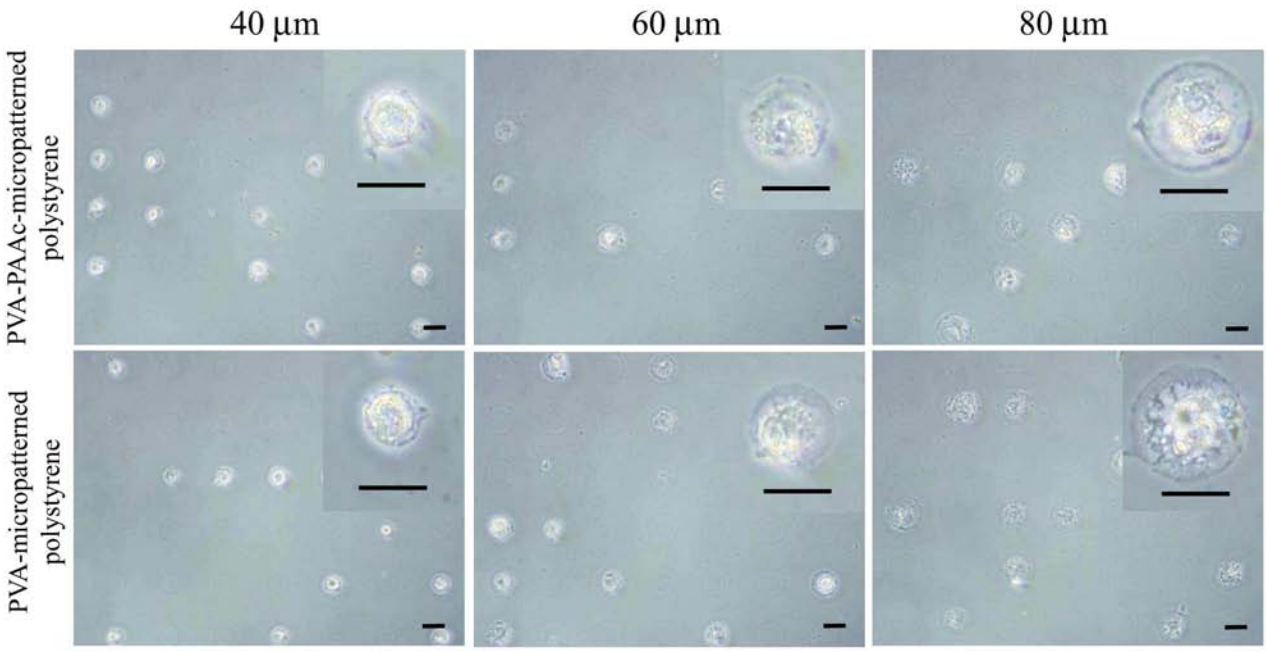

Figure 5.8 Phase contrast photographs of MSCs after culturing for 7 days on the PVA-PAAc- and PVA-micropatterned PSt surfaces in the adipogenic medium. The inserts are enlarged photographs. Scale bars: 50 μm.

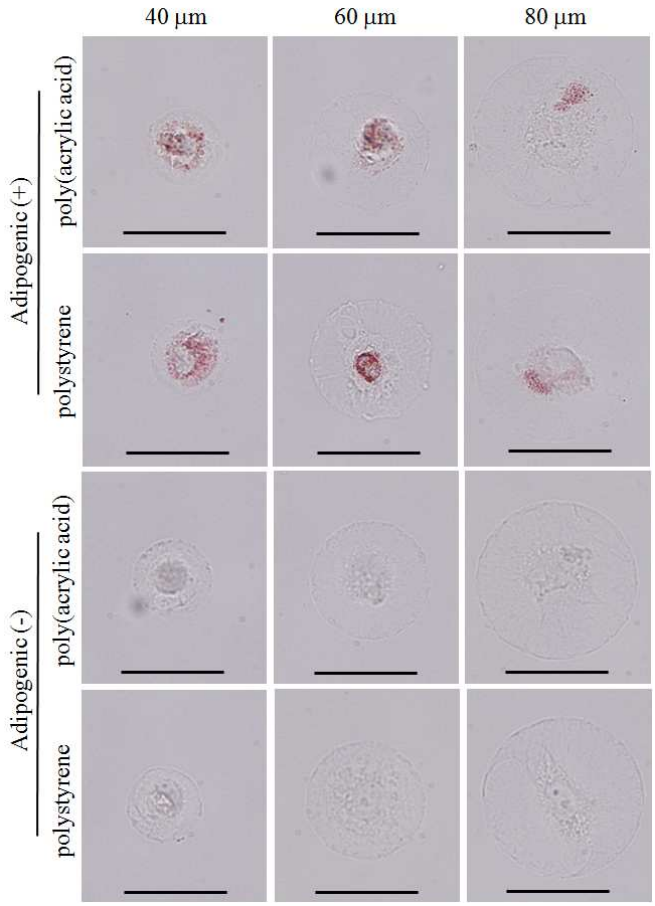

Figure 5.9 Representative optical photographs of MSCs on the PVA-PAAc- and PVA-micropatterned PSt surfaces stained by Oil Red O after culturing in the adipogenic medium (adipogenic +) or the control medium (adipogenic -) for 7 days. Scale bars: 50 μm.

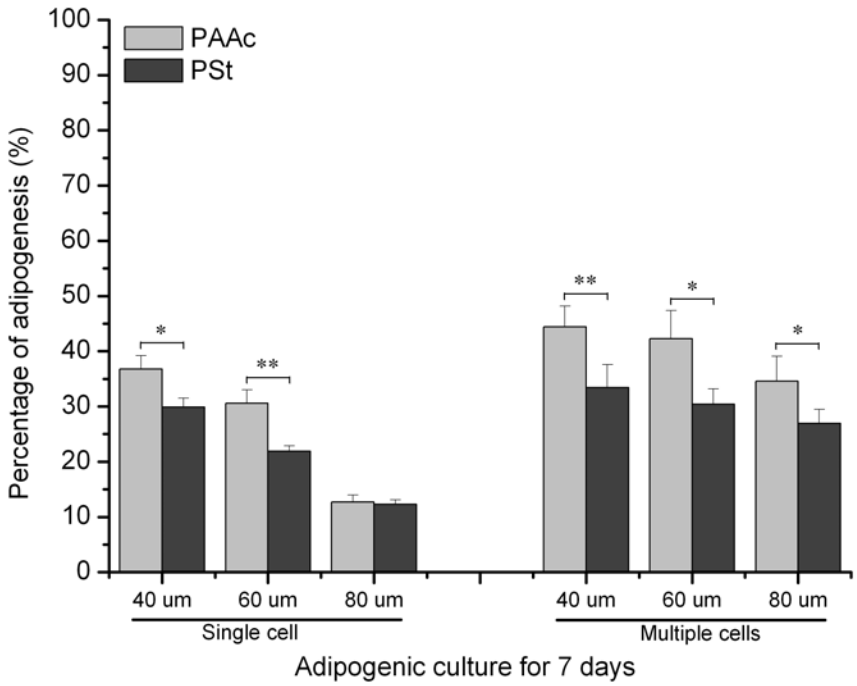

Figure 5.10 The percentage of adipogenic differentiation of MSCs on the PVA-PAAc- and PVA-micropatterned PSt surfaces after culturing in the adipogenic medium for 7 days. Data represent mean ± SD (n = 3). * p<0.05 and ** p<0.01.

5.5 Discussion

It is well-known that biomaterial surface chemistry regulates cell functions including adhesion, survival, proliferation, and differentiation[25-28]. However, most previous works were conducted on non-micropattern surfaces. The conclusions were based on the average results from multiple-cell populations, where the spreading, shape, and behavior of each cell were very heterogeneous. This high cell-to-cell variance of the overall population highlights the importance of single-cell analyses[7,29,30]. To obtain deeper insights on the effects of surface chemistry, negatively charged PAAc and neutral PSt micropatterns were constructed on a commonly used cell-culture surface using UV photolithography. Positively charged polyallylamine (PAAm) micropattern was also prepared. However, it was difficult to obtain single cell array on the PAAm micropattern because of low viability of single MSC on the micropattern. Therefore, the negatively charged surface was used in this study. The electrostatic effect on the functions of individual and multiple MSCs was investigated on different PAAc and PSt micropatterns. The micropatterning method enabled the precise control of cell spreading and shape by modifying the chemical properties of the cell-culture substrates at predefined locations. The circular PAAc and PSt micropatterns allowed for the confinement of single and multiple MSCs and the analysis of the overall cell population at the single- and multiple-cell levels, reducing the heterogeneity of the cell population.

It has been reported that actin cytoskeleton plays an important role in the differentiation of MSCs[31-33]. Therefore, the organization and assembly of the actin filaments of single MSCs were compared between the negatively charged PAAc and neutral PSt micropatterns. The actin structure of single MSCs was affected by the degree of cell spreading, and in the MSCs that adhered to the larger circular micropatterns (60 and 80 μm micropatterns), well-organized stress fibers appeared. This assembly of actin filaments was not

dependent on the surface charge of the underlying substrates. However, as the cell spreading was further restricted (40 μm micropatterns), the arrangement of actin filaments was correlated with the surface charge of the underlying substrate. The actin filaments uniformly distributed on the negatively charged PAAc circles, whereas primarily assembled along the periphery of cell on the neutral PSt circles. More importantly, the assembly of the actin cytoskeleton was highly correlated with intracellular contractility. Large cell spreading and increased contractility favor osteogenic differentiation, while small cell spreading and low contractility favor adipogenic differentiation[34,35]. The different distributions of the actin filaments on the PAAc and PSt micropatterns implied the distinct degree and distribution of intracellular contractility, which could play an important role in the adipogenic differentiation of MSCs[36].

Although most circular micropatterns were occupied by a single MSC immediately after cell seeding, the MSCs inside the micropatterns were dividing, proliferating, and differentiating as they were incubated in the adipogenic culture. Accordingly, it should be valuable to track the behaviors of MSCs in negatively charged PAAc and neutral PSt micropatterns. After culturing for 7 days in the adipogenic medium, the negatively charged PAAc and neutral PSt showed similar effects on cell proliferation. However, larger micropattern promoted the division and proliferation of the MSCs. The effect of micropattern size was consistent with previous reports that more space for cell facilitated cell proliferation[37,38].

The adipogenic differentiation of MSCs on the circular PAAc and PSt micropatterns was analyzed by staining the lipid vacuoles. At the single-cell level, the smaller, negatively charged PAAc micropatterns enhanced adipogenic differentiation. However, the enhancement effect of PAAc was not obvious in the large micropatterns; the effect of PAAc may be counteracted by the area effect, as the adipogenic differentiation decreased when cell spreading increased. At the multiple-cell level, the adipogenic differentiation was also enhanced on the PAAc micropatterns, but the effect of area was not evident. The multiple cells showed higher potential of adipogenic differentiation than did the single cell. Previous work has demonstrated that cell-cell contact strengthened adipogenic differentiation[39]. The result of this study also highlighted the importance of the cell-cell interaction, which can tighten cell-cell contact and limit cell spreading within a preset area of the micropattern. One possible explanation for the stimulatory effect of the negatively charged PAAc micropatterns may be proteins adsorbed from the medium and secreted from the extracellular matrix. Proteins have profound influence on the assembly of cell membrane receptors (such as integrin binding specificity) that transfer the outside signals into the cell[40,41], and subsequent intracellular signal transductions activate gene expression and finally determine the cell fate. García *et al.* has intensively investigated the role of $\alpha_5\beta_1$ integrin on the cell adhesion and osteogenesis using self-assembled monolayer with different chemical groups[42-45]. It is plausible that different but analogous integrin-specific signaling may be associated with the effect of PAAc, given that the integrin expression was dynamic during adipocyte differentiation[46,47].

5.6 Conclusions

PVA-PAAc- and PVA-micropatterned PSt surfaces were prepared using UV photolithography to study the electrostatic effect on the behavior and function of individual and multiple MSCs. The organization and distribution of actin filaments of the individual MSCs were affected by cell spreading and surface charge. The negatively charged PAAc and neutral PSt micropatterns showed similar effects on cell division and proliferation during adipogenic culture. However, the adipogenic differentiation of the MSCs was enhanced on the PAAc micropatterns at the single-cell and multiple-cell levels. This micropatterning method would be useful to construct diverse micropatterns on various substrates with different physicochemical compositions

and topographical features to investigate the corresponding effect of these factors on stem cells.

5.7 References

1. Lutolf, M. P., Gilbert, P. M., Blau, H. M., Designing materials to direct stem-cell fate. *Nature* **462**, 433-441 (2009).
2. Guilak, F., Cohen, D. M., Estes, B. T., Gimble, J. M., Liedtke, W., Chen, C. S., Control of stem cell fate by physical interactions with the extracellular matrix. *Cell Stem Cell* **5**, 17-26 (2009).
3. Marklein, R. A., Burdick, J. A., Controlling stem cell fate with material design. *Adv Mater* **22**, 175-189 (2010).
4. Fisher, O. Z., Khademhosseini, A., Langer, R., Peppas, N. A., Bioinspired materials for controlling stem cell fate. *Accounts Chem Res* **43**, 419-428 (2010).
5. Toh, Y. C., Blagović, K., Voldman, J., Advancing stem cell research with microtechnologies: opportunities and challenges. *Integr Biol* **2**, 305-325 (2010).
6. Kobel, S., Lutolf, M., High-throughput methods to define complex stem cell niches. *BioTechniques* **48**, ix-xxii (2010).
7. Gilbert, P. M., Havenstrite, K. L., Magnusson, K. E. G., Sacco, A., Leonardi, N. A., Kraft, P., Nguyen, N. K., Thrun, S., Lutolf, M. P., Blau, H. M., Substrate elasticity regulates skeletal muscle stem cell self-renewal in culture. *Science* **329**, 1078-1081 (2010).
8. Im, G. I., Kim, H. J., Lee, J. H., Chondrogenesis of adipose stem cells in a porous PLGA scaffold impregnated with plasmid DNA containing SOX trio (SOX-5,-6 and -9) genes. *Biomaterials* **32**, 4385-4392 (2011).
9. Godier-Furnémont, A. F. G., Martens, T. P., Koeckert, M. S., Wan, L., Parksa, J., Araic, K., Zhang, G., Hudson, B., Homma, S., Vunjak-Novakovic, G., Composite scaffold provides a cell delivery platform for cardiovascular repair. *Proc Natl Acad Sci USA* **108**, 7974-7979 (2011).
10. Ruiz, A., Buzanska, L., Gilliland, D., Rauscher, H., Sirghi, L., Sobanski, T., Zychowicz, M., Ceriotti, L., Bretagnol, F., Coecke, S., Colpo, P., Rossi, F., Micro-stamped surfaces for the patterned growth of neural stem cells. *Biomaterials* **29**, 4766-4774 (2008).
11. Song, H. K., Toste, B., Ahmann, K., Hoffman-Kim, D., Palmore, G. T. R., Micropatterns of positive guidance cues anchored to polypyrrole doped with polyglutamic acid: a new platform for characterizing neurite extension in complex environments. *Biomaterials* **27**, 473-484 (2006).
12. Ma, M., Liu, W. F., Hill, P. S., Bratlie, K. M., Siegwart, D. J., Chin, J., Park, M., Guerreiro, J., Anderson, D. G., Development of cationic polymer coatings to regulate foreign-body responses. *Adv Mater* **23**, H189-H194 (2011).
13. Allen, L. T., Fox, E. J., Blute, I., Kelly, Z. D., Rochev, Y., Keenan, A. K., Dawson, K. A., Gallagher, W. M., Interaction of soft condensed materials with living cells: phenotype/transcriptome correlations for the hydrophobic effect. *Proc Natl Acad Sci USA* **100**, 6331-6336 (2003).
14. Brodbeck, W. G., Patel, J., Voskerician, G., Christenson, E., Shive, M. S., Nakayama, Y., Matsuda, T., Ziats, N. P., Anderson, J. M., Biomaterial adherent macrophage apoptosis is increased by hydrophilic and anionic substrates in vivo. *Proc Natl Acad Sci USA* **99**, 10287-10292 (2002).
15. Anderson, D. G., Putnam, D., Lavik, E. B., Mahmood, T. A., Langer, R., Biomaterial microarrays: rapid, microscale screening of polymer-cell interaction. *Biomaterials* **26**, 4892-4897 (2005).

16. Mei, Y., Gerecht, S., Taylor, M., Urquhart, A. J., Bogatyrev, S. R., Cho, S. W., Davies, M. C., Alexander, M. R., Langer, R. S., Anderson, D. G., Mapping the interactions among biomaterials, adsorbed proteins, and human embryonic stem cells. *Adv Mater* **21**, 2781-2786 (2009).
17. Luo, W., Chan, E. W. L., Yousaf, M. N., Tailored electroactive and quantitative ligand density microarrays applied to stem cell differentiation. *J Am Chem Soc* **132**, 2614-2621 (2010).
18. Anderson, D. G., Levenberg, S., Langer, R., Nanoliter-scale synthesis of arrayed biomaterials and application to human embryonic stem cells. *Nat Biotechnol* **22**, 863-866 (2004).
19. Curran, J. M., Chen, R., Hunt, J. A., The guidance of human mesenchymal stem cell differentiation in vitro by controlled modifications to the cell substrate. *Biomaterials* **27**, 4783-4793 (2006).
20. Curran, J. M., Chen, R., Hunt, J. A., Controlling the phenotype and function of mesenchymal stem cells in vitro by adhesion to silane-modified clean glass surfaces. *Biomaterials* **26**, 7057-7067 (2005).
21. Guo, L., Kawazoe, N., Hoshiba, T., Tateishi, T., Chen, G., Zhang, X., Osteogenic differentiation of human mesenchymal stem cells on chargeable polymer-modified surfaces. *J Biomed Mater Res A* **87**, 903-912 (2008).
22. Benoit, D. S. W., Schwartz, M. P., Durney, A. R., Anseth, K. S., Small functional groups for controlled differentiation of hydrogel-encapsulated human mesenchymal stem cells. *Nat Mater* **7**, 816-823 (2008).
23. Guo, L., Kawazoe, N., Fan, Y., Ito, Y., Tanaka, J., Tateishi, T., Zhang, X., Chen, G., Chondrogenic differentiation of human mesenchymal stem cells on photoreactive polymer-modified surfaces. *Biomaterials* **29**, 23-32 (2008).
24. Lanniel, M., Huq, E., Allen, S., Buttery, L., Williams, P. M., Alexander, M. R., Substrate induced differentiation of human mesenchymal stem cells on hydrogels with modified surface chemistry and controlled modulus. *Soft Matter* **7**, 6501-6514 (2011).
25. Brodbeck, W. G., Shive, M. S., Colton, E., Nakayama, Y., Matsuda, T., Anderson, J. M., Influence of biomaterial surface chemistry on the apoptosis of adherent cells. *J Biomed Mater Res* **55**, 661-668 (2001).
26. Shen, M., Horbett, T. A., The effects of surface chemistry and adsorbed proteins on monocyte/macrophage adhesion to chemically modified polystyrene surfaces. *J Biomed Mater Res* **57**, 336-345 (2001).
27. McClary, K. B., Ugarova, T., Grainger, D. W., Modulating fibroblast adhesion, spreading, and proliferation using self-assembled monolayer films of alkylthiolates on gold. *J Biomed Mater Res* **50**, 428-439 (2000).
28. García, A. J., Vega, M. D., Boettiger, D., Modulation of cell proliferation and differentiation through substrate-dependent changes in fibronectin conformation. *Mol Biol Cell* **10**, 785-798 (1999).
29. Lutolf, M. P., Doyonnas, R., Havenstrite, K., Koleckar, K., Blau, H. M., Perturbation of single hematopoietic stem cell fates in artificial niches. *Integr Biol* **1**, 59-69 (2009).
30. Cordey, M., Limacher, M., Kobel, S., Taylor, V., Lutolf, M. P., Enhancing the reliability and throughput of neurosphere culture on hydrogel microwell arrays. *Stem Cells* **26**, 2586-2594 (2008).
31. Tay, C. Y., Yu, H., Pal, M., Leong, W. S., Tan, N. S., Ng, K. W., Leong, D. T., Tan, L. P., Micropatterned matrix directs differentiation of human mesenchymal stem cells towards myocardial lineage. *Exp Cell Res* **316**, 1159-1168 (2010).
32. Rodríguez, J. P., González, M., Ríos, S., Cambiazo, V., Cytoskeletal organization of human mesenchymal stem cells (MSC) changes during their osteogenic differentiation. *J Cell Biochem* **93**, 721-731 (2004).

33. Yourek, G., Hussain, M. A., Mao, J. J., Cytoskeletal changes of mesenchymal stem cells during differentiation. *ASAIO J* **53**, 219-28 (2007).
34. McBeath, R., Pirone, D. M., Nelson, C. M., Bhadriraju, K. Chen, C. S., Cell shape, cytoskeletal tension, and RhoA regulate stem cell lineage commitment. *Dev Cell* **6**, 483-495 (2004).
35. Guvendiren, M., Burdick, J. A., The control of stem cell morphology and differentiation by hydrogel surface wrinkles. *Biomaterials* **31**, 6511-6518 (2010).
36. Kilian, K. A., Bugarija, B., Lahn, B. T., Mrksich, M., Geometric cues for directing the differentiation of mesenchymal stem cells. *Proc Natl Acad Sci USA* **107**, 4872-4877 (2010).
37. Both, S. K., van der Muijsenberg, A. J. C., van Blitterswijk, C. A., de Boer, J., de Bruijn, J. D., A rapid and efficient method for expansion of human mesenchymal stem cells. *Tissue Eng* **13**, 3-9 (2007).
38. Lode, A., Bernhardt, A., Gelinsky, M., Cultivation of human bone marrow stromal cells on three-dimensional scaffolds of mineralized collagen : influence of seeding density on colonization , proliferation and osteogenic differentiation. *Tissue Eng* 400-407 (2008).
39. Tang, J., Peng, R., Ding, J. The regulation of stem cell differentiation by cell-cell contact on micropatterned material surfaces. *Biomaterials* **31**, 2470-2476 (2010).
40. Scott, J. D., Pawson, T., Cell signaling in space and time: where proteins come together and when they're apart. *Science* **326**, 1220-1224 (2009).
41. Giancotti, F. G., Integrin Signaling. *Science* **285**, 1028-1033 (1999).
42. Phillips, J. E., Petrie, T. A., Creighton, F. P., García, A. J., Human mesenchymal stem cell differentiation on self-assembled monolayers presenting different surface chemistries. *Acta Biomater* **6**, 12-20 (2010).
43. Keselowsky, B. G., Collard, D. M., García, A. J. Surface chemistry modulates focal adhesion composition and signaling through changes in integrin binding. *Biomaterials* **25**, 5947-5954 (2004).
44. Keselowsky, B. G., Collard, D. M., García, A. J., Integrin binding specificity regulates biomaterial surface chemistry effects on cell differentiation. *Proc Natl Acad Sci USA* **102**, 5953-5957 (2005).
45. Keselowsky, B. G., Collard, D. M., García, A. J., Surface chemistry modulates fibronectin conformation and directs integrin binding and specificity to control cell adhesion. *J Biomed Mater Res A* **66**, 247-259 (2003).
46. Kawaguchi, N., Sundberg, C., Kveiborg, M., Moghadaszadeh, B., Asmar, M., Dietrich, N., Thodeti, C. K., Nielsen, F. C., Möller, P., Mercurio, A. M., Albrechtsen, R., Wewer, U. M., ADAM12 induces actin cytoskeleton and extracellular matrix reorganization during early adipocyte differentiation by regulating beta1 integrin function. *J Cell Sci* **116**, 3893-3904 (2003).
47. Liu, J., DeYoung, S. M., Zhang, M., Zhang, M., Cheng, A., Saltiel, A. R., Changes in integrin expression during adipocyte differentiation. *Cell Metab* **2**, 165-177 (2005).

Chapter 6

Concluding remarks and future prospects

6.1 Concluding remarks

This thesis summarized the manipulation of stem cell functions by micropatterned polymer surfaces. Diverse micropatterns were constructed on commonly used cell-culture PSt surfaces using photo-reactive polymer and UV photolithography. The different density, spreading, and shape of human MSCs were controlled on the PVA-micropatterned PSt surfaces and their respective effects on the functions of MSCs were systematically investigated. Moreover, PVA-PAAc-micropatterned PSt surface was prepared to study the electrostatic effect on the functions of MSCs with highly controlled and uniform cell shape.

Chapter 1 introduces the origins and types of stem cells, especially mesenchymal stem cells and their differentiation. The main factors that affect stem cell functions are categorized and discussed. The commonly used micropatterning methods are summarized and their applications in cell biology research are illustrated by comparing their advantages and limitations. Representative previous stem cell researches using micropatterning approaches are exemplified. Manipulation of stem cell functions by micropatterned surfaces is motivated.

Chapter 2 describes the manipulation of gradient cell densities of human MSCs on PVA-micropatterned PSt surfaces and the effects of different cell densities on the functions of MSCs. To control different cell densities on a single surface, a micropatterned surface with different area ratios of non-adhesive PVA to cell-adhesive PSt regions was prepared using photo-reactive PVA and UV photolithography. Patterned MSC aggregates with gradient cell densities were generated by culturing the cells on such micropatterned surface. The effects of the cell density gradient on MSC functions such as proliferation and differentiation were investigated. MSC aggregate at a low density proliferated faster than those at a high density. Although MSC aggregates at both low and high densities showed the osteogenic differentiation, the higher cell density of MSC aggregate could initiate the osteogenic differentiation at a faster rate than the low cell density. Additionally, high cell density of MSC aggregate was required to induce the chondrogenic differentiation.

Chapter 3 describes the manipulation of cell spreading of individual human MSCs on

PVA-micropatterned PSt surfaces and the effects of different cell spreading on the functions of MSCs at single-cell level. To control different degrees of cell spreading with the same cell shape, a series of circular cell-adhesive PSt micropatterns with different diameters were created and these micropatterns were surrounded by non-adhesive PVA layer. Cell spreading and differentiation of individual MSCs were investigated. The assembly and organization of the cytoskeleton were regulated by the degree of cell spreading. Individual MSCs on large circular micropatterns exhibited a more highly ordered arrangement of actin filaments than did those on the small circular micropatterns. Furthermore, the differentiation of MSCs was dependent on the degree of cell spreading. Increased cell spreading facilitated the osteogenic differentiation but suppressed the adipogenic differentiation of MSCs.

Chapter 4 describes the manipulation of cell shape of individual human MSCs on PVA-micropatterned PSt surfaces and the effects of different cell shapes on the functions of MSCs at single-cell level. Cell-adhesive PSt geometries of triangle, square, pentagon, hexagon, and circle were surrounded by cell non-adhesive PVA layer to control different cell shapes. These different geometries had the same small surface area for cell spreading. Human MSCs were cultured on the micropatterned surface and the effect of cell shape on the adipogenic differentiation was investigated. The distribution patterns of MSC's actin filaments were similar among these cell shapes and remolded during adipogenesis. The adipogenic differentiation potential of MSCs was similar on the small size triangular, square, pentagonal, hexagonal, and circular geometries according to the lipid vacuoles staining result.

Chapter 5 describes the electrostatic effect of micropatterned surface on the functions of human MSCs. Circular negatively charged PAAc and neutral PSt micropatterns with different diameters were created and surrounded by cell non-adhesive PVA regions using UV photolithography. The assembly and distribution of actin filaments of individual MSCs were correlated with degree of cell spreading and surface charge of underlying substrates. At single-cell level, the adipogenic differentiation was enhanced on PAAc micropatterns and decreased as the increase of circular size. At multiple-cells level, the adipogenic differentiation was stronger on PAAc micropatterns and independent of circular size.

In conclusion, diverse micropatterns were prepared on commonly used cell-culture PSt surfaces using photo-reactive polymer and UV photolithography. The respective effect of cell density, spreading, shape, and surface charge on the functions of stem cells was investigated. This simple micropatterning method using photo-reactive molecules is advantageous for fabricating arbitrary micropatterns on prevalent cell-culture substrates, and cell functions can be directly and systematically investigated on a single surface without external interferences resulting from separate cell culture and pre-coated cell-adhesive molecules. Moreover, it enables the analysis of entire cell populations at both single- and multiple-cell levels, significantly facilitating the identification of the optimal parameters to manipulate the functions of stem cells. The insights derived from these work will be useful to design suitable biomaterials for stem cell research and scaffolds for tissue engineering.

6.2 Future prospects

This research demonstrated the manipulation of stem cell functions using micropatterned surfaces. The important factors of cell environment were precisely controlled using micropatterning method and their

effects on the functions of stem cells were systematically investigated. Further researches and improvements are required to advance the integration between stem cell biology and micropatterning technology.

Fabrication of robust micropatterns on specially modulated cell-culture substrates: Previous reports have demonstrated the critical role of substrate's property such as stiffness and topography on the functions of stem cells. However, the effects of substrate's property were based on the overall data collected from whole cell population. The inherent heterogeneity of cell population should be reduced to investigate the effects on individual stem cells. Therefore, tailor-made micropatterns controlling specific cell numbers could be created on substrates with particular mechanical or chemical features. And the impacts of bottom substrate on individual stem cells of highly controlled and uniform structure could be investigated.

Combination of micropatterns and nano/biotechnology: Stem cells offer an opportunity in studies from drug efficacy to nanomaterial's cytotoxicity test, a necessary step in providing therapeutic products for human use. Most studies are carried out with adherent stem cells grown on a homogenous substrate where cells spread and divide in all directions, resulting in an inherent variability in cell shape, morphology, and behavior. The high cell-to-cell variance of the overall population impedes the success of drug development and nanomaterial screen. The ability of micropatterns to normalize the shape and internal polarity of every individual stem cell provides a tremendous opportunity for solving this critical bottleneck.

Construction of pseudo-three-dimensional micropatterns: The microwell arrays similar to extracellular three-dimensional microenvironment can be constructed by adjusting the coating concentration of photo-reactive polymers. More importantly, the single or multiple bioactive molecules could be tethered on the bottom and side wall of microwells. Therefore, microwell arrays allow the confinement of individual stem cells and analysis of entire stem cell populations at the single cell level, overcoming the problem of heterogeneity of stem cell population. Moreover, the effect of tethered signals on the response and behavior of stem cells could be investigated in a pseudo-three-dimensional manner. Additionally, the influence of spatial geometry of microwell on stem cell functions could be studied by controlling the geometric features of photomask.

List of publications

1. Wei Song, Hongxu Lu, Naoki Kawazoe, Guoping Chen. Adipogenic differentiation of individual mesenchymal stem cell on different geometric micropatterns. Langmuir, 27, 6155-6162 (2011).

2. Wei Song, Hongxu Lu, Naoki Kawazoe, Guoping Chen. Gradient patterning and differentiation of mesenchymal stem cells on micropatterned polymer surface. Journal of Bioactive and Compatible Polymers, 26, 242-256 (2011).

3. Wei Song, Naoki Kawazoe, Guoping Chen. Dependence of spreading and differentiation of mesenchymal stem cells on micropatterned surface area. Journal of Nanomaterials, Article ID 265251, 9 pages (2011).

4. Wei Song, Xinlong Wang, Hongxu Lu, Naoki Kawazoe, Guoping Chen. Adipogenic differentiation of individual mesenchymal stem cells on poly(acrylic acid) and polystyrene micropatterns. Biomacromolecules, submitted (2012).

Acknowledgements

This thesis was accomplished under the supervision from my supervisor Professor Guoping Chen. During the three years Ph. D program, Prof. Chen has devoted to instructing my research and study from selecting the topic and designing the proposal to solving the problem and composing the thesis. His expertise, innovation, and generosity has deeply affected me and greatly encouraged me for my study and life in Japan. His scientific spirit is a model of virtue for my future career and life. It is my great honor to study and work in his group. Therefore, I am taking this opportunity to sincerely giving my millions of thanks to him.

Special thanks must be given to Dr. Naoki Kawazoe for his warm support and encouragement on my doctoral study over the years. His profound knowledge, professional skill, and modest character have deeply impressed me. It is my great pleasure to work and learn from him.

I really appreciate the valuable suggestion and assistance from Dr. Hongxu Lu, Dr. Takashi Hoshiba, and Mrs. Harue Nagata. Dr. Lu has always been supporting me in my study and daily life just like my elder brother. Dr. Hoshiba has given me many important advices on stem cell research. Mrs. Nagata has helped me a lot for my daily life in Tsukuba. And I would like to give my thanks to current members in Tissue Regeneration Unit and former members in Polymeric Biomaterials Group. They are Mr. Hwan Hee Oh, Mr. Koki Hagiwara, Ms. Qin Zhang, Mr. Himansu Nandasekhar, Mr. Hongli Mao, Mr. Yuichi Hirayama, Mr. Radyum Ikono, Ms. Megumi Nozato, Mr. Shangwu Chen, Mr. Xinlong Wang, Dr. Young Gwang Ko, Dr. Wenda Dai, Dr. Michal Jerzy Wozniak, Mrs. Xiaoting Lin, Mr. Michiyuki Yurugi, Ms. Tomoe Yamada, Ms. Fumiko Kamada, Mr. Kazuyuki Sugiyama, and Ms. Akari Tanaka.

I would like to acknowledge thesis committee members: Prof. Yukio Nagasaki, Prof. Takao Aoyagi, and Prof. Tetsushi Taguchi.

I would like to give my most sincere thanks and love to my parents and all friends who are always standing by me and backing my study abroad. I cannot image the life without their selfless love and support.

This work was performed at Tissue Regeneration Unit, International Center for Materials Nanoarchitectonics (MANA), National Institute for Materials Science and Graduate School of Pure and Applied Science of University of Tsukuba.